Programme Area: Carbon Capture and Storage

Project: High Hydrogen

Title: Auto-Ignition of Hydrogen Rich Mixtures in Hot Combustion Products

Abstract:

This deliverable is number 2 of 8 in the project. The current study investigates the impact of fuel reactivity changes caused by the gradual dilution of hydrogen with either methane or carbon monoxide. The impact of nitrogen dilution is also considered. The experimental configuration was chosen to investigate auto-ignition in a turbulent shear layer formed between the fuel jet and a stream of hot combustion products. The document is made up of 117 pages. The results obtained suggest that under the current condition the reactivity of CH4, H2 blends become increasingly reduced by the CH4 component beyond the 50/50 mixture. By contrast, CO mixtures remain much more reactive over the entire range of conditions. A strong impact of dilution has also been shown and the effect is consistent with a reduced ability of the H2 component of the fuel blend to trigger auto-ignition of the carbon containing component.

Context:

Hydrogen is likely to be an increasingly important fuel component in the future. This £3.5m project was designed to advance the safe design and operation of gas turbines, reciprocating engines and combined heat and power systems using hydrogen-based fuels. Through new modelling and large-scale experimental work the project sought to identify the bounds of safe design and operation of high efficiency combined cycle gas turbine and combined heat and power systems operating on a range of fuels with high and variable concentrations of hydrogen. The goal of the project was to increase the range of fuels that can be safely used in power and heat generating plant. The project involved the Health and Safety Laboratory, an agency of the Health and Safety Executive, in collaboration with Imperial Consultants, the consulting arm of Imperial College London.

Report Prepared for Work Package 2 of ETI Project PE02162

Auto-Ignition of Hydrogen Rich Mixtures in Hot Combustion Products

F. Hampp, K.H.H. Goh, H.J. Michels and R.P. Lindstedt[**]

Department of Mechanical Engineering
Imperial College, Exhibition Road, London SW7 2AZ

[**]Corresponding author. Email: p.lindstedt@imperial.ac.uk; Tel: +44-20-7594 7039; Fax: +44-20-7589 3905

Abstract

The current study investigates the impact of fuel reactivity changes caused by the gradual dilution of hydrogen with either methane or carbon monoxide. The impact of nitrogen dilution is also considered. The experimental configuration was chosen to investigate auto-ignition in a turbulent shear layer formed between the fuel jet and a stream of hot combustion products. The study is thus complementary to conventional investigations featuring ignition delay times in laminar mixtures and constitutes a step towards a comprehensive assessment of fuel reactivity in practical systems. Ignition delay times obtained under shock tube conditions are considered in a separate study and comparisons will be presented in subsequent reports. The current results will also be compared with turbulent burning velocity and detonability data obtained in an obstructed shock tube.

The current study investigates binary fuel blends of H_2/CH_4 and H_2/CO. The H_2/CH_4 mixtures cover the full range between the pure components and with intermediate steps of 90/10, 80/20, 70/30, 60/40, 50/50, 40/60 and 25/75. The H_2/CO blends cover mixtures of 90/10, 80/20, 70/30, 60/40, 50/50, 40/60 and 30/70. For each blend a range of hot combustion product temperatures was investigated and the reactivity of the fuel blend determined by measuring the flame lift-off height from 1000 OH chemiluminescence images. The results show that the difference between dilution with CO and CH_4 is notable with comparatively small amounts of added CH_4 causing a noticeable decline in mixture reactivity while a CO content of up to 50% has only a modest impact.

The results obtained suggest that under the current condition the reactivity of CH_4/H_2 blends becomes increasingly reduced by the CH_4 component beyond the 50/50 mixture. By contrast, CO mixtures remain much more reactive over the entire range of conditions. A strong impact of dilution has also been shown and the effect is consistent with a reduced ability of the H_2 component of the fuel blend to trigger auto-ignition of the carbon containing components. The latter conclusion is further supported by the appearance of twin reaction zones in some cases. It should also be pointed out that the latter effect is more pronounced at lower temperatures. Overall, the current results suggest that the quantification of the impact of different blends of hydrocarbons with hydrogen on the fuel reactivity is distinctly possible and that the current work has elucidated several key aspects.

1   Introduction

The test strategy adopted as part of ETI project PE02162 features the initial use of binary fuel blends of H_2/CH_4 and H_2/CO starting from the case of 100% H_2 and with the gradual addition of the second component. The small scale laboratory tests used as basis for future work work within the project uniquely feature four complementary approaches covering a wide range of conditions: (i) A fuel reactivity assessment through the use of ignition delay times obtained from conventional laminar shock tube experiments, (ii) a fuel reactivity assessment via the study of auto-ignition in turbulent flow fields, (iii) the determination of turbulent burning velocities and (iv) the determination of the deflagration to detonation transition (DDT) potential in an obstructed shock tube with optical access.

It must be noted that the actual conditions experienced in a practical device present significant challenges in terms of deriving even a relative assessment of the reactivity of different fuel blends. The exhaust temperatures encountered in a practical scenario will be strongly dependent on the design of the gas turbine and the degree of mixing of the unburnt fuel blend with pre-existing combustion products at the exit plane of the combustor. Hence, the problem is not well-defined and the sensitivity to the exhaust temperature is here considered as an additional parameter. The implications for the project from the increased workload of using a larger number of mixtures can to some extent be mitigated by moderate changes in the overall work programme, notably by emphasising the importance of detonability rather than detonation behaviour of mixtures.

The fuel blends investigated as part of the current study focus on the more reactive end of the spectrum with mixtures ratios of hydrogen to carbon monoxide of 100/0, 90/10, 80/20, 70/30, 60/40, 50/50, 40/60 and 30/70 prior to dilution. The proposed range covers the majority of H_2/CO ratios identified as part of the Literature Review performed as part of Work Package 1 [1]. A narrower range of blends was proposed for the H_2/CH_4 blends encompassing 100/0, 90/10, 80/20, 70/30, 60/40 and 50/50 in line with the obtained mixture information. The latter set of mixtures was subsequently extended, on a best endeavours basis, to include 40/60, 25/75 and 0/100. In addition, a combustion device dependent dilution factor was taken into account. For practical application, it can be assumed that overall lean premixed combustion will be used and/or that significant dilution of the fuel stream will take place prior to conditions of relevance to the current investigation. Hence, it is likely that the overall hydrogen concentration in the mixture prior to combustion will not exceed 25% by volume in a fully premixed mode and, perhaps, less than half of that in the context of a gas turbine combustor. With the further dilution expected in a gas turbine engine, the proposed test matrix will therefore move the hydrogen content towards the lower flammability limit.

The Cabra burner geometry [2, 3, 4, 5, 6] has been successfully used to study the auto-ignition of high velocity fuel streams injected at ambient temperatures in a co-flowing stream of dilute combustion products at temperatures down to 1045 K. Due to the nature of the shear layer driven mixing, the temperature

at the point of ignition will be lower. In the current work, the geometry has been used at as low a temperature as can be achieved while still covering the fuel reactivity range of interest. Gkagkas and Lindstedt [7, 8] modelled the auto-ignition of CH_4 and H_2 mixtures using the transported probability density function approach [9, 10, 11, 12] and clarified the ignition events leading to flame stabilisation. Wang and Pope [13] showed that the auto-ignition chemistry has a direct and significant influence on computed extinction and re-ignition characteristics. The Cabra burner thus has a clear track record in terms of both experimental and computational studies of direct relevance to the current objectives and has been adopted with the intention of providing information pertinent to item (ii) above.

The current report accordingly outlines experimental results aimed at clarifying changes in fuel reactivity caused by a reduction in hydrogen content and covers an assessment via the study of auto-ignition of fuel blends in turbulent flow fields. The latter is of fundamental importance in the context of risks associated with the propensity of mixtures to form flame kernels that may grow into high-speed deflagrations or detonation. Past studies also suggest that state of the art computational methods can also be applied with confidence to elucidate the flow field structure further should the need arise.
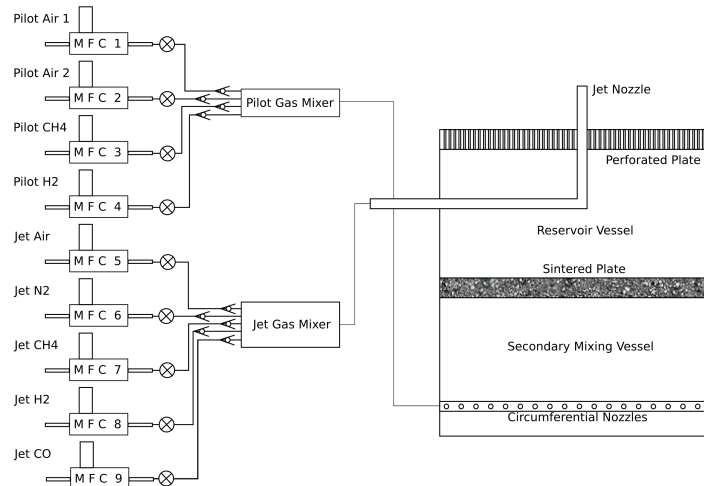
Fig. 1: Schematic of the lifted flame burner test facility

2   Experimental Configuration

2.1   Burner Configuration

The design of the current vitiated coflow burner is based on the Cabra burner [2] and the current version is shown schematically in Fig. 1. Several modifications were implemented to fulfil the safety requirements for the current experiments and to ensure homogenised mixtures in the vitiated coflow and for the fuel-air mixture in the central jet nozzle. Furthermore, the burner was modified to permit a larger number of gas components used to create the hot combustion products in the coflow and in the central core jet. The mixing of the reactant streams used to create the combustion products was initially performed in a primary mixing chamber with the resulting gas mixture subsequently passed to a circumferential ring featuring 32 radial nozzles used to inject the gas mixture into a secondary mixing vessel.

Fig. 2: Photograph of the lifted flame burner

A sintered plate with a maximum pore size of 76 μm [14] was used as a flame arrestor and to separate the secondary mixing chamber from the reservoir

leading up to the perforated disc used to stabilise the flames producing the hot combustion products. The reservoir vessel was sealed using a plate with a diameter of 210 mm perforated with 2200 holes of diameter 1.58 mm resulting in a blockage ratio of 87%. A lean premixed flame was stabilised on each of the 2200 holes providing a controlled combustion product stream that surrounded the centre nozzle. The gas mixture components for the central jet were also injected into a gas mixer. To improve the homogenisation, a sintered disk, with identical maximum pore size to that outlined above (76 μm), was inserted just before the outlet of the gas mixer. Additionally, the sintered plate served as flame arrester should flash back occur in the central fuel jet. The homogenised gas mixtures were subsequently passed directly to a jet nozzle with an inner diameter $D = 4.2$ mm. The central jet nozzle outlet is located 70 mm from the perforated pilot plate to ensure uniform properties of the coflowing combustion products. A photograph of the burner facility is shown in Fig. 2, while Fig. 3 depicts the inside of the burner by means of a computer assisted design illustration.
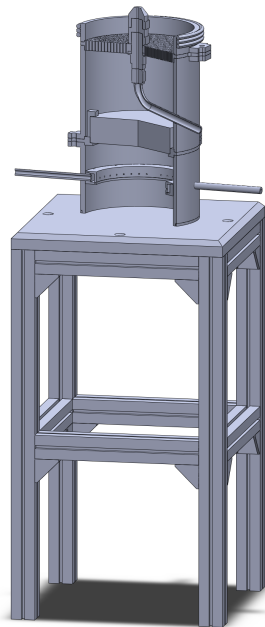
Fig. 3: Sectioned computer assisted design image of the burner

2.2   Safety Precautions

The explosion (e.g. hydrogen) and toxicity (e.g. carbon monoxide) hazards associated with the reactant gases used in the current study demand a reliable safety control system that prohibits the injection of unburned reactants into the laboratory cell or the process exhaust extraction system. Thus, two Omega thermocouples [15] were installed to monitor and record the temperature of the combustion products in the vitiated coflowing stream. The first thermocouple was of an R-type that features a fast response time and provides highly accurate temperature measurements while the second thermocouple was a shielded K-type that is robust and hence acted as backup safety system. If either one of the thermocouples detected a temperature lower than a defined safe temperature, a shut off signal is sent to the fuel mass flow controllers (MFC). The safe temperature was defined as high as feasible such that the response time for shut down was optimised ($< 1s$) while allowing for minor temperature variations resulting from normal operation. The full set of operating procedures, safety assessments and the associated documentation is available upon request.

2.3   Measurement and Analysis Arrangements

The main objective of the current experimental study was to investigate the influence of the hydrogen content of binary gas mixtures with methane and carbon monoxide upon the reactivity of the mixture.

The flame lift-off height is a direct measure of the reactivity of the fuel blend and related to the ignition delay time through the Lagrangian history of a fluid element undergoing auto-ignition. The initial data obtained in the current study therefore amounts to the determination of the lift-off height as a function of the mixture composition and the temperature of the vitiated coflow of combustion products. For mixtures containing hydrocarbons (or fragments thereof) the natural choice is to image excited state CH^* light emissions. However, the current mixture matrix has a strong focus on the upper reactivity side of the H_2 fuel blends – including pure H_2. Most mixtures are expected to offer a weak or no CH^* signal but a strong OH^* signal that is invisible to the human eye and can not be analysed in such a manner. As consequence, OH^* chemiluminescence was used to detect the flame position using an interline-transfer CCD-camera (LaVision Intense Camera [16]) with an acquisition size of $1376 \ x \ 1040 \ pixels$ and a intensified relay optics (IRO) unit (intensifier type $25 \ mm \ V7670U-70-P43$, photocathode S20, phosphor P43) to capture the instantaneous OH radical distribution. The intensifier gain was adjusted from 70 to 85 to compensate for the weaker signal obtained with increasingly stretched reaction zones. The exposure time of the camera and intensifier was set to $50 \ \mu s$ and the image interrogation region was set to $250 \ mm$.

To achieve statistically independent data, 1000 images were captured for each set of conditions with repetition rates of $9 \ Hz$ or $15 \ Hz$. To improve the signal to noise ratio, a background subtraction of the raw images was performed to reduce noise. As the background noise is dependent on the intensifier gain, a set

of 100 images was taken for each gain used. Following the actual measurements for a particular fuel mixture, the corresponding average background image was subtracted from the raw images. A sample image of an instantaneous OH^* signal with a high signal to noise ratio resulting from a concentrated reaction zone of a hydrogen/carbon monoxide mixture is shown in Fig. 4.
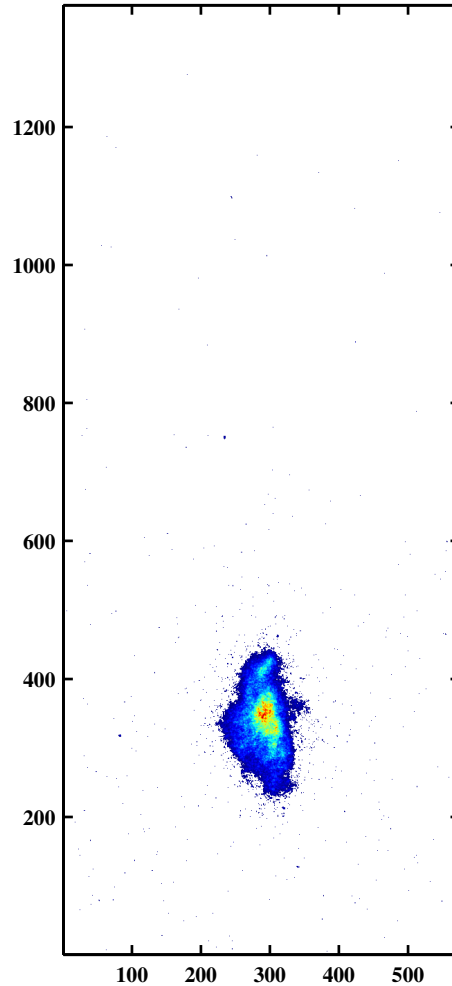
Fig. 4: Instantaneous OH^* signal with high signal to noise ratio

By contrast, Fig. 5 depicts an OH^* signal with significantly lower signal to noise ratio resulting from a stretched reaction zone of a hydrogen/methane mixture. Subsequently, further calculations, i.e. determination of the average, root mean square, and instantaneous flame lift-off height, were performed on the basis of the corrected images. Finally, the temperature of the combustion

products in the coflow were recorded with a repetition rate of $\sim 3\ Hz$ throughout the whole experiment using an R-type thermocouple in order to determine any fluctuations or drift in the mean temperature. The latter measurements were used to provide an uncertainty estimate.
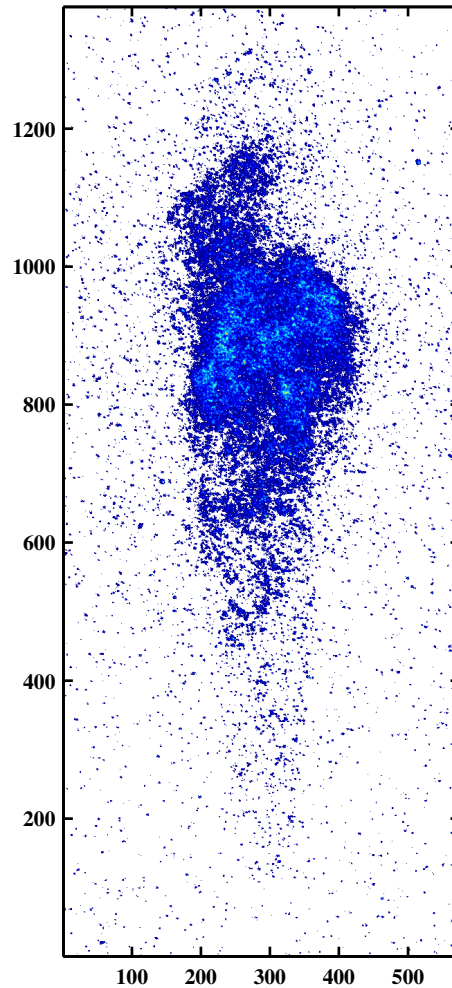
Fig. 5: Instantaneous OH^* signal with low signal to noise ratio

3   Experimental Conditions

3.1   Jet Conditions and Syngas Mixtures

The current study investigates binary fuel blends of H_2/CH_4 and H_2/CO. The H_2/CH_4 mixtures cover the full range between the pure components and with

intermediate steps of 90/10, 80/20, 70/30, 60/40, 50/50, 40/60 and 25/75. The H_2/CO blends cover mixtures of 90/10, 80/20, 70/30, 60/40, 50/50, 40/60 and 30/70. Furthermore, dilution of the fuel blend with nitrogen was also investigated. The wide spectrum of proposed gas mixtures results in considerable differences in gas properties, e.g. the unburned gas density (ρ_u), as well as reactivities. A detailed summary of all investigated gas mixtures is presented in Table 20. The intrusion of a free jet into an essentially stagnant medium is primarily governed by the momentum ($M_j = \rho_u u_j^2$) of the jet, rather than the jet velocity u_j, and we have chosen to conserve the momentum of the jet. A further advantage is that the Reynolds number remains approximately constant. The value of the jet momentum was defined such that the jet velocity of the mixture that exhibits the highest reactivity has an exit jet velocity value $u_j \approx 100 \ m/s$. The resulting jet momentum is $M_j = 0.125 \ N$. The conservation of momentum results, due to the differences in mixture densities, in a varying jet velocity which is calculated by:

$$u_j = \sqrt{\frac{M_j}{\rho_u}} \tag{1}$$

The jet velocity was accordingly varied from $u_j = 100.1 \ m/s$ for the case of pure H_2-air mixtures to $u_j = 89.13 \ m/s$ for the corresponding pure CH_4-air case. The equivalence ratio for all mixtures was maintained constant at $\Phi_j = 0.8$ and the required mole fractions in the fuel jet were calculated as shown in Eq. (2),

$$\chi_{CH_4} \cdot CH_4 + \chi_{H_2} \cdot H_2 + \chi_{CO} \cdot CO + \beta_j \cdot O_2 + 3.76 \cdot \beta_j \cdot N_2 \rightarrow$$
$$(\chi_{CH_4} + \chi_{CO}) \cdot CO_2 + (2 \cdot \chi_{CH_4} + \chi_{H_2}) \cdot H_2O + (\beta_j - \alpha_j) \cdot O_2 + 3.76 \cdot \beta_j \cdot N_2$$

$$\chi_{Air} = 4.76 \cdot \beta_j \tag{2}$$

where $\alpha_j = (2 \cdot \chi_{CH_4} + \frac{\chi_{H_2}}{2} + \frac{\chi_{CO}}{2})$ and $\beta_j = \frac{\alpha_j}{\Phi}$. Additionally, a further set of mixtures were diluted with N_2 by adding the same amount of N_2 as already introduced via the air stream. The additional N_2 mole fraction was calculated from:

$$d = \frac{3.76}{4.76} \cdot \chi_{Air}$$

$$\chi_{N_2} = \frac{d}{1+d} \tag{3}$$

Accordingly, a total of 34 fuel blends were investigated which each covering a suitable temperature range. The conditions used for all mixtures are presented in Appendix A.

3.2   The Coflow of Hot Combustion Products

The wide range of fuel blends investigated leads to significant variation in mixture reactivity. As a consequence, the temperature of the coflowing combustion products must be adjusted in order to stabilise lifted flames for all of the proposed mixture conditions. In the current work, the pilot temperature was modified by adding small quantities of CH_4 into the pilot gas stream starting

from a pure H_2-air stream. The CH_4 addition has a strong effect on the pilot temperature with 2 $slpm$ CH_4, compared to a total flow rate of ~ 2075 $slpm$ (standard litre per minute), increasing the temperature ~ 20 K. Detailed pilot conditions are presented in Appendix A for each of the mixtures investigated. The equivalence ratio of the pilot varies somewhat as it is utilised for temperature control as shown in Eq. (4),

$$a \cdot CH_4 + b \cdot H_2 + \beta_p \cdot O_2 + 3.76 \cdot \beta_p \cdot N_2 \rightarrow$$
$$a \cdot CO_2 + (2a + b) \cdot H_2O + (\beta_p - \alpha_p) \cdot O_2 + 3.76 \cdot \beta_p \cdot N_2 \tag{4}$$

where $\alpha_p = (2a + \frac{b}{2})$ and $\beta_p = \frac{\alpha_p}{\Phi}$. The difference of $(\beta_p - \alpha_p)$ represents an estimate for the residual O_2 concentration in the burned gas of the pilot stream.

4 Experimental Procedure

4.1 Control of the Experiment

A purpose designed LabView [17] interface was programmed to control experimental parameters and to initiate shutdown procedures. The interface allows an accurate setting of operating conditions, monitoring of flow rates and temperatures and also writes essential parameters to a log file. The velocities, equivalence ratios, unburned gas densities and molecular weights (MW) of the reactant streams, as well as the estimated residual O_2 concentration in the hot coflow, are also calculated and displayed. All flow rates were accurately regulated using Bronkhorst EL-FLOW Select series flow controllers [18] with an error of less than $\pm 0.5\%$ of full scale.

4.2 Operational Boundaries

Prior to the actual experiments, the potential constraints of the test facilities were explored with respect to flow velocities, coflow temperatures and the range of possible reactant stream compositions.

The lower flow velocity limit for the coflow of hot combustion products was defined by the flashback of the pilot flames stabilised on the perforated plate discussed above. This limit was not exhausted as sufficiently low pilot velocities were achieved before flashback occurred. The upper pilot velocity was bounded by the capacity limit of the mass flow controllers (MFCs). In total, four MFCs were connected to the pilot gas mixer. Two air lines were drawn from the Howden air compressor facility located in the Department of Mechanical Engineering and fitted with MFCs with a total flow rate of 2045 $slpm$ ($4.405 * 10^{-2}$ kg/s), one MFC was allocated to CH_4 with a maximum flow rate of 140.1 $slpm$ ($1.667 * 10^{-3}$ kg/s) and a fourth MFC regulated the H_2 flow rate up to 235.0 $slpm$ ($3.500 * 10^{-4}$ kg/s).

The lower coflow temperature limit is restricted by the blow-off of the pilot flames used to generate the hot combustion products. The current study necessitated a comprehensive investigation and a lower temperature limit of

$T_{p,low} = 1045 \ K$ was established while maintaining stable combustion suitably insensitive to minor flow fluctuations. The corresponding conditions, which are here defined as the base case, featured an air flow rate of 1850 $slpm$ and a H_2 flow rate of 220 $slpm$. The corresponding equivalence ratio is $\Phi \approx 0.28$. The upper temperature limit of the coflow stream is restricted by the material properties of the nozzle. This limit was not exploited due to the focus on lower temperatures in the current study.

The lower and upper limits of the core jet velocity are dependent on the reactivity of the mixture and restricted by flashback and blow-off respectively. The boundaries were explored indirectly by means of varying the coflow temperature. Raising the coflow temperature results in a higher reactivity of the mixture and stabilises the flame closer to the nozzle exit. The flashback limit and flame stabilisation on the actual nozzle were avoided. A reduction in the coflow temperature results in a reduced mixture reactivity eventually leading to flame extinction following blow-off. The latter limit was investigated thoroughly as the main objective implies the need to stabilise all mixtures at the lowest possible temperature.

Entrainment of ambient air into the hot pilot stream restricts the maximum lift-off height that can be determined reliably. The limit is defined as the height where the vitiated coflow stream becomes mixed with ambient air and thus does not provide a controlled environment. The upper limit for the flame lift-off height was found to be around $X/D \geq 50$, which is reflected in a significant increase in measurement uncertainties. Therefore, all data points with a flame lift-off height of $X/D \geq 50$ were excluded from further analysis.

5   Post-processing and Lift-off Height Definition

The large number of different mixtures and the use of an average of five temperatures per mixture resulted in a total of approximately $165,000$ instantaneous flame images. The number of images necessitated the development of an automatic flame location algorithm and a purpose written C++ algorithm was used to detect the flame lift-off height in each instantaneous image. The flame lift-off height is here detected by means of the steepest gradient in the average OH^* concentration which approximates the location of the strongest reaction zone. The IMX reader from LaVision [16] is implemented to import the instantaneous OH^* image. Subsequently, the following steps are performed to assess the flame lift-off height from the input data:

1. Integration over all pixels in vertical direction results in an average distribution locating horizontal position of the flame.

2. Pixels which are located far left or far right from the flame are excluded from the subsequent analysis.

3. Integration in the horizontal direction of the remaining pixels which leads to an average (potentially noisy) signal locating the flame in vertical direction.

Tab. 1: Fuel mixtures investigated in the scope of H_2/CH_4 blending

Mixture	u_j $[m/s]$	χ_{H_2}	χ_{CH_4}	χ_{CO}	χ_{N_2}	χ_{Air}
$H_2\ 100\% - Air$	100.1	0.2516	0.0000	0.0000	0.0000	0.7484
$H_2\ 90\% - CH_4\ 10\% - Air$	96.82	0.1849	0.0205	0.0000	0.0000	0.7946
$H_2\ 80\% - CH_4\ 20\% - Air$	94.74	0.1389	0.0347	0.0000	0.0000	0.8264
$H_2\ 70\% - CH_4\ 30\% - Air$	93.29	0.1052	0.0451	0.0000	0.0000	0.8497
$H_2\ 60\% - CH_4\ 40\% - Air$	92.23	0.0795	0.0530	0.0000	0.0000	0.8675
$H_2\ 50\% - CH_4\ 50\% - Air$	91.42	0.0593	0.0593	0.0000	0.0000	0.8815
$H_2\ 40\% - CH_4\ 60\% - Air$	90.78	0.0429	0.0643	0.0000	0.0000	0.8928
$H_2\ 25\% - CH_4\ 75\% - Air$	90.08	0.0240	0.0710	0.0000	0.0000	0.9050
$H_2\ 0\% - CH_4\ 100\% - Air$	89.17	0.0000	0.0775	0.0000	0.0000	0.9225

4. A moving average filter was applied in combination with a gradient detection algorithm.

5. The overall steepest gradient is found iteratively, starting from a coarse filtering range over the whole signal and up to a fine filtering range over a small section locating the flame lift-off height precisely.

6. The respective steepest gradient is found iteratively by means of a central difference scheme.

7. The mean flame lift-off height and the root mean square value are subsequently calculated from the detected instantaneous flame lift-off heights.

Subsequently the mean flame lift-off height and root mean square value were stored along with the reciprocal temperature and auto-ignition delay time. This operation allows a sufficiently quick and reliable detection of the mean flame lift-off height for all cases.

6   Results and Discussion

The main objective of the current investigation is to determine the influence of blending components (CH_4 and CO) on the reactivity of H_2 based fuel blends. Binary fuel mixtures of H_2/CH_4 have been studied by a significant number of researchers, though typically not under conditions of relevance to the current study [19, 20, 21, 22, 23].

Investigations covering fuel blends of H_2/CO, on the other hand, are uncommon and mainly related to research on syngas utilisation and fuel flexibility [24, 25, 26]. Lieuwen et al. [25] reports the auto-ignition delay times for various H_2/CH_4 and H_2/CO mixtures at $\Phi = 0.4$ and $P = 15\ atm$ obtained from numerical investigations. In the following sections, the impact of gradually substituting H_2 by either CH_4 or CO is reported while the equivalence ratio of the core jet was maintained at $\Phi_j = 0.8$. Moreover, the jet momentum was kept constant which leads to a varying jet velocity due to changes in the unburned gas density as detailed above. The coflow temperature was utilised as further parameter and varied within the operating limits for each mixture. A

summary of all investigated fuel blends and conditions is presented in Table 20 in Appendix A.
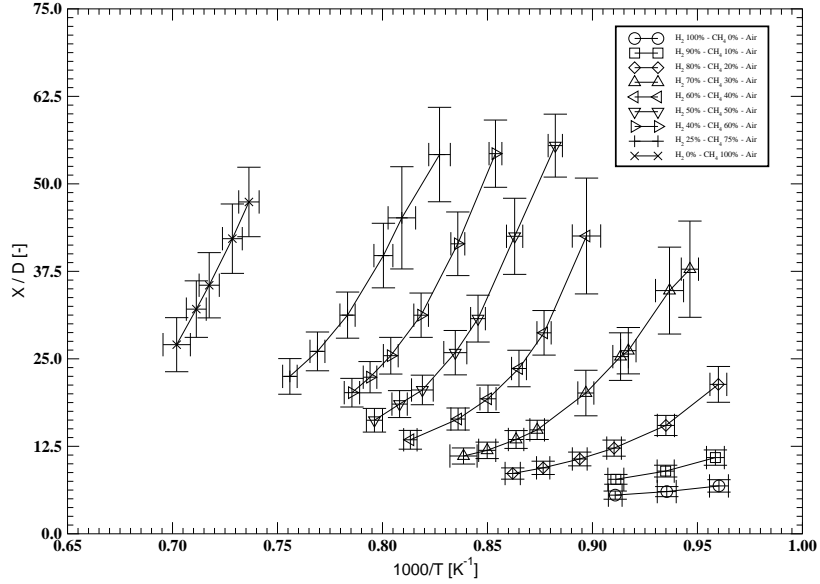
Fig. 6: Dimensionless flame lift-off height of H_2 based fuels with gradual CH_4 blending

6.1 Mixtures of Hydrogen with Methane

The case of H_2 based fuel mixtures with CH_4 as the blending component were investigated starting with pure hydrogen. Methane was introduced incrementally until H_2 was completely substituted by CH_4. The fuel mixture compositions for the investigated cases are listed in Table 1. The relative reactivity E_r was measured indirectly based on the flame lift-off height variation as a function of temperature as defined in Section 5. A standard Arrhenius diagram was found suitable for this purpose. However, it must be pointed out that E_r is not a conventional activation energy (e.g. E_A) as it is influenced by both chemistry and flow statistics. The conventional activation energies, free of such considerations, will also be determined as part of the current work as outlined in the introduction above and in the final Work Package 1 report [1]. A low flame lift-off height indicates high activity and vice versa. The flame lift-off height, measured in mm, is subsequently related to the nozzle diameter $D = 4.2\ mm$ leading to the dimensionless lift-off height X/D.

The most straightforward visualisation of the flame lift-off height is on the basis of the mean image which was calculated for each mixture and coflow temperature using a set of 1000 instantaneous images. Samples of the mean flame location are therefore shown in Fig. 26 to Fig. 34 in Appendix A for all

investigated H_2/CH_4 fuel blends and for three of the coflow temperature. As discussed above, significant differences in the mixture reactivity necessitated adjustments of the coflow temperature range on a case to case basis. Detailed conditions for all mixtures and pilot temperatures are listed in Tables 21 to 29 in Appendix A.
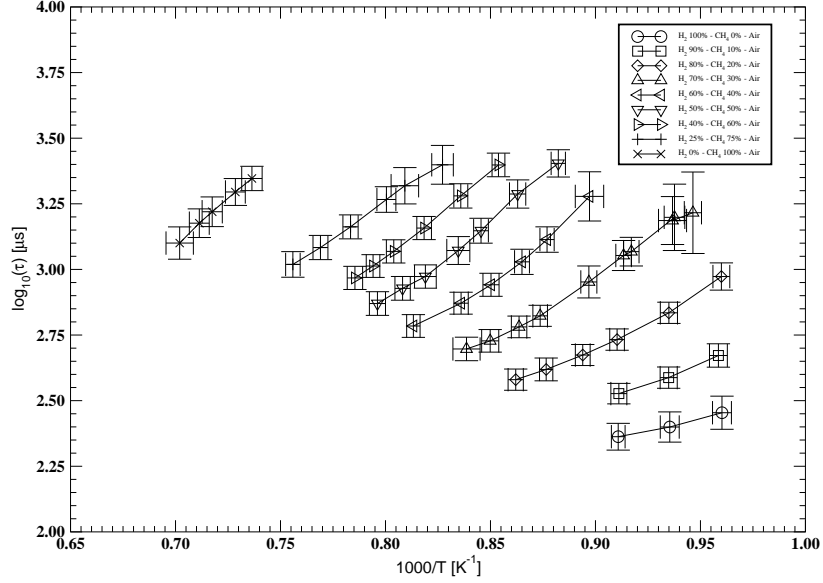
Fig. 7: Auto-ignition delay time of H_2 based fuels with gradual CH_4 blending

The measured dimensionless lift-off heights X/D are plotted in Fig. 6 versus $1000/T\ K^{-1}$ for all mixtures listed in Table 1. The data clearly illustrates that the flame lift-off height increases significantly with successive H_2 substitutions by CH_4. As discussed earlier, an increase in the flame lift-off height is directly related to a decrease in relative reactivity. The sharp impact of H_2 substitution with CH_4 was also reported by Lieuwen et al. [25]. Comparing the case of pure H_2 with mixtures of 10% and 20% CH_4 at the lower pilot temperature limit of $T_p \approx 1040\ K$ reveals an increase of X/D from 6.846, via 10.89 to 21.35 corresponding to increases of 59% and 96%, respectively. The cases featuring pure H_2 and with a 10% CH_4 substitution are restricted to a maximum coflow temperature of $T_p \approx 1095\ K$ due to the risk of flashback. The temperature range for the 20% CH_4 fuel blend could be extended up to $T_p \approx 1160\ K$. The increase in T_p is another indicator of a reduced mixture reactivity and suggests a significant decrease compared to the undiluted case and that with 10% CH_4. The measurements show that mixtures with a further substitution of H_2, leading to fuel blends with CH_4 fraction > 30%, cannot be stabilised at the lower coflow temperature limit due to the reduced reactivity. For the case of 30% CH_4 a minimum temperature $T_p \approx 1090\ K$ is required and, as a further

consequence of the lower reactivity, the upper temperature limit is raised to $T_p \approx 1190 \ K$. Furthermore, a strong increase in the temperature sensitivity, as compared to the mixtures with an increased H_2 content, is observed as indicated by the steeper gradient. Further substitution of H_2 with CH_4 continues the same trend with an increase in required minimum and possible maximum coflow temperatures.
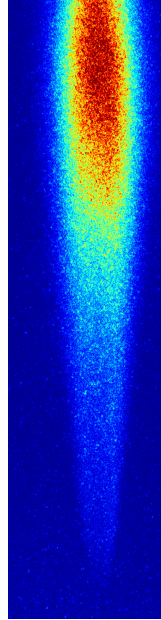
Fig. 8: Separation of the reaction zones in H_2/CH_4 mixtures

Comparisons on a basis of X/D data is sufficient to illustrate the behaviour of the different mixtures. Interestingly, it may be noted that the lift-off height appears to consist of two slopes for the more methane rich mixtures. At higher temperatures, the initial slope appears related to the hydrogen content of the mixture, while at lower temperatures the slope approaches that of the pure methane case. The trend becomes more pronounced for H_2 contents $\leq 70\%$. An analysis of the corresponding OH^* images suggest that the H_2 content acts as an initiator of chemical reaction, but that the effect is not sufficiently strong to trigger a rapid ignition of CH_4 at lower temperatures and with reduced amounts of hydrogen. Hence, there is a tendency for reaction zones to separate in H_2/CH_4 mixtures. The separation of the reaction zones is illustrated in Fig. 8 by the signal tail cased by OH^* below the main reaction zone.

It is possible to translate the lift-off height to an approximate auto-ignition delay time on the basis of the flame lift-off height and jet bulk velocity as shown

in Eq. (5).

$$\tau = \frac{X}{\sqrt{(M_j/\rho_{u,j})}} \tag{5}$$

It is important to note that the current expression does not correspond to a conventional definition as it is influenced by turbulence and mixture inhomogeneities in the shear layer formed between the core jet and the coflow of hot combustion products. However, the slope of the resulting curves in a conventional Arrhenius diagram suggest a near linear behaviour for a substantial number of the considered cases as shown in Fig. 7, where the auto-ignition delay times are plotted in the form of $log_{10}(\tau)$ against $1000/T$. Furthermore, the spreading of the curves suggests a nearly linear dependency on the H_2 concentration. The latter finding is supported by other investigators [19, 20] who calculated the auto-ignition delay time using Eq. (6), where γ is the hydrogen mole fraction with τ_{mix}, τ_{CH_4} and τ_{H_2} the ignition delay times for the mixture, pure methane and pure hydrogen respectively. The relationship was suggested to be accurate for a H_2 blending range from 0% CH_4 up to and including 40% CH_4.

$$\tau_{mix} = \tau_{H_2}^{\gamma} \cdot \tau_{CH_4}^{(1-\gamma)} \tag{6}$$

A quantitative interpretation of the auto-ignition delay time requires an analytical fit to the experimental data. Comparing the slopes of the fitted functions with the logarithm of an Arrhenius form allows an estimate of the relative reactivity as shown in Eq. (7),

$$\tau = A \cdot e^{E_r/(R \cdot T)}$$

$$log_{10}(\tau) = log_{10}(A) + log_{10}(e^{E_r/R \cdot T})$$

$$log_{10}(\tau) = log_{10}(A) + 0.4343 \cdot \frac{E_r}{R} \cdot \frac{1}{T} \tag{7}$$

$$m \cdot \frac{1}{T} = 0.4343 \cdot \frac{E_r}{R} \cdot \frac{1}{T} \Rightarrow E_r = \frac{m \cdot R}{0.4343}$$

where A a pre-exponential factor, R the universal gas constant and m is the slope of the fitted linear function. The inferred logarithmic Arrhenius functions are listed for all H_2/CH_4 fuel mixtures in Table 2. The listed fits reveal a progressive increase in the slope with a decreasing H_2 fraction for fuel blends up to a mixture ratio of 50/50 H_2/CH_4. The relative reactivity determined using Eq. (7) are also shown.

Reductions in the H_2 content below 50% introduces some scatter in the results. Mixtures with a CH_4 fraction $\geq$ 50% are stabilised at a significantly higher flame lift-off height, which increases the uncertainties in the current simplified analysis. Accordingly, a selective further analysis will be performed using transported probability density function methods (e.g. [7]) and reported as part of future work. Nevertheless, it should also be pointed out that the mixture with 25% hydrogen is at the very limit of the range for the MFC used and that

Tab. 2: Linear functions fitted to the logarithm of the auto-ignition delay time data and calculated relative reactivity E_r for H_2/CH_4 fuel blends

Mixture	Arrhenius Fit	E_r J/mol
H_2 100% $-$ Air	$log_{10}(\tau) = \frac{1850}{T} + 0.6745$	$3.542E+04$
H_2 90% $-$ CH_4 10% $-$ Air	$log_{10}(\tau) = \frac{3062}{T} - 0.2668$	$5.861E+04$
H_2 80% $-$ CH_4 20% $-$ Air	$log_{10}(\tau) = \frac{3973}{T} - 0.8656$	$7.607E+04$
H_2 70% $-$ CH_4 30% $-$ Air	$log_{10}(\tau) = \frac{5168}{T} - 1.667$	$9.893E+04$
H_2 60% $-$ CH_4 40% $-$ Air	$log_{10}(\tau) = \frac{5862}{T} - 2.018$	$1.122E+05$
H_2 50% $-$ CH_4 50% $-$ Air	$log_{10}(\tau) = \frac{6366}{T} - 2.222$	$1.219E+05$
H_2 40% $-$ CH_4 60% $-$ Air	$log_{10}(\tau) = \frac{6360}{T} - 2.037$	$1.217E+05$
H_2 25% $-$ CH_4 75% $-$ Air	$log_{10}(\tau) = \frac{5669}{T} - 1.124$	$1.085E+05$
H_2 0% $-$ CH_4 100% $-$ Air	$log_{10}(\tau) = \frac{7104}{T} - 1.881$	$1.360E+05$

measurements were performed on a best-endeavours effort for this case. Hence, the uncertainties for the other mixtures should probably not be exaggerated. Finally, the corresponding conventional ignition delay times will be determined as part of the current work package and will also be reported as part of future work.

The relative reactivity can also be determined based on the highest temperatures for each data set by simply removing the lower temperature data from the analysis. Such a procedure is not recommended in the current context, but results in the linear relationship given in Eq. (6). Table 3 lists the relative reactivities (E_r) (see Table 2), the inferred values for the high temperature range ($E_{r,h}$) and the theoretical values ($E_{r,t}$) obtained using Eq. (6). It is evident that the values obtained by the linear relationship match the relative reactivity values at the higher temperature very well, with the exception of the case 25% H_2/75% CH_4.

6.2   Hydrogen Blending with Carbon Monoxide

The second fuel blend component, carbon monoxide, was studied in a similar manner to that outlined above and the cases investigated are listed in Table 4. The corresponding flame lift-off heights, determined in the same way as for the H_2/CH_4 blends, are shown in Fig. 9. As shown for the CH_4 blends, the lift-off height increases with the introduction of CO. However, compared to the CH_4 mixtures, the trend is much less pronounced, as is particularly evident for mixtures with a CO content lower than 50%. The result corresponds qualitatively very well with the results reported by Lieuwen et al. [25] and can be

Tab. 3: Linear functions fitted to the logarithm of the auto-ignition delay time data and calculated relative reactivity E_r for H_2/CH_4 fuel blends

Mixture	$E_r \ J/mol$	$E_{r,h} \ J/mol$	$E_{r,t} \ J/mol$
$H_2 \ 100\% - Air$	$3.542E+04$	$3.542E+04$	$3.542E+04$
$H_2 \ 90\% - CH_4 \ 10\% - Air$	$5.861E+04$	$4.908E+04$	$4.668E+04$
$H_2 \ 80\% - CH_4 \ 20\% - Air$	$7.607E+04$	$5.640E+04$	$5.795E+04$
$H_2 \ 70\% - CH_4 \ 30\% - Air$	$9.893E+04$	$6.465E+04$	$6.921E+04$
$H_2 \ 60\% - CH_4 \ 40\% - Air$	$1.122E+05$	$8.059E+04$	$8.048E+04$
$H_2 \ 50\% - CH_4 \ 50\% - Air$	$1.219E+05$	$8.632E+04$	$9.175E+04$
$H_2 \ 40\% - CH_4 \ 60\% - Air$	$1.217E+05$	$1.047E+05$	$1.030E+05$
$H_2 \ 25\% - CH_4 \ 75\% - Air$	$1.085E+05$	$1.065E+05$	$1.199E+05$
$H_2 \ 0\% - CH_4 \ 100\% - Air$	$1.360E+05$	$1.481E+01$	$1.481E+05$

Tab. 4: Fuel mixtures investigated in the scope of H_2/CO blending

Mixture	$u_j \ [m/s]$	χ_{H_2}	χ_{CH_4}	χ_{CO}	χ_{N_2}	χ_{Air}
$H_2 \ 100\% - Air$	100.1	0.2516	0.0000	0.0000	0.0000	0.7484
$H_2 \ 90\% - CO \ 10\% - Air$	98.66	0.2264	0.0000	0.0252	0.0000	0.7484
$H_2 \ 80\% - CO \ 20\% - Air$	97.28	0.2013	0.0000	0.0503	0.0000	0.7484
$H_2 \ 70\% - CO \ 30\% - Air$	95.95	0.1761	0.0000	0.0755	0.0000	0.7484
$H_2 \ 60\% - CO \ 40\% - Air$	94.68	0.1509	0.0000	0.1006	0.0000	0.7484
$H_2 \ 50\% - CO \ 50\% - Air$	93.45	0.1258	0.0000	0.1258	0.0000	0.7484
$H_2 \ 40\% - CO \ 60\% - Air$	92.28	0.1006	0.0000	0.1509	0.0000	0.7484
$H_2 \ 30\% - CO \ 70\% - Air$	91.14	0.0755	0.0000	0.1761	0.0000	0.7484

directly related to the higher intrinsic reactivity of CO compared to CH_4. In this context it may be noted that all investigated H_2/CO fuel blends could be stabilised at the lowest possible coflow temperature of $T_p \approx 1040 \ K$ and that the reaction zone separation obtained for some H_2/CH_4 mixtures was not observed. The results suggest a comparatively low impact of H_2 substitution with CO. Furthermore, mixtures with a H_2 concentration down to 60% could only be investigated in the same narrow temperature range as the pure H_2 case due to the risk of flashback.

Further substitution of H_2 with CO shows an increasingly strong effect on the relative mixture reactivity. This suggests that the auto-ignition affinity of H_2/CO mixtures is governed by H_2 up to a volumetric mixture fraction of 50/50. A further CO addition results in a more significant increase in flame lift-off height at a given temperature and a more pronounced non-linearity. Furthermore, the upper temperature limit could be extended and permitted the investigation of a wider temperature range.

Tab. 5: Linear functions fitted to the logarithm of the auto-ignition delay time data and calculated relative reactivity E_r for H_2/CO fuel blends

Mixture	Arrhenius Fit	$E_r \; J/mol$
$H_2 \; 100\% - Air$	$log_{10}(\tau) \; = \; \frac{1850}{T} + 0.6745$	$3.542E + 04$
$H_2 \; 90\% - CO \; 10\% - Air$	$log_{10}(\tau) \; = \; \frac{2376}{T} + 0.2237$	$4.549E + 04$
$H_2 \; 80\% - CO \; 20\% - Air$	$log_{10}(\tau) \; = \; \frac{2384}{T} + 0.2695$	$4.562E + 04$
$H_2 \; 70\% - CO \; 30\% - Air$	$log_{10}(\tau) \; = \; \frac{2530}{T} + 0.1932$	$4.844E + 04$
$H_2 \; 60\% - CO \; 40\% - Air$	$log_{10}(\tau) \; = \; \frac{2835}{T} - 0.01727$	$5.427E + 04$
$H_2 \; 50\% - CO \; 50\% - Air$	$log_{10}(\tau) \; = \; \frac{3029}{T} - 0.1124$	$5.799E + 04$
$H_2 \; 40\% - CO \; 60\% - Air$	$log_{10}(\tau) \; = \; \frac{2986}{T} + 0.01974$	$5.716E + 04$
$H_2 \; 30\% - CO \; 70\% - Air$	$log_{10}(\tau) \; = \; \frac{3194}{T} - 0.06546$	$6.114E + 04$

A qualitatively similar behaviour was observed by Fotache et al. [26] for H_2/CO fuel blends in a study featuring ignition against a hot air stream in a counterflow (opposed jet) arrangement. Three ignition regimes were defined: (1) A hydrogen dominated regime for $100\% < \chi_{H_2} < 17\%$, (2) a transition regime spanning from $17\% < \chi_{H_2} < 7\%$ and (3) a hydrogen catalysed regime for $\chi_{H_2} < 7\%$. According to this classification, all mixtures investigated in the current study are within the hydrogen dominated ignition regime. However, a noticeable increase in the ignition temperature for volumetric hydrogen concentrations of $\chi_{H_2} < 12.58\%$ ($\chi_{H_2} = 12.58\%$ corresponds to the $50\% \; H_2/50\% \; CO$ mixture) was observed in the experimental data with the ignition temperature remaining constant for a $\chi_{H_2} > 12.58\%$ followed by an increase of approximately $20 \; K$ when $12.58\% > \chi_{H_2} > 7.55\%$. This latter agrees well with modelling approach by Sung et al. [24]. Such observations are consistent with results presented in Fig. 9, which show a significant influence on the flame lift-off height when the CO blending fraction exceeds 50%. Therefore, the current findings suggest that the hydrogen dominated regime is much narrower, with the transition regime starting with $\chi_{H_2} < 50\%$ as suggested by Sung et al. [24].

The corresponding auto-ignition delay times are shown in Fig. 10 and display the linearity between $log_{10}(\tau)$ and the reciprocal of the temperature. The significantly lower maximum lift-off height of H_2/CO fuel blends, compared to the H_2/CH_4 mixtures discussed above, reduces the uncertainties associated with the current simplified analysis, though mixtures with a CO content exceeding 50% show some scatter. The fitting of an Arrhenius-like function to the ignition delay time data reveals that the slope steadily increases with the possible exception of the case with $40\% \; H_2$. The corresponding Arrhenius fits are listed in Table 5 along with the calculated values for the relative reactivity.
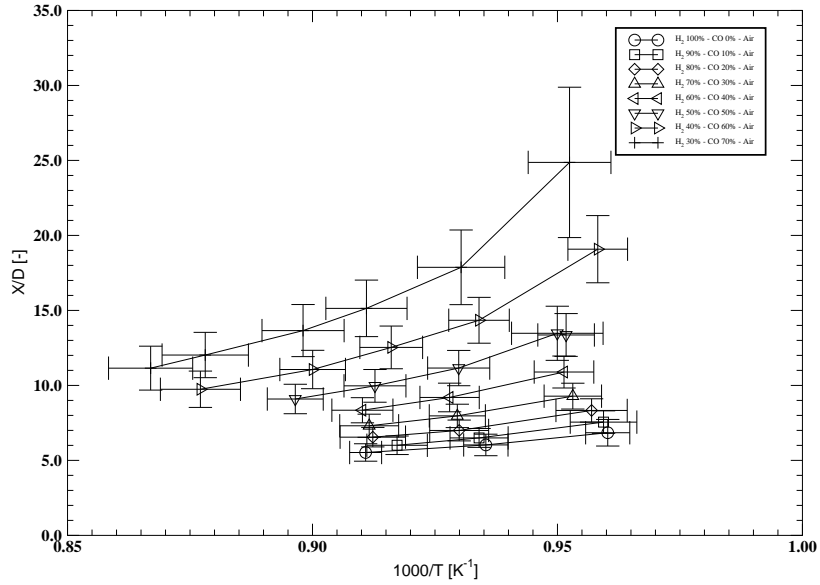
Fig. 9: Flame lift-off height of H_2 based fuels with gradual CO blending

6.3   Hydrogen Blending with a Constant CH_4 or CO Fraction

The different impacts of introducing CH_4 or CO in blends with H_2 is further analysed in the following sections in order to provide a direct comparison between mixtures with the same amount of substitution on a molar basis.

6.3.1   Mixtures with 90% Hydrogen

A comparison of mixtures with 90% H_2 blended with CH_4 or CO shows a clear difference in behaviour. It is evident, as shown in Fig. 11, that the addition of 10% CH_4 has a significant impact compared to the corresponding case with CO addition. Such differences caused by the addition of CH_4 and CO have also been reported in the context of laminar burning velocities [22] and for computed ignition delay times [25]. To quantify the actual differences between CH_4 and CO blending in the context of auto-ignition in a turbulent flow field, Table 6 lists the determined auto-ignition delay times for both mixtures. A comparison with pure H_2 at the lowest possible pilot temperature of $T_p \approx 1040$ K is also made. The addition of 10% CO results in an increase in τ of 12%, while an addition of 10% CH_4 leads to an increase of 65%. This finding suggests that the introduction of small quantities of CH_4 has a much more significant impact on the ignition characteristics of H_2 than the corresponding introduction of CO.
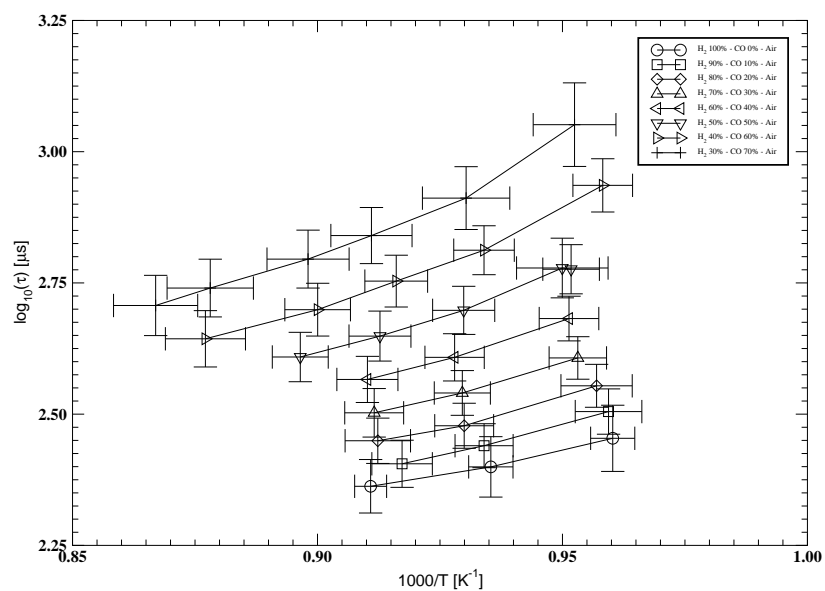
Fig. 10: Auto-ignition delay time of H_2 based fuels with gradual CO blending
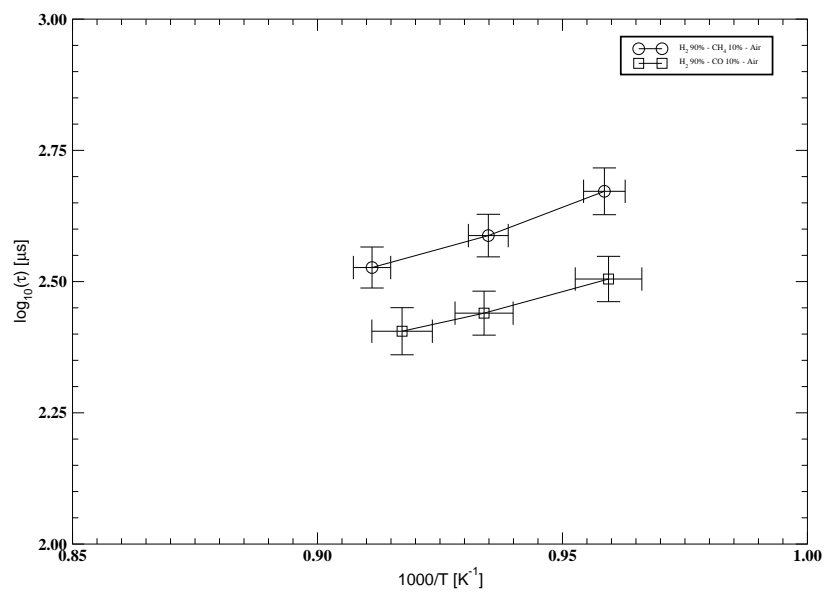
Fig. 11: Auto-ignition delay time of 90% H_2; comparison between CH_4 and CO blending

Tab. 6: Auto-ignition delay time comparison for 90% Hydrogen based fuels

Mixture	Pilot Temperature K	τ μs
H_2 $100\% - Air$	1041	284.4
H_2 $90\% - CH_4$ $10\% - Air$	1043	469.9
H_2 $90\% - CO$ $10\% - Air$	1042	319.8

Tab. 7: Arrhenius fit and relative reactivity E_r comparison for 90% hydrogen based fuels

Mixture	Arrhenius Fit	E_r J/mol
H_2 $100\% - Air$	$log_{10}(\tau) = \frac{1850}{T} + 0.6745$	$3.542E+04$
H_2 $90\% - CH_4$ $10\% - Air$	$log_{10}(\tau) = \frac{3062}{T} - 0.2668$	$5.861E+04$
H_2 $90\% - CO$ $10\% - Air$	$log_{10}(\tau) = \frac{2376}{T} + 0.2237$	$4.549E+04$

The fitted Arrhenius functions further illustrate the differences. As shown in Table 7, the inferred relative reactivities differ significantly for the two blending components. While the ratio of $E_{r,H_2/CH_4}/E_{r,H_2}$ increases to ~ 1.65, the ratio of $E_{r,H_2/CO}/E_{r,H_2}$ remains at ~ 1.28.

6.3.2 Mixtures with 80% Hydrogen

A further substitution of H_2 to produce mixtures with 80% H_2 amplifies the differences observed for the 90% H_2 case. While the H_2/CO mixture is barely affected by the additional replacement, the reactivity of the H_2/CH_4 mixture decreases radically. This finding agrees well, qualitatively, with the behaviour reported by Lieuwen et al. [25]. The actual changes in the auto-ignition delay times are shown in Table 8 and the addition of 20% CH_4 leads to an increase of auto-ignition delay time by a factor of ~ 3.3 at a pilot temperature of $T_p \approx$ 1040 K. By contrast the addition of CO results in a raise of a factor ~ 1.3.

To relate the behaviour over a range of temperatures, a more suitable com-

Tab. 8: Auto-ignition delay time comparison for 80% Hydrogen based fuels

Mixture	Pilot Temperature K	τ μs
H_2 $100\% - Air$	1041	284.4
H_2 $80\% - CH_4$ $20\% - Air$	1041	939.7
H_2 $80\% - CO$ $20\% - Air$	1045	358.1

Tab. 9: Arrhenius fit and relative reactivity E_r comparison for 80% hydrogen based fuels

Mixture	Arrhenius Fit	$E_r \ J/mol$
$H_2 \ 100\% - Air$	$log_{10}(\tau) \ = \ \frac{1850}{T} + 0.6745$	$3.542E + 04$
$H_2 \ 80\% - CH_4 \ 20\% - Air$	$log_{10}(\tau) \ = \ \frac{3973}{T} - 0.8656$	$7.607E + 04$
$H_2 \ 80\% - CO \ 20\% - Air$	$log_{10}(\tau) \ = \ \frac{2384}{T} + 0.2695$	$4.562E + 04$

parison can be obtained via the inferred relative reactivity values listed in Table 9. The increase in blending fraction, regardless of CH_4 or CO, increases the value of E_r. For the current blending ratio, the impact of the introduction of CO on the ignition characteristic of the mixture appears straightforward since:

$$\frac{\tau_{H_2}}{\tau_{H_2/CO}} \approx \frac{E_{r,H_2}}{E_{r,H_2/CO}} \tag{8}$$

However, for the case of CH_4 the blending the ratio is not conserved and, instead, the following applies:

$$\frac{\tau_{H_2}}{\tau_{H_2/CH_4}} \geq \frac{E_{r,H_2}}{E_{r,H_2/CH_4}} \tag{9}$$

The effect suggests that the influence of CH_4 on the ignition characteristic of the mixture is more profound at lower temperatures. The finding is supported by the slightly non-linear characteristics depicted in Fig. 12. Inferring the relative reactivity in a narrow temperature range around 1040 K leads to a much higher value of the reactivity barrier that sustains the ignition delay time ratio.

6.3.3 Mixtures with 70% to 50% Hydrogen

The tendencies discussed for the 90% and 80% H_2 mixtures are carried forward and further amplified with increasing blending factors. The relative reactivity of 50% H_2/CH_4 mixtures is reduced to a level where a comparison at similar temperatures is no longer possible due to the lack of overlapping measurements. The sample auto-ignition delay times and the respective coflow temperatures are listed in Table 10. The auto-ignition delay times for the lowest pilot temperature investigated for the H_2/CO mixtures are also listed in Table 10. The reported values clearly indicate significant discrepancies between the two blending components. While ignition delay times for the H_2/CO mixtures remain of the same order as for the pure H_2 case, those for H_2/CH_4 show much reduced reactivity. The Arrhenius fits as well as the relative reactivity values for the cases 70% to 50% hydrogen are shown in Table 11. The comparisons show that the CH_4 blending component introduces a much stronger temperature dependency.

Tab. 10: Auto-ignition delay time comparison for 70%, 60% and 50% Hydrogen based fuels

Mixture	Pilot Temperature K	τ μs
H_2 70% − CH_4 30% − Air	1095	1130
H_2 70% − CO 30% − Air	1097	318.1
H_2 70% − CO 30% − Air	1049	404.6
H_2 60% − CH_4 40% − Air	1115	1898
H_2 60% − CO 40% − Air	1099	368.3
H_2 60% − CO 40% − Air	1051	481.0
H_2 50% − CH_4 50% − Air	1133	2535
H_2 50% − CO 50% − Air	1115	406.3
H_2 50% − CO 50% − Air	1051	597.2

Tab. 11: Arrhenius fit and relative reactivity E_r comparison for 70%, 60% and 50% hydrogen based fuels

Mixture	Arrhenius Fit	E_r J/mol
H_2 100% − Air	$log_{10}(\tau) = \frac{1850}{T} + 0.6745$	$3.542E + 04$
H_2 70% − CH_4 30% − Air	$log_{10}(\tau) = \frac{5168}{T} - 1.667$	$9.893E + 04$
H_2 70% − CO 30% − Air	$log_{10}(\tau) = \frac{2530}{T} + 0.1932$	$4.844E + 04$
H_2 60% − CH_4 40% − Air	$log_{10}(\tau) = \frac{5862}{T} - 2.018$	$1.122E + 05$
H_2 60% − CO 40% − Air	$log_{10}(\tau) = \frac{2835}{T} - 0.01727$	$5.427E + 04$
H_2 50% − CH_4 50% − Air	$log_{10}(\tau) = \frac{6366}{T} - 2.222$	$1.219E + 05$
H_2 50% − CO 50% − Air	$log_{10}(\tau) = \frac{3029}{T} - 0.1124$	$5.799E + 04$
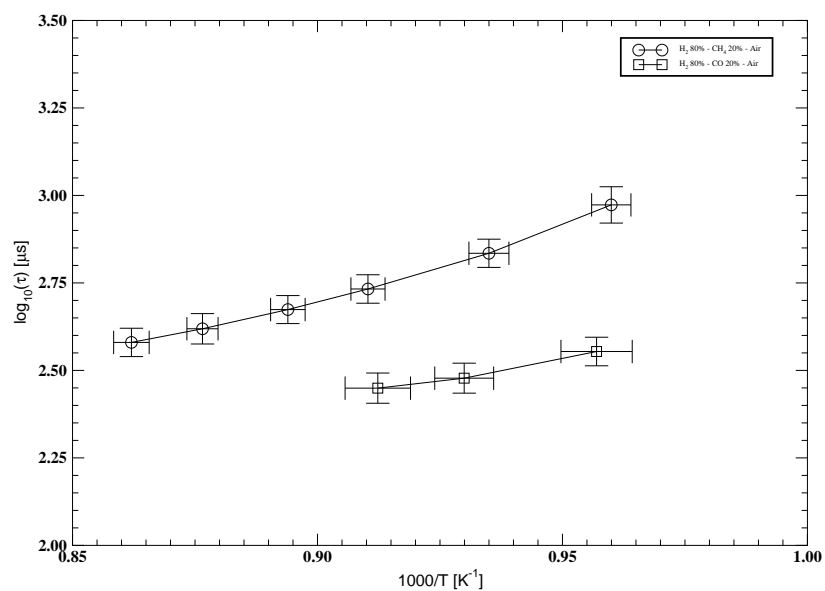
Fig. 12: Auto-ignition delay time of 80% H_2; comparison between CH_4 and CO blending
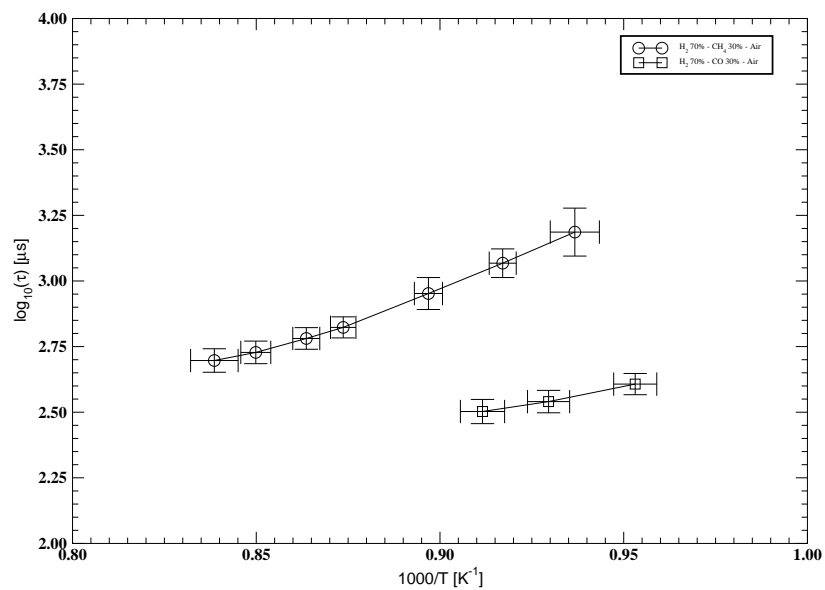
Fig. 13: Auto-ignition delay time of 70% H_2; comparison between CH_4 and CO blending
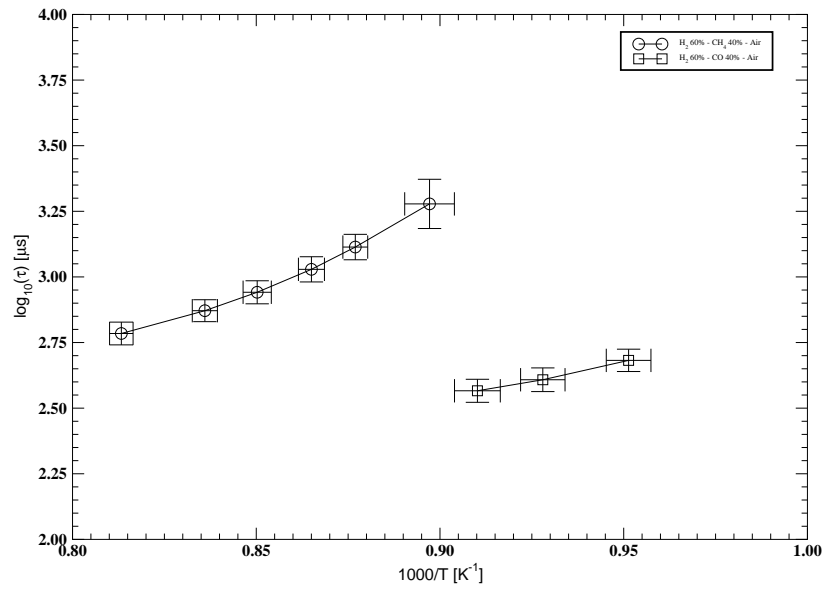
Fig. 14: Auto-ignition delay time of 60% H_2; comparison between CH_4 and CO blending
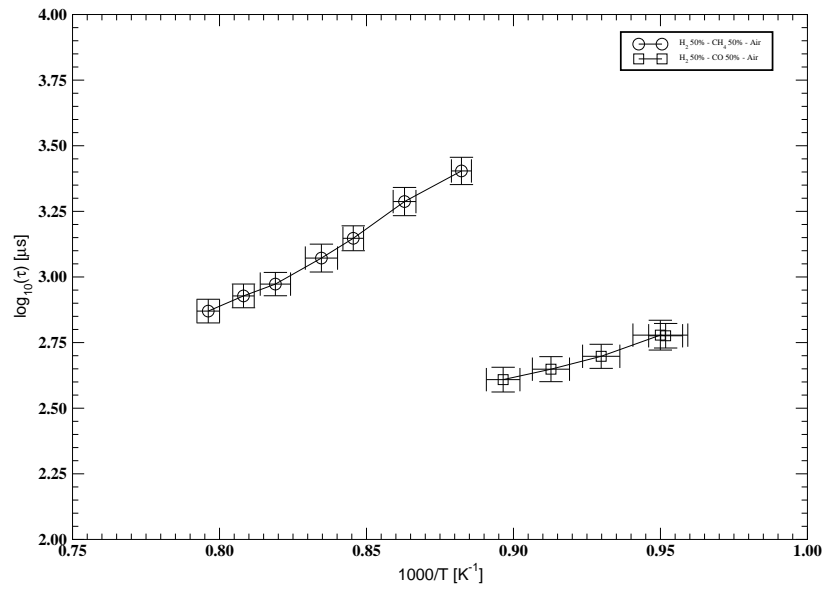
Fig. 15: Auto-ignition delay time of 50% H_2; comparison between CH_4 and CO blending

Tab. 12: Auto-ignition delay time comparison for 40% Hydrogen based fuels

Mixture	Pilot Temperature K	$\tau\ \mu s$
$H_2\ 40\% - CH_4\ 60\% - Air$	1171	2501
$H_2\ 40\% - CO\ 60\% - Air$	1044	862.7

Tab. 13: Arrhenius fit and relative reactivity E_r comparison for 40% hydrogen based fuels

Mixture	Arrhenius Fit	$E_r\ J/mol$
$H_2\ 40\% - CH_4\ 60\% - Air$	$log_{10}(\tau)\ =\ \frac{6360}{T} - 2.037$	$1.217E + 05$
$H_2\ 40\% - CO\ 60\% - Air$	$log_{10}(\tau)\ =\ \frac{2986}{T} + 0.01974$	$5.716E + 04$

The $log_{10}(\tau)$ versus the reciprocal temperature is plotted for all three blending ratios in Figs. 13, 14 and 15 for decreasing values of the H_2 mole fraction. While the slope of the H_2/CO mixture, depicted in Fig. 13, is close to be perfectly linear, the gradient in the H_2/CH_4 line is a function of temperature. This suggests that the addition of 30% CH_4 introduces a temperature dependency on the ignition characteristics. The same behaviour is observed in Fig. 14, which shows the impact of a 40% blending factor. As shown in Fig. 15, the non-linearity of the H_2/CH_4 remains present for the 50/50 mixture. However, it is also evident that by then a slight non-linearity as a function of the coflow temperature is also introduced for the H_2/CO mixture. This suggests that the impact of CO blending is also gradually becoming dependent on the coflow temperature, but at much higher dilution levels as compared CH_4. The finding suggests that the ignition characteristics of the mixture has moved into the transition regime for blending factors $> 50\%\ CO$.

6.3.4   Mixtures with 40% Hydrogen

The mixtures consisting of 60% CH_4 and 60% CO continue the trend discussed above. Thus the effect of CH_4 addition remains significantly stronger than for CO. However, as compared to the 50% H_2 cases, the influence of CO on the mixture reactivity is amplified as shown in Table 12. It should also be noted that at the higher coflow temperatures required to stabilise the CH_4 flames, the slope becomes essentially linear. The difference in reactivity is also evident from the values of the relative reactivity. The significantly larger gradient obtained for H_2/CH_4 is evident.
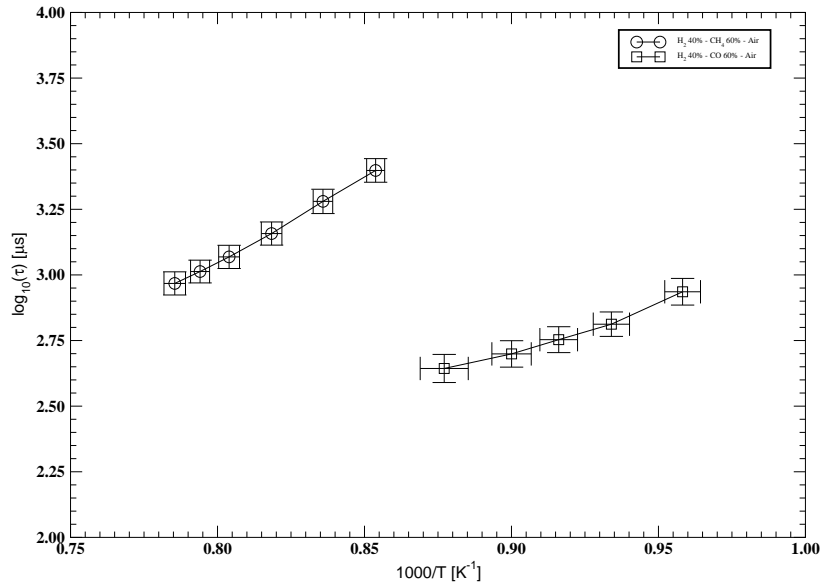
Fig. 16: Auto-ignition delay time of 40% H_2; comparison between CH_4 and CO blending

As suggested for the 50% H_2/CO mixture, the impact of CO on the ignition characteristic of the mixture becomes apparent exceeding 50% CO. This is supported by the slope of H_2/CO in Fig. 16. It is evident that the $log_{10}(\tau)$ has a certain non-linearity with respect to reciprocal coflow temperature, which, once again, is an indicator that the ignition characteristics of CO manifests itself increasingly with decreasing temperature.

6.4 Hydrogen Blending with Methane and Nitrogen Dilution

The composition of syngas is strongly dependent on the primary feedstock, i.e. coal, biomass, waste, but also on the process, e.g. gasifying agent. While oxyfuel gasification produces a rather clean gas, only traces of diluents are present in such a feedstock while gasification with air leads to a high N_2 content. The dilution introduces an inert mass which, compared to the non-diluted case, reduces the fuel concentrations, adds a heat sink into the mixtures, and affects third body reactions. A definition for the auto-ignition delay time which allows such effects is commonly used [27].

Tab. 14: Fuel mixtures investigated in the scope of H_2/CH_4 blending and further N_2 dilution

Mixture	$u_j \ [m/s]$	χ_{H_2}	χ_{CH_4}	χ_{CO}	χ_{N_2}	χ_{Air}
$H_2 \ 100\% - N_2 - Air$	95.54	0.1581	0.0000	0.0000	0.3715	0.4704
$H_2 \ 90\% - CH_4 \ 10\% - N_2 - Air$	93.60	0.1136	0.0126	0.0000	0.3856	0.4882
$H_2 \ 80\% - CH_4 \ 20\% - N_2 - Air$	92.37	0.0840	0.0210	0.0000	0.3950	0.5000
$H_2 \ 70\% - CH_4 \ 30\% - N_2 - Air$	91.52	0.0630	0.0270	0.0000	0.4016	0.5084
$H_2 \ 60\% - CH_4 \ 40\% - N_2 - Air$	90.90	0.0470	0.0315	0.0000	0.4066	0.5147
$H_2 \ 50\% - CH_4 \ 50\% - N_2 - Air$	90.43	0.0349	0.0349	0.0000	0.4105	0.5197
$H_2 \ 40\% - CH_4 \ 60\% - N_2 - Air$	90.06	0.0251	0.0377	0.0000	0.4136	0.5236
$H_2 \ 0\% - CH_4 \ 100\% - N_2 - Air$	89.13	0.0000	0.0448	0.0000	0.4215	0.5336
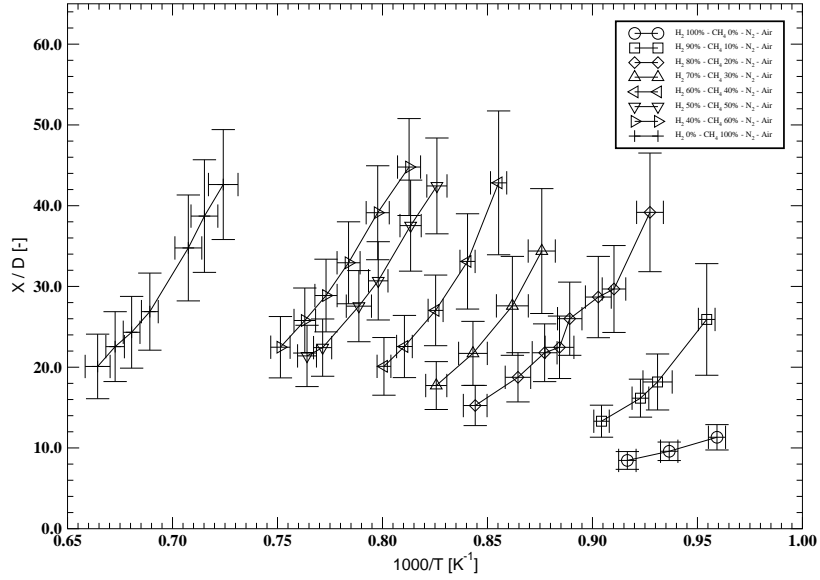
Fig. 17: Flame lift-off height of H_2 based, N_2 diluted, fuels with gradual CH_4 blending

The frequent appearance of highly diluted syngas necessitates an investigation of the impact upon the reactivity of fuel blends. In the current work, the fuel mixtures discussed above were diluted with N_2 with the added mole fraction calculated via Eq. 3. The resulting mole fractions, along with the jet velocity, of the fuel mixtures $H_2/CH_4/N_2$ studied in this section are listed in Table 14. As shown here, the fuel mole fractions, and therefore concentrations, are considerably reduced compared to the non-diluted mixtures.
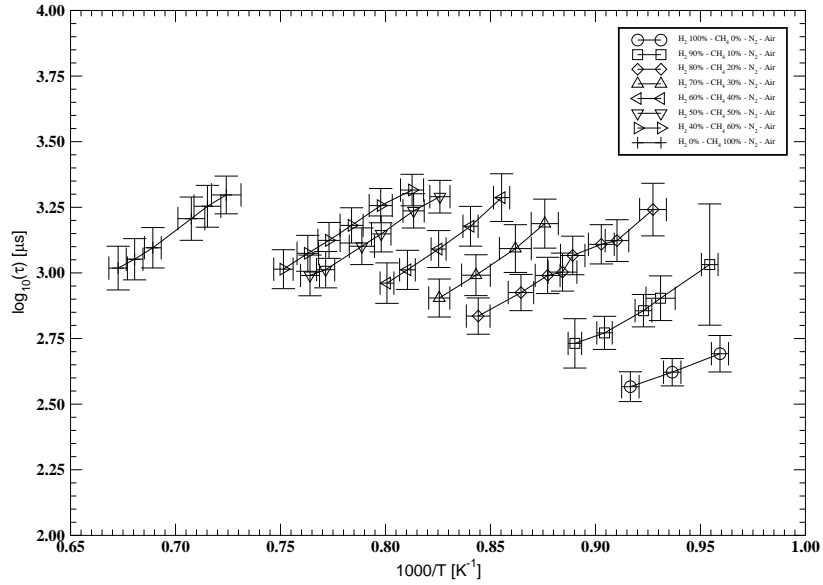
Fig. 18: Auto-ignition delay time of H_2 based, N_2 diluted, fuels with gradual CH_4 blending

The measured flame lift-off heights are shown in Fig. 17 and it is evident that the substitution of H_2 with CH_4 has, similar to the non-diluted case, a strong impact on the mixture reactivity. It can also be observed that the impact of CH_4 blending is more pronounced for the N_2 diluted mixtures. Such an effect can be expected since dilution generally slows down the reaction progress resulting in a larger flame lift-off height. A comparison of the pure H_2/N_2 blend with a mixture containing 10% CH_4 shows a sharp increase of the flame lift-off height. The findings reported in Fig. 17 suggest that a blending factor of only 10% CH_4 has a strong influence on the mixture reactivity with the diluted mixture already located in the transition regime, while the non-diluted fuel blend remains in the H_2 dominated regime. For higher CH_4 blending factors, the influence of N_2 dilution is also evident from the need to use higher coflow temperatures to achieve similar flame lift-off heights as compared to the undiluted cases. This follows from the fact that the maximum feasible flame lift-off height is reached at much lower fuel blending factors than for the non-diluted cases. In the extreme example of 100% CH_4, the investigated temperature range is $1355\ K < T_p < 1425\ K$ for the non-diluted mixture, while the diluted mixture required a temperature range of $1380\ K < T_p < 1480\ K$.

The auto-ignition delay times, determined as discussed above, are shown in Fig. 18. The linearity as a function of reciprocal temperature is maintained with N_2 dilution. However, the actual auto-ignition delay time, its slope, and therefore the relative reactivity E_r, is affected by the dilution. A more detailed comparison between the diluted and non-diluted mixtures can be found below.

Tab. 15: Linear functions fitted to the logarithm of the auto-ignition delay time data and calculated relative reactivity E_r for $H_2/CH_4/N_2$ fuel blends

Mixture	Arrhenius Fit	E_r J/mol
$H_2\ 100\% - N_2 - Air$	$log_{10}(\tau) = \frac{2947}{T} - 0.1358$	$5.641E+04$
$H_2\ 90\% - CH_4\ 10\% - N_2 - Air$	$log_{10}(\tau) = \frac{4740}{T} - 1.505$	$9.074E+04$
$H_2\ 80\% - CH_4\ 20\% - N_2 - Air$	$log_{10}(\tau) = \frac{4755}{T} - 1.183$	$9.102E+04$
$H_2\ 70\% - CH_4\ 30\% - N_2 - Air$	$log_{10}(\tau) = \frac{5596}{T} - 1.721$	$1.071E+05$
$H_2\ 60\% - CH_4\ 40\% - N_2 - Air$	$log_{10}(\tau) = \frac{5889}{T} - 1.761$	$1.127E+05$
$H_2\ 50\% - CH_4\ 50\% - N_2 - Air$	$log_{10}(\tau) = \frac{5012}{T} - 0.8478$	$9.596E+04$
$H_2\ 40\% - CH_4\ 60\% - N_2 - Air$	$log_{10}(\tau) = \frac{4999}{T} - 0.7394$	$9.570E+04$
$H_2\ 0\% - CH_4\ 100\% - N_2 - Air$	$log_{10}(\tau) = \frac{5577}{T} - 0.7401$	$1.068E+05$

Tab. 16: Fuel mixtures investigated in the scope of H_2/CO blending and further N_2 dilution

Mixture	$u_j\ [m/s]$	χ_{H_2}	χ_{CH_4}	χ_{CO}	χ_{N_2}	χ_{Air}
$H_2\ 100\% - N_2 - Air$	95.54	0.1581	0.0000	0.0000	0.3715	0.4704
$H_2\ 90\% - CO\ 10\% - N_2 - Air$	94.75	0.1423	0.0000	0.0158	0.3715	0.4704
$H_2\ 80\% - CO\ 20\% - N_2 - Air$	93.97	0.1265	0.0000	0.0316	0.3715	0.4704
$H_2\ 70\% - CO\ 30\% - N_2 - Air$	93.21	0.1107	0.0000	0.0474	0.3715	0.4704
$H_2\ 60\% - CO\ 40\% - N_2 - Air$	92.47	0.0949	0.0000	0.0632	0.3715	0.4704
$H_2\ 50\% - CO\ 50\% - N_2 - Air$	91.74	0.0791	0.0000	0.0791	0.3715	0.4704
$H_2\ 40\% - CO\ 60\% - N_2 - Air$	91.04	0.0632	0.0000	0.0949	0.3715	0.4704
$H_2\ 30\% - CO\ 70\% - N_2 - Air$	90.35	0.0474	0.0000	0.1107	0.3715	0.4704

The fitted logarithmic Arrhenius functions are shown in Table 15 along with the determined relative reactivity. The functions indicate a continuous increase of the gradient, and therefore relative reactivity up to 40% CH_4 addition. The relative reactivity barriers (E_r) for mixtures of $H_2 \geq 60\%$ are consistently higher than the values for the non-diluted cases.

6.5 Hydrogen Blending with Carbon Monoxide and Nitrogen Dilution

The impact of N_2 dilution on H_2/CO fuel blends was also investigated by applying the method shown in Eq. (3). The mixture compositions for all cases are listed in Table 16. The dimensionless flame lift-off heights for the listed mixtures are shown in Fig. 19. The impact of CO addition to diluted H_2 mixtures suggests a slightly different behaviour compared to the non-diluted counterparts. It is evident that small quantities of CO (e.g. 10%) have noticeable impact on

the mixture reactivity and, therefore, flame lift-off heights. The curves are also more spread out, i.e. an increasing CO fraction has a more distinct impact on the flame lift-off height than observed for the non-diluted counterpart. However, since the 100% H_2/N_2 mixture already features a significantly decreased reactivity it can be suggested that the dilution effect is rather strong in the current system where the dynamics between mixture reactivity and flow comes to the fore.

The auto-ignition delay times for the $H_2/CO/N_2$ mixtures are shown in Fig. 20. It is evident that, similar to the non-diluted mixtures, low CO fuel fractions have a very moderate impact on the mixture ignition characteristics. It is obvious that up to and including the 70% $H_2/30\%$ CO mixture, the reactivity of hydrogen dominates the mixture reactivity. Starting with the 60% $H_2/40\%$ CO mixture, the slopes of the auto-ignition delay time curves show a slight non-linearity which indicates the increasing influence of CO on the mixture reactivity. The fitted Arrhenius functions along with the determined values for the relative reactivity are shown in Table 17. The relative reactivity increases consistently with an increasing H_2 substitution. It is evident that at a fuel blending ratio of 60% $H_2/40\%$ CO/N_2 a distinct shift is observed in the increase of the relative reactivity barrier. The relative reactivity of the mixtures are approximately governed by Eq. (10):

$$E_r \;=\; m \cdot \chi_{H_2} + t \;\; for \; H_2 \geq 60\%$$

$$E_r \;=\; 3.4 \cdot m \cdot \chi_{H_2} + 1.45 \cdot t \;\; for \; H_2 \leq 60\% \tag{10}$$

where m and t are the gradient and intercept, respectively, obtained via least squares linear fit to the data.
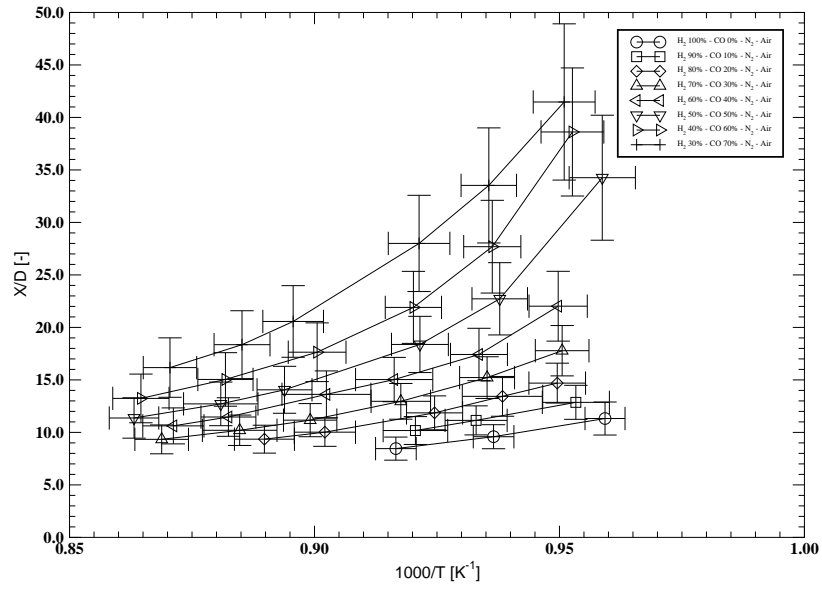
Fig. 19: Flame lift-off height of H_2 based, N_2 diluted, fuels with gradual CO blending
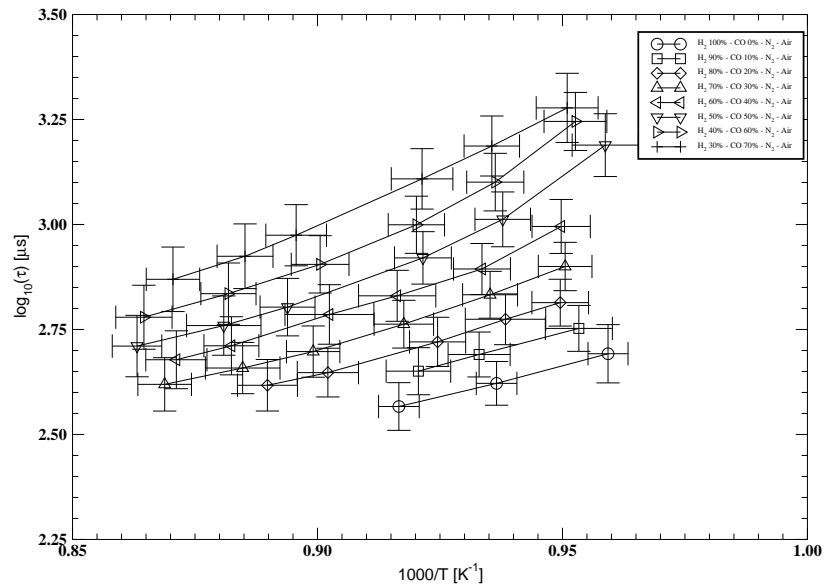
Fig. 20: Auto-ignition delay time of H_2 based, N_2 diluted, fuels with gradual CO blending
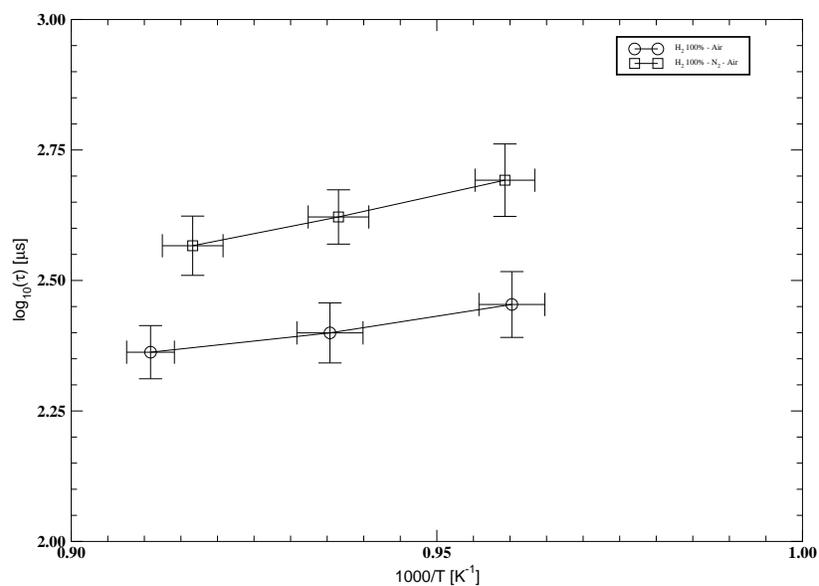
Fig. 21: Effect of N_2 dilution on the auto-ignition delay time of 100% H_2
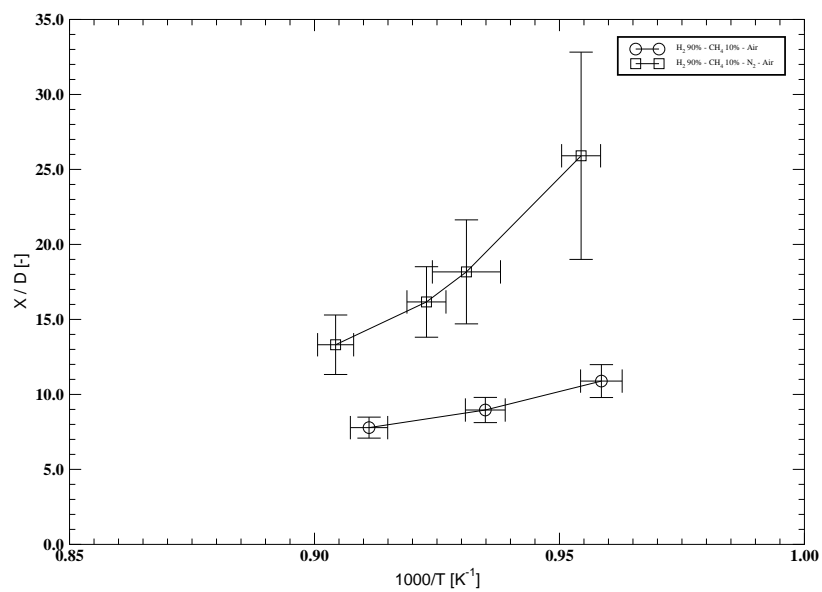
Fig. 22: Effect of N_2 dilution on the auto-ignition delay time of fuel mixture 90% H_2/10% CH_4

Tab. 17: Linear functions fitted to the logarithm of the auto-ignition delay time data and calculated relative reactivity E_r for $H_2/CO/N_2$ fuel blends

Mixture	Arrhenius Fit	E_r J/mol
$H_2\ 100\% - N_2 - Air$	$log_{10}(\tau) = \frac{2947}{T} - 0.1358$	$5.641E+04$
$H_2\ 90\% - CO\ 10\% - N_2 - Air$	$log_{10}(\tau) = \frac{3105}{T} - 0.2077$	$5.945E+04$
$H_2\ 80\% - CO\ 20\% - N_2 - Air$	$log_{10}(\tau) = \frac{3335}{T} - 0.3564$	$6.384E+04$
$H_2\ 70\% - CO\ 30\% - N_2 - Air$	$log_{10}(\tau) = \frac{3449}{T} - 0.3909$	$6.602E+04$
$H_2\ 60\% - CO\ 40\% - N_2 - Air$	$log_{10}(\tau) = \frac{3483}{T} - 0.3592$	$6.668E+04$
$H_2\ 50\% - CO\ 50\% - N_2 - Air$	$log_{10}(\tau) = \frac{4050}{T} - 0.8018$	$7.754E+04$
$H_2\ 40\% - CO\ 60\% - N_2 - Air$	$log_{10}(\tau) = \frac{4436}{T} - 1.071$	$8.492E+04$
$H_2\ 30\% - CO\ 70\% - N_2 - Air$	$log_{10}(\tau) = \frac{4952}{T} - 1.452$	$9.479E+04$

Tab. 18: Effect of N_2 dilution on the relative reactivity and auto-ignition delay time of fuel blends with 90% H_2/10% CH_4

Mixture	T_p K	X/D	τ μs
$H_2\ 90\% - CH_4\ 10\% - Air$	1043	10.87	469.9
$H_2\ 90\% - CH_4\ 10\% - N_2 - Air$	1048	25.98	1076

7   The Impact of Dilution on Mixture Reactivity

The N_2 dilution effects on the current fuel lean premixed flames of binary H_2 based fuel blends are analysed further in the current section. The influence of N_2 dilution on a pure H_2 premixed flame is considered first. At the lowest coflow temperature, the flame corresponding to the non-diluted case is stabilised at a lift-off height of $X/D = 6.846$ ($\tau = 284\ \mu s$), while N_2 dilution results in a lift-off height of $X/D = 11.32$ ($\tau = 492\ \mu s$). The corresponding increase is $\sim 65\%$. The lower reactivity of the diluted cases is the result of a broadening of the reaction zone due to heat extraction by the inert gas. The effect of N_2 dilution on pure H_2 is illustrated in Fig. 21 in terms of the auto-ignition delay time. The results show that the N_2 diluted mixture exhibits a significantly lower reactivity and therefore a longer auto-ignition delay time at a constant coflow temperature.

(a)   (b)
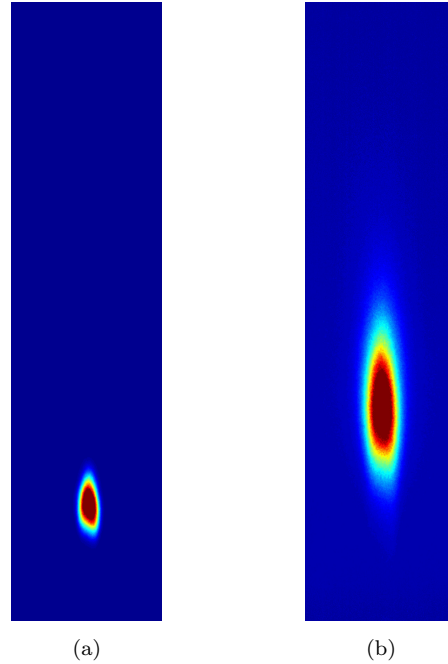
Fig. 23: OH^* Chemiluminescence: (a) H_2 $90\% - CH_4$ 10% at $T_p \approx 1075$ K; (b)
H_2 $90\% - CH_4$ $10\% - N_2$ at $T_p \approx 1075$ K

A fuel blending fraction of 10% CH_4 had a modest effect on the ignition characteristics of non-diluted mixtures, while the diluted corresponding mixture showed a significant impact. The flame lift-off heights for the cases of 90% $H_2/10\%$ CH_4 and 90% $H_2/10\%$ CH_4/N_2 are shown in Fig. 22.

The dimensionless lift-off height is chosen here as an illustration. A small amount of CH_4 induced blending is detected in the non-diluted case. The effect is amplified with N_2 dilution as the fuel concentrations are significantly reduced which has a direct impact on the amount of heat release and the auto-ignition delay time. The earlier discussed effect of the separation of the reaction zones is in the N_2 diluted case more distinct. This finding and the stretching of the reaction zone is illustrated in Fig. 23. To quantify the difference in reactivity, Table 18 lists the dimensionless flame lift-off height and the determined auto-ignition delay time for both mixtures. An increase in the auto-ignition delay time by a factor of ~ 2.5 is observed for the N_2 diluted scenario.

Tab. 19: Effect of N_2 dilution on the relative reactivity and auto-ignition delay time of fuel blends with 60% H_2/40% CO

Mixture	T_p K	X/D	τ μs
H_2 60% $- CO$ 40% $- Air$	1051	10.79	481.0
H_2 60% $- CO$ 40% $- N_2 - Air$	1053	21.97	989.1
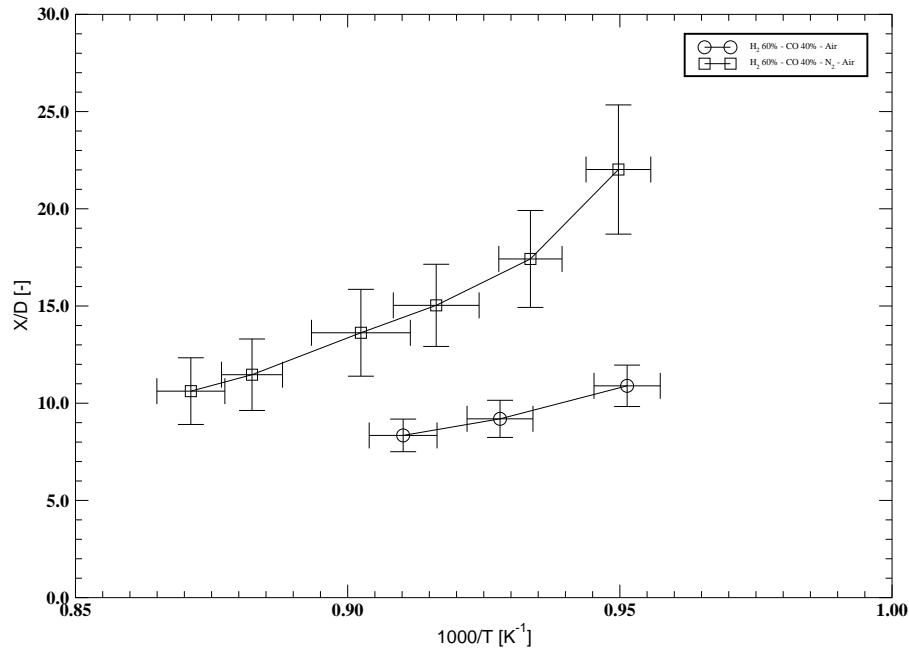
Fig. 24: Effect of N_2 dilution on the auto-ignition delay time of fuel mixture 60% H_2/40% CO

For the case with CO blending, Fig. 24 shows the effect of N_2 dilution on a mixture of 60% H_2/40% CO. As discussed previously, the ignition characteristics of CO becomes more predominant as indicated by the extended reaction zone. At higher temperatures, the evident linearity suggests a predominant H_2 ignition regime, while at lower temperatures the impact of CO becomes apparent and the mixture is transferred into the transition regime. A reason for this behaviour might be the difference in auto-ignition temperatures of the separate components or a failure by the hydrogen component to release sufficient energy on a suitable time scale to trigger ignition of the carbon containing fuel mixture component. Such an observation is consistent with noted differences

in behaviour between CO and CH_4 and should ideally be investigated further. The effect can be inferred from the emerging non-linearity at lower temperatures which indicates the increasing impact of CO blending on the ignition character-istics of the mixture. Therefore, dilution appears to have an indirect influence on the ignition characteristics of H_2/CO mixtures through a delayed auto-ignition. The actual auto-ignition delay times and dimensional flame lift-off heights are shown in Table 19. The auto-ignition delay time increases by a factor of ~ 2 for the N_2 diluted case. The OH^* chemiluminescence of the $60\% \, H_2/40\% \, CO$ is shown in Fig. 25 which supports the discussion of an extended reaction zone for the diluted case.

<div align="center">(a)   (b)</div>
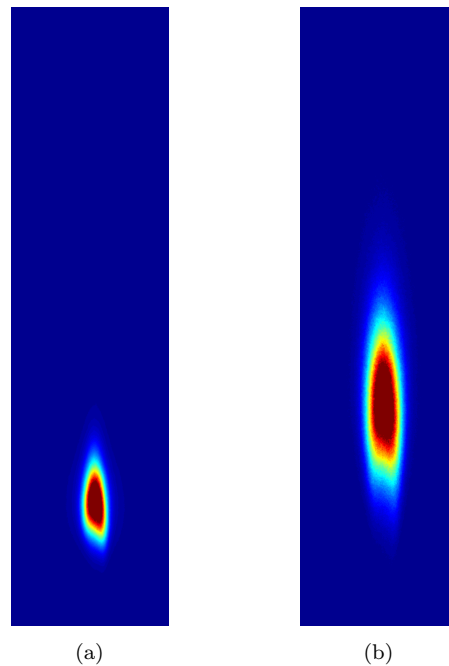
Fig. 25: OH^* Chemiluminescence: (a) $H_2 \, 60\% - CO \, 40\%$ at $T_p \approx 1051 \; K$; (b) $H_2 \, 60\% - CO \, 40\% - N_2$ at $T_p \approx 1053 \; K$

As detailed in the discussion above, the N_2 dilution of turbulent lean pre-mixed flames has a significant impact on the flame lift-off height. This is pri-marily due to the extraction of heat from the reaction zone by the diluent which, consequently, slow down the reaction progress and results in a broadening effect of the reaction zone. In terms of the auto-ignition delay time, the introduction of a diluent reduces the concentration of fuel components which, in turn, affect the ignition delay. Overall, it appears that the current experimental series has served to emphasise the importance of dilution effects in the context of flowing systems.

8   Conclusions

The current study has investigated the impact of fuel reactivity changes caused by the gradual dilution of hydrogen with either methane or carbon monoxide. The impact of nitrogen dilution added to both of these cases was also considered. Binary fuel blends of H_2/CH_4 were investigated over the full range between the pure components and with intermediate steps of 90/10, 80/20, 70/30, 60/40, 50/50, 40/60 and 25/75. The H_2/CO blends cover mixtures of 90/10, 80/20, 70/30, 60/40, 50/50, 40/60 and 30/70. For each blend a range of hot combustion product temperatures was investigated and the reactivity of the fuel blends determined by measuring the flame lift-off height from 1000 OH chemiluminescence images.

The results show that the difference between dilution with CO and CH_4 is notable and that comparatively small amounts of added CH_4 cause a decline in mixture reactivity while a CO content of up to 50% has a modest impact. The results obtained suggest that under the current condition the reactivity of CH_4/H_2 blends becomes increasingly dominated by the CH_4 component beyond the 50/50 mixture. By contrast, CO mixtures remain much more reactive over the entire range of conditions.

The strong impact of dilution has also been shown and the effect is consistent with a reduced ability of the H_2 component of the fuel blend to trigger auto-ignition of the carbon containing components. The latter conclusion is further supported by the appearance of twin reaction zones for the less reactive cases. It should also be pointed out that the latter effect is more pronounced at lower temperatures. Overall, the current results suggest that the quantification of the impact of different blends of hydrocarbons with hydrogen on the fuel reactivity is distinctly possible and that the current work has elucidated several key aspects.

The current conclusions are preliminary and will be augmented by data sets comprising ignition delay times obtained under laminar shock tube conditions, as well as turbulent burning velocity and detonability data, with the latter obtained in an obstructed shock tube. It should also be noted that the current approximate link between the flame lift-off height and the auto-ignition delay time can be significantly improved by a more extended modeling study should this prove desirable following an assessment of the complete data base including results from the other linked invstigations.

A Supplementary Tables

Tab. 20: Summary of projected Syngas Mixtures

Mixture	u_j [m/s]	Re	H_2 slpm	CH_4 slpm	CO slpm	N_2 slpm	Air slpm
H_2 100% − Air	100.1	$2.049E+04$	20.94	0.000	0.000	0.000	62.28
H_2 90% − $CH_4$10% − Air	96.82	$2.127E+04$	14.88	1.650	0.000	0.000	63.95
H_2 80% − $CH_4$20% − Air	94.74	$2.180E+04$	10.94	2.733	0.000	0.000	65.08
H_2 70% − $CH_4$30% − Air	93.29	$2.218E+04$	8.158	3.497	0.000	0.000	65.89
H_2 60% − $CH_4$40% − Air	92.23	$2.247E+04$	6.095	4.063	0.000	0.000	66.51
H_2 50% − $CH_4$50% − Air	91.42	$2.270E+04$	4.506	4.506	0.000	0.000	66.99
H_2 40% − $CH_4$60% − Air	90.78	$2.288E+04$	3.237	4.852	0.000	0.000	67.37
H_2 20% − $CH_4$80% − Air	89.83	$2.316E+04$	1.344	5.377	0.000	0.000	67.96
H_2 0% − $CH_4$100% − Air	89.17	$2.299E+04$	0.000	5.746	0.000	0.000	68.38
H_2 100% − Air	100.1	$2.049E+04$	20.94	0.000	0.000	0.000	62.28
H_2 90% − CO10% − Air	98.66	$2.078E+04$	18.57	0.000	2.067	0.000	61.38
H_2 80% − CO20% − Air	97.28	$2.107E+04$	16.28	0.000	4.068	0.000	60.52
H_2 70% − CO30% − Air	95.95	$2.136E+04$	14.05	0.000	6.022	0.000	59.69
H_2 60% − CO40% − Air	94.68	$2.165E+04$	11.88	0.000	7.918	0.000	58.90
H_2 50% − CO50% − Air	93.45	$2.193E+04$	9.773	0.000	9.773	0.000	58.14
H_2 40% − CO60% − Air	92.28	$2.222E+04$	7.717	0.000	11.58	0.000	57.42
H_2 30% − CO70% − Air	91.14	$2.250E+04$	5.720	0.000	13.34	0.000	56.70
H_2 100% − N_2 − Air	95.54	$2.164E+04$	12.56	0.000	0.000	29.51	37.36
H_2 90% − $CH_4$10% − N_2 − Air	93.60	$2.215E+04$	8.839	0.9803	0.000	30.00	37.98
H_2 80% − $CH_4$20% − N_2 − Air	92.37	$2.249E+04$	6.450	1.612	0.000	30.33	38.39
H_2 70% − $CH_4$30% − N_2 − Air	91.52	$2.272E+04$	4.793	2.054	0.000	30.55	38.68
H_2 60% − $CH_4$40% − N_2 − Air	90.90	$2.291E+04$	3.552	2.380	0.000	30.73	38.89
H_2 50% − $CH_4$50% − N_2 − Air	90.43	$2.296E+04$	2.623	2.623	0.000	30.86	39.07
H_2 40% − $CH_4$60% − N_2 − Air	90.06	$2.315E+04$	1.879	2.822	0.000	30.96	39.20
H_2 0% − $CH_4$100% − N_2 − Air	89.13	$2.321E+04$	0.000	3.319	0.000	31.23	39.53
H_2 100% − N_2 − Air	95.54	$2.164E+04$	12.56	0.000	0.000	29.51	37.36
H_2 90% − CO10% − N_2 − Air	94.75	$2.182E+04$	11.21	0.000	1.244	29.26	37.05
H_2 80% − CO20% − N_2 − Air	93.97	$2.199E+04$	9.881	0.000	2.468	29.02	36.74
H_2 70% − CO30% − N_2 − Air	93.21	$2.217E+04$	8.577	0.000	3.673	28.79	36.45
H_2 60% − CO40% − N_2 − Air	92.47	$2.235E+04$	7.295	0.000	4.858	28.56	36.16
H_2 50% − CO50% − N_2 − Air	91.74	$2.253E+04$	6.032	0.000	6.032	28.33	35.87
H_2 40% − CO60% − N_2 − Air	91.04	$2.271E+04$	4.783	0.000	7.182	28.11	35.60
H_2 30% − CO70% − N_2 − Air	90.35	$2.288E+04$	3.560	0.000	8.314	27.90	35.33

Tab. 21: Experimental conditions for the mixture $H_2 - Air$ for varying pilot conditions, where subindices j and p refer to the jet and pilot, respectively

$\chi_{H_2,j}$ [−]	$\chi_{CH_4,j}$ [−]	$\chi_{CO,j}$ [−]	$\chi_{N_2,j}$ [−]	$\chi_{Air,j}$ [−]	MW_j [kg/kmol]	$\rho_{u,j}$ [kg/m³]	$\mu_{u,j}$ [µPa·s]	u_j [m/s]	Re_j [−]	$\chi_{H_2,p}$ [−]	$\chi_{CH_4,p}$ [−]	$\chi_{Air,p}$ [−]	u_p [m/s]	T_p [K]
0.2516	0.0000	0.0000	0.0000	0.7484	22.16	0.8977	18.42	100.1	2.049E+04	0.1041	0.0000	0.8959	0.994	1041
0.2516	0.0000	0.0000	0.0000	0.7484	22.16	0.8977	18.42	100.1	2.049E+04	0.1084	0.0000	0.8916	0.998	1069
0.2516	0.0000	0.0000	0.0000	0.7484	22.16	0.8977	18.42	100.1	2.049E+04	0.1127	0.0000	0.8873	1.003	1092

Tab. 22: Experimental conditions for the mixture $H_2\ 90\% - CH_4\ 10\% - Air$ for varying pilot conditions

$\chi_{H_2,j}$ [−]	$\chi_{CH_4,j}$ [−]	$\chi_{CO,j}$ [−]	$\chi_{N_2,j}$ [−]	$\chi_{Air,j}$ [−]	MW_j [kg/kmol]	$\rho_{u,j}$ [kg/m³]	$\mu_{u,j}$ [μPa · s]	u_j [m/s]	Re_j [−]	$\chi_{H_2,p}$ [−]	$\chi_{CH_4,p}$ [−]	$\chi_{Air,p}$ [−]	u_p [m/s]	T_p [K]
0.1849	0.0205	0.0000	0.0000	0.7946	23.69	0.9597	18.35	96.82	2.127E+04	0.1041	0.0000	0.8959	0.994	1043
0.1849	0.0205	0.0000	0.0000	0.7946	23.69	0.9597	18.35	96.82	2.127E+04	0.1084	0.0000	0.8916	0.998	1070
0.1849	0.0205	0.0000	0.0000	0.7946	23.69	0.9597	18.35	96.82	2.127E+04	0.1127	0.0000	0.8873	1.003	1098

Tab. 23: Experimental conditions for the mixture H_2 80% − CH_4 20% − Air for varying pilot conditions

$X_{H_2,j}$ [−]	$X_{CH_4,j}$ [−]	$X_{CO,j}$ [−]	$X_{N_2,j}$ [−]	$X_{Air,j}$ [−]	MW_j [kg/kmol]	$\rho_{u,j}$ [kg/m³]	$\mu_{u,j}$ [μPa·s]	u_j [m/s]	Re_j [−]	$X_{H_2,p}$ [−]	$X_{CH_4,p}$ [−]	$X_{Air,p}$ [−]	u_p [m/s]	T_p [K]
0.1389	0.0347	0.0000	0.0000	0.8264	24.75	1.0025	18.30	94.74	2.180E+04	0.1041	0.0000	0.8959	0.994	1042
0.1389	0.0347	0.0000	0.0000	0.8264	24.75	1.0025	18.30	94.74	2.180E+04	0.1084	0.0000	0.8916	0.998	1070
0.1389	0.0347	0.0000	0.0000	0.8264	24.75	1.0025	18.30	94.74	2.180E+04	0.1127	0.0000	0.8873	1.003	1099
0.1389	0.0347	0.0000	0.0000	0.8264	24.75	1.0025	18.30	94.74	2.180E+04	0.1126	0.0010	0.8864	1.004	1119
0.1389	0.0347	0.0000	0.0000	0.8264	24.75	1.0025	18.30	94.74	2.180E+04	0.1225	0.0022	0.8854	1.005	1141
0.1389	0.0347	0.0000	0.0000	0.8264	24.75	1.0025	18.30	94.74	2.180E+04	0.1124	0.0031	0.8845	1.006	1160

Tab. 24: Experimental conditions for the mixture H_2 70% − CH_4 30% − Air for varying pilot conditions

$\chi_{H_2,j}$ [-]	$\chi_{CH_4,j}$ [-]	$\chi_{CO,j}$ [-]	$\chi_{N_2,j}$ [-]	$\chi_{Air,j}$ [-]	MW_j [kg/kmol]	$\rho_{u,j}$ [kg/m³]	$\mu_{u,j}$ [μPa·s]	u_j [m/s]	Re_j [-]	$\chi_{H_2,p}$ [-]	$\chi_{CH_4,p}$ [-]	$\chi_{Air,p}$ [-]	u_p [m/s]	T_p [K]
0.1052	0.0451	0.0000	0.0000	0.8497	25.52	1.0338	18.26	93.29	2.218E+04	0.1063	0.0000	0.8937	0.9961	1042
0.1052	0.0451	0.0000	0.0000	0.8497	25.52	1.0338	18.26	93.29	2.218E+04	0.1125	0.0000	0.8875	1.003	1068
0.1052	0.0451	0.0000	0.0000	0.8497	25.52	1.0338	18.26	93.29	2.218E+04	0.1084	0.0000	0.8916	0.9985	1067
0.1052	0.0451	0.0000	0.0000	0.8497	25.52	1.0338	18.26	93.29	2.218E+04	0.1127	0.0000	0.8873	1.003	1090
0.1052	0.0451	0.0000	0.0000	0.8497	25.52	1.0338	18.26	93.29	2.218E+04	0.1126	0.0010	0.8928	1.004	1095
0.1052	0.0451	0.0000	0.0000	0.8497	25.52	1.0338	18.26	93.29	2.218E+04	0.1125	0.0017	0.8858	1.005	1115
0.1052	0.0451	0.0000	0.0000	0.8497	25.52	1.0338	18.26	93.29	2.218E+04	0.1124	0.0024	0.8862	1.006	1145
0.1052	0.0451	0.0000	0.0000	0.8497	25.52	1.0338	18.26	93.29	2.218E+04	0.1124	0.0031	0.8845	1.006	1158
0.1052	0.0451	0.0000	0.0000	0.8497	25.52	1.0338	18.26	93.29	2.218E+04	0.1123	0.0041	0.8837	1.007	1177
0.1052	0.0451	0.0000	0.0000	0.8497	25.52	1.0338	18.26	93.29	2.218E+04	0.1122	0.0048	0.8831	1.008	1192

Tab. 25: Experimental conditions for the mixture H_2 60% $- CH_4$ 40% $- Air$ for varying pilot conditions

$\chi_{H_2,j}$ [-]	$\chi_{CH_4,j}$ [-]	$\chi_{CO,j}$ [-]	$\chi_{N_2,j}$ [-]	$\chi_{Air,j}$ [-]	MW_j [kg/kmol]	$\rho_{u,j}$ [kg/m³]	$\mu_{u,j}$ [μPa·s]	u_j [m/s]	Re_j [-]	$\chi_{H_2,p}$ [-]	$\chi_{CH_4,p}$ [-]	$\chi_{Air,p}$ [-]	u_p [m/s]	T_p [K]
0.0795	0.0530	0.0000	0.0000	0.8675	26.11	1.0577	18.23	92.23	2.247E+04	0.1127	0.0000	0.8873	1.003	1115
0.0795	0.0530	0.0000	0.0000	0.8675	26.11	1.0577	18.23	92.23	2.247E+04	0.1126	0.0010	0.8864	1.004	1140
0.0795	0.0530	0.0000	0.0000	0.8675	26.11	1.0577	18.23	92.23	2.247E+04	0.1125	0.0022	0.8854	1.005	1156
0.0795	0.0530	0.0000	0.0000	0.8675	26.11	1.0577	18.23	92.23	2.247E+04	0.1124	0.0031	0.8845	1.006	1176
0.0795	0.0530	0.0000	0.0000	0.8675	26.11	1.0577	18.23	92.23	2.247E+04	0.1123	0.0041	0.8837	1.007	1176
0.0795	0.0530	0.0000	0.0000	0.8675	26.11	1.0577	18.23	92.23	2.247E+04	0.1121	0.0050	0.8828	1.008	1196
0.0795	0.0530	0.0000	0.0000	0.8675	26.11	1.0577	18.23	92.23	2.247E+04	0.1119	0.0069	0.8812	1.010	1230

Tab. 26: Experimental conditions for the mixture H_2 50% − CH_4 50% − Air for varying pilot conditions

$\chi_{H_2,j}$ [−]	$\chi_{CH_4,j}$ [−]	$\chi_{CO,j}$ [−]	$\chi_{N_2,j}$ [−]	$\chi_{Air,j}$ [−]	MW_j [kg/kmol]	$\rho_{u,j}$ [kg/m³]	$\mu_{u,j}$ [μPa·s]	u_j [m/s]	Re_j [−]	$\chi_{H_2,p}$ [−]	$\chi_{CH_4,p}$ [−]	$\chi_{Air,p}$ [−]	u_p [m/s]	T_p [K]
0.0593	0.0593	0.0000	0.0000	0.8815	26.58	1.0765	18.21	91.42	2.270E+04	0.1125	0.0022	0.8854	1.005	1133
0.0593	0.0593	0.0000	0.0000	0.8815	26.58	1.0765	18.21	91.42	2.270E+04	0.1123	0.0033	0.8843	1.007	1159
0.0593	0.0593	0.0000	0.0000	0.8815	26.58	1.0765	18.21	91.42	2.270E+04	0.1122	0.0045	0.8833	1.008	1183
0.0593	0.0593	0.0000	0.0000	0.8815	26.58	1.0765	18.21	91.42	2.270E+04	0.1121	0.0052	0.8826	1.009	1198
0.0593	0.0593	0.0000	0.0000	0.8815	26.58	1.0765	18.21	91.42	2.270E+04	0.1120	0.0064	0.8816	1.010	1221
0.0593	0.0593	0.0000	0.0000	0.8815	26.58	1.0765	18.21	91.42	2.270E+04	0.1119	0.0071	0.8810	1.011	1237
0.0593	0.0593	0.0000	0.0000	0.8815	26.58	1.0765	18.21	91.42	2.270E+04	0.1118	0.0081	0.8801	1.011	1256

Tab. 27: Experimental conditions for the mixture H_2 40% $- CH_4$ 60% $- Air$ for varying pilot conditions

$\chi_{H_2,j}$ [-]	$\chi_{CH_4,j}$ [-]	$\chi_{CO,j}$ [-]	$\chi_{N_2,j}$ [-]	$\chi_{Air,j}$ [-]	MW_j [kg/kmol]	$\rho_{u,j}$ [kg/m³]	$\mu_{u,j}$ [μPa·s]	u_j [m/s]	Re_j [-]	$\chi_{H_2,p}$ [-]	$\chi_{CH_4,p}$ [-]	$\chi_{Air,p}$ [-]	u_p [m/s]	T_p [K]
0.0429	0.0643	0.0000	0.0000	0.8928	26.95	1.0918	18.19	90.78	2.288E+04	0.1123	0.0038	0.8839	1.007	1171
0.0429	0.0643	0.0000	0.0000	0.8928	26.95	1.0918	18.19	90.78	2.288E+04	0.1121	0.0050	0.8828	1.008	1196
0.0429	0.0643	0.0000	0.0000	0.8928	26.95	1.0918	18.19	90.78	2.288E+04	0.1120	0.0064	0.8816	1.010	1222
0.0429	0.0643	0.0000	0.0000	0.8928	26.95	1.0918	18.19	90.78	2.288E+04	0.1119	0.0076	0.8805	1.011	1244
0.0429	0.0643	0.0000	0.0000	0.8928	26.95	1.0918	18.19	90.78	2.288E+04	0.1118	0.0083	0.8799	1.012	1259
0.0429	0.0643	0.0000	0.0000	0.8928	26.95	1.0918	18.19	90.78	2.288E+04	0.1117	0.0090	0.8793	1.012	1273

Tab. 28: Experimental conditions for the mixture H_2 25% $- CH_4$ 75% $- Air$ for varying pilot conditions

$X_{H_2,j}$ [-]	$X_{CH_4,j}$ [-]	$X_{CO,j}$ [-]	$X_{N_2,j}$ [-]	$X_{Air,j}$ [-]	MW_j [kg/kmol]	$\rho_{u,j}$ [kg/m³]	$\mu_{u,j}$ [μPa·s]	u_j [m/s]	Re_j [-]	$X_{H_2,p}$ [-]	$X_{CH_4,p}$ [-]	$X_{Air,p}$ [-]	u_p [m/s]	T_p [K]
0.0240	0.0710	0.0000	0.0000	0.9050	27.37	1.1149	18.16	90.08	2.323E+04	0.1121	0.0057	0.8822	1.009	1209
0.0240	0.0710	0.0000	0.0000	0.9050	27.37	1.1149	18.16	90.08	2.323E+04	0.1119	0.0069	0.8812	1.010	1236
0.0240	0.0710	0.0000	0.0000	0.9050	27.37	1.1149	18.16	90.08	2.323E+04	0.1119	0.0076	0.8805	1.011	1249
0.0240	0.0710	0.0000	0.0000	0.9050	27.37	1.1149	18.16	90.08	2.323E+04	0.1117	0.0090	0.8793	1.012	1277
0.0240	0.0710	0.0000	0.0000	0.9050	27.37	1.1149	18.16	90.08	2.323E+04	0.1116	0.0102	0.8782	1.014	1300
0.0240	0.0710	0.0000	0.0000	0.9050	27.37	1.1149	18.16	90.08	2.323E+04	0.1114	0.0114	0.8772	1.015	1323

Tab. 29: Experimental conditions for the mixture H_2 0% − CH_4 100% − Air for varying pilot conditions

$\chi_{H_2,j}$ [−]	$\chi_{CH_4,j}$ [−]	$\chi_{CO,j}$ [−]	$\chi_{N_2,j}$ [−]	$\chi_{Air,j}$ [−]	MW_j [kg/kmol]	$\rho_{u,j}$ [kg/m³]	$\mu_{u,j}$ [μPa·s]	u_j [m/s]	Re_j [−]	$\chi_{H_2,p}$ [−]	$\chi_{CH_4,p}$ [−]	$\chi_{Air,p}$ [−]	u_p [m/s]	T_p [K]
0.0000	0.0775	0.0000	0.0000	0.9225	27.94	1.1149	18.16	89.17	2.299E+04	0.1046	0.0155	0.8799	1.012	1358
0.0000	0.0775	0.0000	0.0000	0.9225	27.94	1.1149	18.16	89.17	2.299E+04	0.1046	0.0162	0.8793	1.012	1373
0.0000	0.0775	0.0000	0.0000	0.9225	27.94	1.1149	18.16	89.17	2.299E+04	0.1045	0.0171	0.8784	1.013	1394
0.0000	0.0775	0.0000	0.0000	0.9225	27.94	1.1149	18.16	89.17	2.299E+04	0.1044	0.0180	0.8776	1.014	1406
0.0000	0.0775	0.0000	0.0000	0.9225	27.94	1.1149	18.16	89.17	2.299E+04	0.1043	0.0190	0.8768	1.015	1425

Tab. 30: Experimental conditions for the mixture H_2 90% $- CO$ 10% $- Air$ for varying pilot conditions

$\chi_{H_2,j}$ [-]	$\chi_{CH_4,j}$ [-]	$\chi_{CO,j}$ [-]	$\chi_{N_2,j}$ [-]	$\chi_{Air,j}$ [-]	MW_j [kg/kmol]	$\rho_{u,j}$ [kg/m³]	$\mu_{u,j}$ [μPa·s]	u_j [m/s]	Re_j [-]	$\chi_{H_2,p}$ [-]	$\chi_{CH_4,p}$ [-]	$\chi_{Air,p}$ [-]	u_p [m/s]	T_p [K]
0.2264	0.0000	0.0252	0.0000	0.7484	22.82	0.9243	18.43	98.66	2.078E+04	0.1028	0.0000	0.8972	0.9922	1042
0.2264	0.0000	0.0252	0.0000	0.7484	22.82	0.9243	18.43	98.66	2.078E+04	0.1074	0.0000	0.8926	0.9973	1071
0.2264	0.0000	0.0252	0.0000	0.7484	22.82	0.9243	18.43	98.66	2.078E+04	0.1073	0.0010	0.8918	0.9982	1090

Tab. 31: Experimental conditions for the mixture $H_2\ 80\% - CO\ 20\% - Air$ for varying pilot conditions

$\chi_{H_2,j}$ [−]	$\chi_{CH_4,j}$ [−]	$\chi_{CO,j}$ [−]	$\chi_{N_2,j}$ [−]	$\chi_{Air,j}$ [−]	MW_j [kg/kmol]	$\rho_{u,j}$ [kg/m³]	$\mu_{u,j}$ [μPa·s]	u_j [m/s]	Re_j [−]	$\chi_{H_2,p}$ [−]	$\chi_{CH_4,p}$ [−]	$\chi_{Air,p}$ [−]	u_p [m/s]	T_p [K]
0.2013	0.0000	0.0503	0.0000	0.7484	23.47	0.9508	18.44	97.28	2.107E+04	0.1028	0.0000	0.8972	0.9922	1045
0.2013	0.0000	0.0503	0.0000	0.7484	23.47	0.9508	18.44	97.28	2.107E+04	0.1074	0.0000	0.8926	0.9973	1075
0.2013	0.0000	0.0503	0.0000	0.7484	23.47	0.9508	18.44	97.28	2.107E+04	0.1073	0.0010	0.8918	0.9982	1096

Tab. 32: Experimental conditions for the mixture H_2 70% − CO 30% − Air for varying pilot conditions

$X_{H_2,j}$ [−]	$X_{CH_4,j}$ [−]	$X_{CO,j}$ [−]	$X_{N_2,j}$ [−]	$X_{Air,j}$ [−]	MW_j [kg/kmol]	$\rho_{u,j}$ [kg/m^3]	$\mu_{u,j}$ [$\mu Pa \cdot s$]	u_j [m/s]	Re_j [−]	$X_{H_2,p}$ [−]	$X_{CH_4,p}$ [−]	$X_{Air,p}$ [−]	u_p [m/s]	T_p [K]
0.1761	0.0000	0.0755	0.0000	0.7484	24.12	0.9774	18.44	95.95	2.136E+04	0.1028	0.0000	0.8972	0.9922	1049
0.1761	0.0000	0.0755	0.0000	0.7484	24.12	0.9774	18.44	95.95	2.136E+04	0.1074	0.0000	0.8926	0.9973	1076
0.1761	0.0000	0.0755	0.0000	0.7484	24.12	0.9774	18.44	95.95	2.136E+04	0.1073	0.0010	0.8918	0.9982	1097

Tab. 33: Experimental conditions for the mixture H_2 60% − CO 40% − Air for varying pilot conditions

$X_{H_2,j}$ [−]	$X_{CH_4,j}$ [−]	$X_{CO,j}$ [−]	$X_{N_2,j}$ [−]	$X_{Air,j}$ [−]	MW_j [kg/kmol]	$\rho_{u,j}$ [kg/m³]	$\mu_{u,j}$ [μPa·s]	u_j [m/s]	Re_j [−]	$X_{H_2,p}$ [−]	$X_{CH_4,p}$ [−]	$X_{Air,p}$ [−]	u_p [m/s]	T_p [K]
0.1509	0.0000	0.1006	0.0000	0.7484	24.78	1.0040	18.44	94.68	2.165E+04	0.1028	0.0000	0.8972	0.9922	1051
0.1509	0.0000	0.1006	0.0000	0.7484	24.78	1.0040	18.44	94.68	2.165E+04	0.1074	0.0000	0.8926	0.9973	1078
0.1509	0.0000	0.1006	0.0000	0.7484	24.78	1.0040	18.44	94.68	2.165E+04	0.1073	0.0010	0.8918	0.9982	1099

Tab. 34: Experimental conditions for the mixture $H_2\ 50\% - CO\ 50\% - Air$ for varying pilot conditions

$\chi_{H_2,j}$ [-]	$\chi_{CH_4,j}$ [-]	$\chi_{CO,j}$ [-]	$\chi_{N_2,j}$ [-]	$\chi_{Air,j}$ [-]	MW_j [kg/kmol]	$\rho_{u,j}$ [kg/m³]	$\mu_{u,j}$ [μPa·s]	u_j [m/s]	Re_j [-]	$\chi_{H_2,p}$ [-]	$\chi_{CH_4,p}$ [-]	$\chi_{Air,p}$ [-]	u_p [m/s]	T_p [K]
0.1258	0.0000	0.1258	0.0000	0.7484	25.43	1.0305	18.44	93.45	2.193E+04	0.1028	0.0000	0.8972	0.9922	1051
0.1258	0.0000	0.1258	0.0000	0.7484	25.43	1.0305	18.44	93.45	2.193E+04	0.1062	0.0010	0.8929	0.9970	1075
0.1258	0.0000	0.1258	0.0000	0.7484	25.43	1.0305	18.44	93.45	2.193E+04	0.1061	0.0019	0.8920	0.9980	1096
0.1258	0.0000	0.1258	0.0000	0.7484	25.43	1.0305	18.44	93.45	2.193E+04	0.1060	0.0029	0.8911	0.9990	1115

Tab. 35: Experimental conditions for the mixture $H_2\ 40\% - CO\ 60\% - Air$ for varying pilot conditions

$\chi_{H_2,j}$ [−]	$\chi_{CH_4,j}$ [−]	$\chi_{CO,j}$ [−]	$\chi_{N_2,j}$ [−]	$\chi_{Air,j}$ [−]	MW_j [kg/kmol]	$\rho_{u,j}$ [kg/m³]	$\mu_{u,j}$ [μPa·s]	u_j [m/s]	Re_j [−]	$\chi_{H_2,p}$ [−]	$\chi_{CH_4,p}$ [−]	$\chi_{Air,p}$ [−]	u_p [m/s]	T_p [K]
0.1006	0.0000	0.1509	0.0000	0.7484	26.08	1.0571	18.44	92.28	2.222E+04	0.1028	0.0000	0.8972	0.9922	1044
0.1006	0.0000	0.1509	0.0000	0.7484	26.08	1.0571	18.44	92.28	2.222E+04	0.1074	0.0000	0.8926	0.9973	1071
0.1006	0.0000	0.1509	0.0000	0.7484	26.08	1.0571	18.44	92.28	2.222E+04	0.1073	0.0010	0.8918	0.9982	1092
0.1006	0.0000	0.1509	0.0000	0.7484	26.08	1.0571	18.44	92.28	2.222E+04	0.1072	0.0019	0.8909	0.9992	1111
0.1006	0.0000	0.1509	0.0000	0.7484	26.08	1.0571	18.44	92.28	2.222E+04	0.1070	0.0029	0.8901	1.000	1140

Tab. 36: Experimental conditions for the mixture $H_2\ 30\% - CO\ 70\% - Air$ for varying pilot conditions

$\chi_{H_2,j}$ [-]	$\chi_{CH_4,j}$ [-]	$\chi_{CO,j}$ [-]	$\chi_{N_2,j}$ [-]	$\chi_{Air,j}$ [-]	MW_j [kg/kmol]	$\rho_{u,j}$ [kg/m³]	$\mu_{u,j}$ [μPa·s]	u_j [m/s]	Re_j [-]	$\chi_{H_2,p}$ [-]	$\chi_{CH_4,p}$ [-]	$\chi_{Air,p}$ [-]	u_p [m/s]	T_p [K]
0.0755	0.0000	0.1761	0.0000	0.7484	26.74	1.0837	18.44	91.14	2.250E+04	0.1028	0.0000	0.8972	0.9922	1050
0.0755	0.0000	0.1761	0.0000	0.7484	26.74	1.0837	18.44	91.14	2.250E+04	0.1074	0.0000	0.8926	0.9973	1075
0.0755	0.0000	0.1761	0.0000	0.7484	26.74	1.0837	18.44	91.14	2.250E+04	0.1073	0.0010	0.8918	0.9982	1098
0.0755	0.0000	0.1761	0.0000	0.7484	26.74	1.0837	18.44	91.14	2.250E+04	0.1072	0.0019	0.8909	1.000	1113
0.0755	0.0000	0.1761	0.0000	0.7484	26.74	1.0837	18.44	91.14	2.250E+04	0.1070	0.0031	0.8899	1.004	1139
0.0755	0.0000	0.1761	0.0000	0.7484	26.74	1.0837	18.44	91.14	2.250E+04	0.1069	0.0038	0.8892	1.010	1153

Tab. 37: Experimental conditions for the mixture $H_2 - N_2 - Air$ for varying pilot conditions

$\chi_{H_2,j}$ [-]	$\chi_{CH_4,j}$ [-]	$\chi_{CO,j}$ [-]	$\chi_{N_2,j}$ [-]	$\chi_{Air,j}$ [-]	MW_j [kg/kmol]	$\rho_{u,j}$ [kg/m³]	$\mu_{u,j}$ [μPa·s]	u_j [m/s]	Re_j [-]	$\chi_{H_2,p}$ [-]	$\chi_{CH_4,p}$ [-]	$\chi_{Air,p}$ [-]	u_p [m/s]	T_p [K]
0.1581	0.0000	0.0000	0.3715	0.4704	24.33	0.9870	18.31	95.54	2.164E+04	0.1127	0.0000	0.8873	1.003	1042
0.1581	0.0000	0.0000	0.3715	0.4704	24.33	0.9870	18.31	95.54	2.164E+04	0.1125	0.0014	0.8860	1.004	1068
0.1581	0.0000	0.0000	0.3715	0.4704	24.33	0.9870	18.31	95.54	2.164E+04	0.1124	0.0026	0.8850	1.006	1091

Tab. 38: Experimental conditions for the mixture $H_2\ 90\% - CH_4\ 10\% - N_2 - Air$ for varying pilot conditions

$\chi_{H_2,j}$ [−]	$\chi_{CH_4,j}$ [−]	$\chi_{CO,j}$ [−]	$\chi_{N_2,j}$ [−]	$\chi_{Air,j}$ [−]	MW_j [kg/kmol]	$\rho_{u,j}$ [kg/m³]	$\mu_{u,j}$ [μPa·s]	u_j [m/s]	Re_j [−]	$\chi_{H_2,p}$ [−]	$\chi_{CH_4,p}$ [−]	$\chi_{Air,p}$ [−]	u_p [m/s]	T_p [K]
0.1136	0.0126	0.0000	0.3856	0.4882	25.35	1.0285	18.25	93.60	2.215E+04	0.1127	0.0000	0.8873	1.003	1048
0.1136	0.0126	0.0000	0.3856	0.4882	25.35	1.0285	18.25	93.60	2.215E+04	0.1125	0.0014	0.8860	1.004	1074
0.1136	0.0126	0.0000	0.3856	0.4882	25.35	1.0285	18.25	93.60	2.215E+04	0.1124	0.0026	0.8850	1.006	1084
0.1136	0.0126	0.0000	0.3856	0.4882	25.35	1.0285	18.25	93.60	2.215E+04	0.1124	0.0026	0.8850	1.006	1106
0.1136	0.0126	0.0000	0.3856	0.4882	25.35	1.0285	18.25	93.60	2.215E+04	0.1123	0.0036	0.8841	1.007	1123

Tab. 39: Experimental conditions for the mixture H_2 80% $- CH_4$ 20% $- N_2 - Air$ for varying pilot conditions

$\chi_{H_2,j}$ [-]	$\chi_{CH_4,j}$ [-]	$\chi_{CO,j}$ [-]	$\chi_{N_2,j}$ [-]	$\chi_{Air,j}$ [-]	MW_j [kg/kmol]	$\rho_{u,j}$ [kg/m³]	$\mu_{u,j}$ [μPa·s]	u_j [m/s]	Re_j [-]	$\chi_{H_2,p}$ [-]	$\chi_{CH_4,p}$ [-]	$\chi_{Air,p}$ [-]	u_p [m/s]	T_p [K]
0.0840	0.0210	0.0000	0.3950	0.5000	26.03	1.0560	18.22	92.37	2.249E+04	0.1074	0.0000	0.8926	0.9973	1078
0.0840	0.0210	0.0000	0.3950	0.5000	26.03	1.0560	18.22	92.37	2.249E+04	0.1072	0.0013	0.8914	0.9986	1099
0.0840	0.0210	0.0000	0.3950	0.5000	26.03	1.0560	18.22	92.37	2.249E+04	0.1060	0.0022	0.8918	0.9982	1107
0.0840	0.0210	0.0000	0.3950	0.5000	26.03	1.0560	18.22	92.37	2.249E+04	0.1060	0.0029	0.8911	0.9990	1125
0.0840	0.0210	0.0000	0.3950	0.5000	26.03	1.0560	18.22	92.37	2.249E+04	0.1059	0.0038	0.8903	0.9999	1130
0.0840	0.0210	0.0000	0.3950	0.5000	26.03	1.0560	18.22	92.37	2.249E+04	0.1058	0.0048	0.8894	1.0009	1157
0.0840	0.0210	0.0000	0.3950	0.5000	26.03	1.0560	18.22	92.37	2.249E+04	0.1057	0.0058	0.8875	1.0019	1185

Tab. 40: Experimental conditions for the mixture $H_2\ 70\% - CH_4\ 30\% - N_2 - Air$ for varying pilot conditions

$X_{H_2,j}$ [−]	$X_{CH_4,j}$ [−]	$X_{CO,j}$ [−]	$X_{N_2,j}$ [−]	$X_{Air,j}$ [−]	MW_j [kg/kmol]	$\rho_{u,j}$ [kg/m³]	$\mu_{u,j}$ [μPa·s]	u_j [m/s]	Re_j [−]	$X_{H_2,p}$ [−]	$X_{CH_4,p}$ [−]	$X_{Air,p}$ [−]	u_p [m/s]	T_p [K]
0.0630	0.0270	0.0000	0.4016	0.5084	26.52	1.0756	18.20	91.52	2.272E+04	0.1062	0.0012	0.8926	0.9973	1101
0.0630	0.0270	0.0000	0.4016	0.5084	26.52	1.0756	18.20	91.52	2.272E+04	0.1060	0.0026	0.8914	0.9987	1123
0.0630	0.0270	0.0000	0.4016	0.5084	26.52	1.0756	18.20	91.52	2.272E+04	0.1059	0.0036	0.8905	0.9997	1142
0.0630	0.0270	0.0000	0.4016	0.5084	26.52	1.0756	18.20	91.52	2.272E+04	0.1058	0.0046	0.8896	1.001	1160
0.0630	0.0270	0.0000	0.4016	0.5084	26.52	1.0756	18.20	91.52	2.272E+04	0.1057	0.0058	0.8886	1.002	1186
0.0630	0.0270	0.0000	0.4016	0.5084	26.52	1.0756	18.20	91.52	2.272E+04	0.1055	0.0070	0.8875	1.003	1211

Tab. 41: Experimental conditions for the mixture $H_2\ 60\% - CH_4\ 40\% - N_2 - Air$ for varying pilot conditions

$X_{H_2,j}$ [-]	$X_{CH_4,j}$ [-]	$X_{CO,j}$ [-]	$X_{N_2,j}$ [-]	$X_{Air,j}$ [-]	MW_j [kg/kmol]	$\rho_{u,j}$ [kg/m³]	$\mu_{u,j}$ [μPa·s]	u_j [m/s]	Re_j [-]	$X_{H_2,p}$ [-]	$X_{CH_4,p}$ [-]	$X_{Air,p}$ [-]	u_p [m/s]	T_p [K]
0.0630	0.0270	0.0000	0.4016	0.5084	26.52	1.0756	18.20	91.52	2.272E+04	0.1058	0.0048	0.8894	1.001	1147
0.0630	0.0270	0.0000	0.4016	0.5084	26.52	1.0756	18.20	91.52	2.272E+04	0.1057	0.0055	0.8888	1.002	1169
0.0630	0.0270	0.0000	0.4016	0.5084	26.52	1.0756	18.20	91.52	2.272E+04	0.1056	0.0065	0.8879	1.003	1190
0.0630	0.0270	0.0000	0.4016	0.5084	26.52	1.0756	18.20	91.52	2.272E+04	0.1055	0.0074	0.8871	1.004	1212
0.0630	0.0270	0.0000	0.4016	0.5084	26.52	1.0756	18.20	91.52	2.272E+04	0.1054	0.0084	0.8862	1.004	1234
0.0630	0.0270	0.0000	0.4016	0.5084	26.52	1.0756	18.20	91.52	2.272E+04	0.1053	0.0091	0.8856	1.005	1249

Tab. 42: Experimental conditions for the mixture H_2 $50\% - CH_4$ $50\% - N_2 - Air$ for varying pilot conditions

$X_{H_2,j}$ [-]	$X_{CH_4,j}$ [-]	$X_{CO,j}$ [-]	$X_{N_2,j}$ [-]	$X_{Air,j}$ [-]	MW_j [kg/kmol]	$\rho_{u,j}$ [kg/m³]	$\mu_{u,j}$ [μPa·s]	u_j [m/s]	Re_j [-]	$X_{H_2,p}$ [-]	$X_{CH_4,p}$ [-]	$X_{Air,p}$ [-]	u_p [m/s]	T_p [K]
0.0349	0.0349	0.0000	0.4105	0.5197	27.16	1.0985	18.17	90.43	2.296E+04	0.1056	0.0068	0.8876	1.003	1211
0.0349	0.0349	0.0000	0.4105	0.5197	27.16	1.0985	18.17	90.43	2.296E+04	0.1055	0.0077	0.8869	1.004	1229
0.0349	0.0349	0.0000	0.4105	0.5197	27.16	1.0985	18.17	90.43	2.296E+04	0.1053	0.0089	0.8858	1.005	1253
0.0349	0.0349	0.0000	0.4105	0.5197	27.16	1.0985	18.17	90.43	2.296E+04	0.1053	0.0097	0.8851	1.006	1268
0.0349	0.0349	0.0000	0.4105	0.5197	27.16	1.0985	18.17	90.43	2.296E+04	0.1051	0.0108	0.8841	1.007	1296
0.0349	0.0349	0.0000	0.4105	0.5197	27.16	1.0985	18.17	90.43	2.296E+04	0.1050	0.0117	0.8833	1.008	1309

Tab. 43: Experimental conditions for the mixture H_2 40% − CH_4 60% − N_2 − Air for varying pilot conditions

$X_{H_2,j}$ [−]	$X_{CH_4,j}$ [−]	$X_{CO,j}$ [−]	$X_{N_2,j}$ [−]	$X_{Air,j}$ [−]	MW_j [kg/kmol]	$\rho_{u,j}$ [kg/m³]	$\mu_{u,j}$ [μPa·s]	u_j [m/s]	Re_j [−]	$X_{H_2,p}$ [−]	$X_{CH_4,p}$ [−]	$X_{Air,p}$ [−]	u_p [m/s]	T_p [K]
0.0251	0.0377	0.0000	0.4136	0.5236	27.39	1.1109	18.15	90.06	2.315E+04	0.1054	0.0079	0.8867	1.004	1230
0.0251	0.0377	0.0000	0.4136	0.5236	27.39	1.1109	18.15	90.06	2.315E+04	0.1054	0.0086	0.8860	1.005	1254
0.0251	0.0377	0.0000	0.4136	0.5236	27.39	1.1109	18.15	90.06	2.315E+04	0.1052	0.0100	0.8847	1.006	1276
0.0251	0.0377	0.0000	0.4136	0.5236	27.39	1.1109	18.15	90.06	2.315E+04	0.1051	0.0110	0.8839	1.007	1293
0.0251	0.0377	0.0000	0.4136	0.5236	27.39	1.1109	18.15	90.06	2.315E+04	0.1050	0.0122	0.8828	1.008	1311
0.0251	0.0377	0.0000	0.4136	0.5236	27.39	1.1109	18.15	90.06	2.315E+04	0.1049	0.0133	0.8818	1.010	1331

Tab. 44: Experimental conditions for the mixture H_2 0% − CH_4 0% − N_2 − Air for varying pilot conditions

$X_{H_2,j}$ [-]	$X_{CH_4,j}$ [-]	$X_{CO,j}$ [-]	$X_{N_2,j}$ [-]	$X_{Air,j}$ [-]	MW_j [kg/kmol]	$\rho_{u,j}$ [kg/m³]	$\mu_{u,j}$ [µPa·s]	u_j [m/s]	Re_j [-]	$X_{H_2,p}$ [-]	$X_{CH_4,p}$ [-]	$X_{Air,p}$ [-]	u_p [m/s]	T_p [K]
0.0000	0.0448	0.0000	0.4215	0.5336	27.96	1.1245	18.13	89.13	2.321E+04	0.1045	0.0171	0.8784	1.013	1381
0.0000	0.0448	0.0000	0.4215	0.5336	27.96	1.1245	18.13	89.13	2.321E+04	0.1044	0.0180	0.8776	1.014	1398
0.0000	0.0448	0.0000	0.4215	0.5336	27.96	1.1245	18.13	89.13	2.321E+04	0.1042	0.0199	0.8759	1.016	1314
0.0000	0.0448	0.0000	0.4215	0.5336	27.96	1.1245	18.13	89.13	2.321E+04	0.1041	0.0208	0.8751	1.017	1451
0.0000	0.0448	0.0000	0.4215	0.5336	27.96	1.1245	18.13	89.13	2.321E+04	0.1040	0.0217	0.8743	1.018	1469
0.0000	0.0448	0.0000	0.4215	0.5336	27.96	1.1245	18.13	89.13	2.321E+04	0.1038	0.0231	0.8731	1.020	1487

Tab. 45: Experimental conditions for the mixture H_2 90% − CO 10% − N_2 − Air for varying pilot conditions

$X_{H_2,j}$ [−]	$X_{CH_4,j}$ [−]	$X_{CO,j}$ [−]	$X_{N_2,j}$ [−]	$X_{Air,j}$ [−]	MW_j [kg/kmol]	$\rho_{u,j}$ [kg/m³]	$\mu_{u,j}$ [μPa·s]	u_j [m/s]	Re_j [−]	$X_{H_2,p}$ [−]	$X_{CH_4,p}$ [−]	$X_{Air,p}$ [−]	u_p [m/s]	T_p [K]
0.1423	0.0000	0.0158	0.3715	0.4704	24.74	1.0037	18.31	94.75	2.182E+04	0.1063	0.0000	0.8937	0.9961	1049
0.1423	0.0000	0.0158	0.3715	0.4704	24.74	1.0037	18.31	94.75	2.182E+04	0.1062	0.0007	0.8931	0.9968	1072
0.1423	0.0000	0.0158	0.3715	0.4704	24.74	1.0037	18.31	94.75	2.182E+04	0.1061	0.0014	0.8924	0.9975	1086

Tab. 46: Experimental conditions for the mixture H_2 80% − CO 20% − N_2 − Air for varying pilot conditions

$\chi_{H_2,j}$ [−]	$\chi_{CH_4,j}$ [−]	$\chi_{CO,j}$ [−]	$\chi_{N_2,j}$ [−]	$\chi_{Air,j}$ [−]	MW_j [kg/kmol]	$\rho_{u,j}$ [kg/m³]	$\mu_{u,j}$ [μPa·s]	u_j [m/s]	Re_j [−]	$\chi_{H_2,p}$ [−]	$\chi_{CH_4,p}$ [−]	$\chi_{Air,p}$ [−]	u_p [m/s]	T_p [K]
0.1265	0.0000	0.0316	0.3715	0.4704	25.15	1.0204	18.31	93.97	2.199E+04	0.1037	0.0000	0.8963	0.9932	1052
0.1265	0.0000	0.0316	0.3715	0.4704	25.15	1.0204	18.31	93.97	2.199E+04	0.1054	0.0000	0.8946	0.9951	1066
0.1265	0.0000	0.0316	0.3715	0.4704	25.15	1.0204	18.31	93.97	2.199E+04	0.1062	0.0007	0.8931	0.9968	1082
0.1265	0.0000	0.0316	0.3715	0.4704	25.15	1.0204	18.31	93.97	2.199E+04	0.1060	0.0022	0.8918	0.9982	1109
0.1265	0.0000	0.0316	0.3715	0.4704	25.15	1.0204	18.31	93.97	2.199E+04	0.1059	0.0031	0.8909	0.9992	1124

Tab. 47: Experimental conditions for the mixture H_2 70% − CO 30% − N_2 − Air for varying pilot conditions

$X_{H_2,j}$ [−]	$X_{CH_4,j}$ [−]	$X_{CO,j}$ [−]	$X_{N_2,j}$ [−]	$X_{Air,j}$ [−]	MW_j [kg/kmol]	$\rho_{u,j}$ [kg/m³]	$\mu_{u,j}$ [μPa·s]	u_j [m/s]	Re_j [−]	$X_{H_2,p}$ [−]	$X_{CH_4,p}$ [−]	$X_{Air,p}$ [−]	u_p [m/s]	T_p [K]
0.1107	0.0000	0.0474	0.3715	0.4704	25.56	1.0370	18.31	93.21	2.217E+04	0.1037	0.0000	0.8963	0.9932	1052
0.1107	0.0000	0.0474	0.3715	0.4704	25.56	1.0370	18.31	93.21	2.217E+04	0.1063	0.0000	0.8937	0.9961	1069
0.1107	0.0000	0.0474	0.3715	0.4704	25.56	1.0370	18.31	93.21	2.217E+04	0.1062	0.0010	0.8929	0.9970	1090
0.1107	0.0000	0.0474	0.3715	0.4704	25.56	1.0370	18.31	93.21	2.217E+04	0.1060	0.0022	0.8918	0.9982	1112
0.1107	0.0000	0.0474	0.3715	0.4704	25.56	1.0370	18.31	93.21	2.217E+04	0.1059	0.0031	0.8909	0.9992	1130
0.1107	0.0000	0.0474	0.3715	0.4704	25.56	1.0370	18.31	93.21	2.217E+04	0.1058	0.0041	0.8901	1.000	1151

Tab. 48: Experimental conditions for the mixture $H_2\ 60\% - CO\ 40\% - N_2 - Air$ for varying pilot conditions

$\chi_{H_2,j}$ [-]	$\chi_{CH_4,j}$ [-]	$\chi_{CO,j}$ [-]	$\chi_{N_2,j}$ [-]	$\chi_{Air,j}$ [-]	MW_j [kg/kmol]	$\rho_{u,j}$ [kg/m³]	$\mu_{u,j}$ [μPa·s]	u_j [m/s]	Re_j [-]	$\chi_{H_2,p}$ [-]	$\chi_{CH_4,p}$ [-]	$\chi_{Air,p}$ [-]	u_p [m/s]	T_p [K]
0.0949	0.0000	0.0632	0.3715	0.4704	25.97	1.0537	18.31	92.47	2.235E+04	0.1028	0.0000	0.8972	0.9922	1053
0.0949	0.0000	0.0632	0.3715	0.4704	25.97	1.0537	18.31	92.47	2.235E+04	0.1063	0.0000	0.8937	0.9961	1071
0.0949	0.0000	0.0632	0.3715	0.4704	25.97	1.0537	18.31	92.47	2.235E+04	0.1062	0.0010	0.8929	0.9970	1091
0.0949	0.0000	0.0632	0.3715	0.4704	25.97	1.0537	18.31	92.47	2.235E+04	0.1059	0.0031	0.8909	0.9992	1108
0.0949	0.0000	0.0632	0.3715	0.4704	25.97	1.0537	18.31	92.47	2.235E+04	0.1058	0.0041	0.8901	1.000	1133
0.0949	0.0000	0.0632	0.3715	0.4704	25.97	1.0537	18.31	92.47	2.235E+04	0.1057	0.0050	0.8892	1.001	1148

Tab. 49: Experimental conditions for the mixture $H_2\ 50\% - CO\ 50\% - N_2 - Air$ for varying pilot conditions

$\chi_{H_2,j}$ [-]	$\chi_{CH_4,j}$ [-]	$\chi_{CO,j}$ [-]	$\chi_{N_2,j}$ [-]	$\chi_{Air,j}$ [-]	MW_j [kg/kmol]	$\rho_{u,j}$ [kg/m³]	$\mu_{u,j}$ [μPa·s]	u_j [m/s]	Re_j [-]	$\chi_{H_2,p}$ [-]	$\chi_{CH_4,p}$ [-]	$\chi_{Air,p}$ [-]	u_p [m/s]	T_p [K]
0.0791	0.0000	0.0791	0.3715	0.4704	26.39	1.0704	18.31	91.74	2.253E+04	0.1028	0.0000	0.8972	0.9922	1043
0.0791	0.0000	0.0791	0.3715	0.4704	26.39	1.0704	18.31	91.74	2.253E+04	0.1063	0.0000	0.8937	0.9961	1066
0.0791	0.0000	0.0791	0.3715	0.4704	26.39	1.0704	18.31	91.74	2.253E+04	0.1062	0.0012	0.8926	0.9970	1085
0.0791	0.0000	0.0791	0.3715	0.4704	26.39	1.0704	18.31	91.74	2.253E+04	0.1060	0.0029	0.8911	0.9992	1119
0.0791	0.0000	0.0791	0.3715	0.4704	26.39	1.0704	18.31	91.74	2.253E+04	0.1059	0.0038	0.8903	1.000	1135
0.0791	0.0000	0.0791	0.3715	0.4704	26.39	1.0704	18.31	91.74	2.253E+04	0.1058	0.0048	0.8894	1.001	1159

Tab. 50: Experimental conditions for the mixture H_2 40% $- CO$ 60% $- N_2 - Air$ for varying pilot conditions

$\chi_{H_2,j}$ [-]	$\chi_{CH_4,j}$ [-]	$\chi_{CO,j}$ [-]	$\chi_{N_2,j}$ [-]	$\chi_{Air,j}$ [-]	MW_j [kg/kmol]	$\rho_{u,j}$ [kg/m³]	$\mu_{u,j}$ [μPa·s]	u_j [m/s]	Re_j [-]	$\chi_{H_2,p}$ [-]	$\chi_{CH_4,p}$ [-]	$\chi_{Air,p}$ [-]	u_p [m/s]	T_p [K]
0.0632	0.0000	0.0949	0.3715	0.4704	26.80	1.0872	18.31	91.04	2.271E+04	0.1028	0.0000	0.8972	0.9922	1050
0.0632	0.0000	0.0949	0.3715	0.4704	26.80	1.0872	18.31	91.04	2.271E+04	0.1063	0.0000	0.8937	0.9961	1068
0.0632	0.0000	0.0949	0.3715	0.4704	26.80	1.0872	18.31	91.04	2.271E+04	0.1062	0.0010	0.8929	0.9970	1087
0.0632	0.0000	0.0949	0.3715	0.4704	26.80	1.0872	18.31	91.04	2.271E+04	0.1060	0.0022	0.8918	0.9982	1110
0.0632	0.0000	0.0949	0.3715	0.4704	26.80	1.0872	18.31	91.04	2.271E+04	0.1059	0.0034	0.8907	0.9994	1134
0.0632	0.0000	0.0949	0.3715	0.4704	26.80	1.0872	18.31	91.04	2.271E+04	0.1058	0.0046	0.8896	1.001	1157

Tab. 51: Experimental conditions for the mixture $H_2\ 30\% - CO\ 70\% - N_2 - Air$ for varying pilot conditions

$x_{H_2,j}$ [-]	$x_{CH_4,j}$ [-]	$x_{CO,j}$ [-]	$x_{N_2,j}$ [-]	$x_{Air,j}$ [-]	MW_j [kg/kmol]	$\rho_{u,j}$ [kg/m³]	$\mu_{u,j}$ [μPa·s]	u_j [m/s]	Re_j [-]	$x_{H_2,p}$ [-]	$x_{CH_4,p}$ [-]	$x_{Air,p}$ [-]	u_p [m/s]	T_p [K]
0.0474	0.0000	0.1107	0.3715	0.4704	27.21	1.1039	18.31	90.35	2.288E+04	0.1028	0.0000	0.8972	0.9922	1052
0.0474	0.0000	0.1107	0.3715	0.4704	27.21	1.1039	18.31	90.35	2.288E+04	0.1063	0.0000	0.8937	0.9961	1069
0.0474	0.0000	0.1107	0.3715	0.4704	27.21	1.1039	18.31	90.35	2.288E+04	0.1061	0.0019	0.8920	0.9980	1085
0.0474	0.0000	0.1107	0.3715	0.4704	27.21	1.1039	18.31	90.35	2.288E+04	0.1059	0.0034	0.8907	0.9994	1116
0.0474	0.0000	0.1107	0.3715	0.4704	27.21	1.1039	18.31	90.35	2.288E+04	0.1059	0.0038	0.8903	0.9999	1130
0.0474	0.0000	0.1107	0.3715	0.4704	27.21	1.1039	18.31	90.35	2.288E+04	0.1058	0.0048	0.8894	1.001	1149

B Supplementary Figures

B.1 Hydrogen Blends with Methane

<div align="center">(a)   (b)   (c)</div>
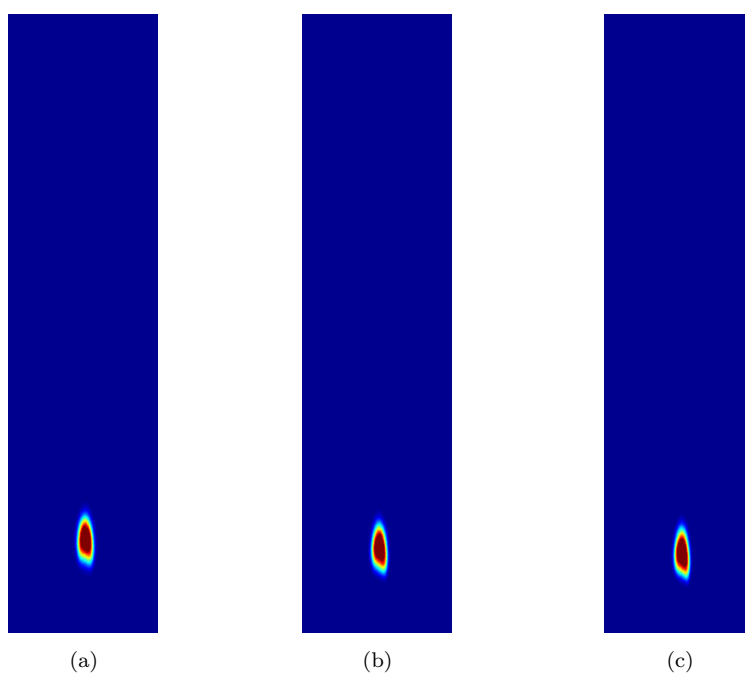
Fig. 26: OH^* Chemiluminescence for H_2 100%: (a) at $T_p \approx 1040\ K$; (b) at $T_p \approx 1070\ K$; (c) at $T_p \approx 1095\ K$;

(a)   (b)   (c)
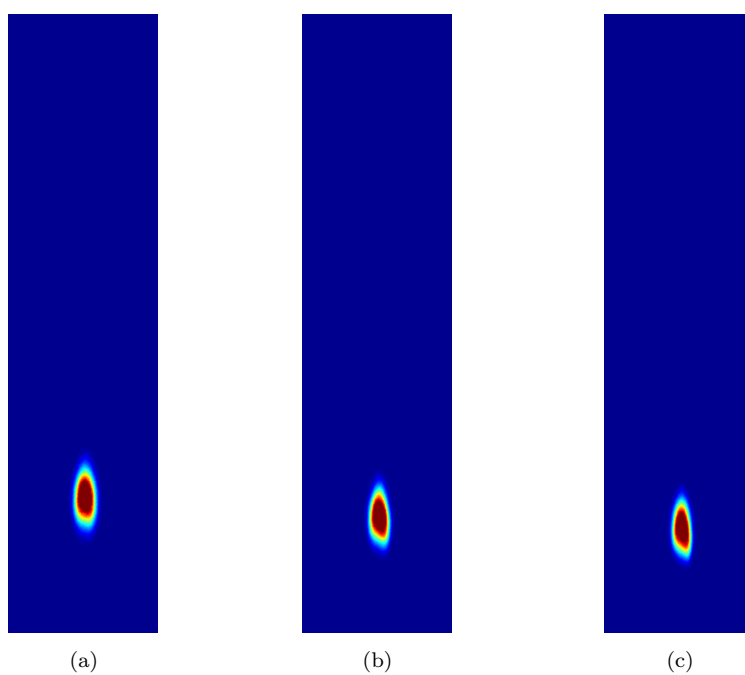
Fig. 27: OH^* Chemiluminescence for H_2 $90\% - CH_4$ 10%: (a) at $T_p \approx 1040\ K$; (b) at $T_p \approx 1070\ K$; (c) at $T_p \approx 1095\ K$;
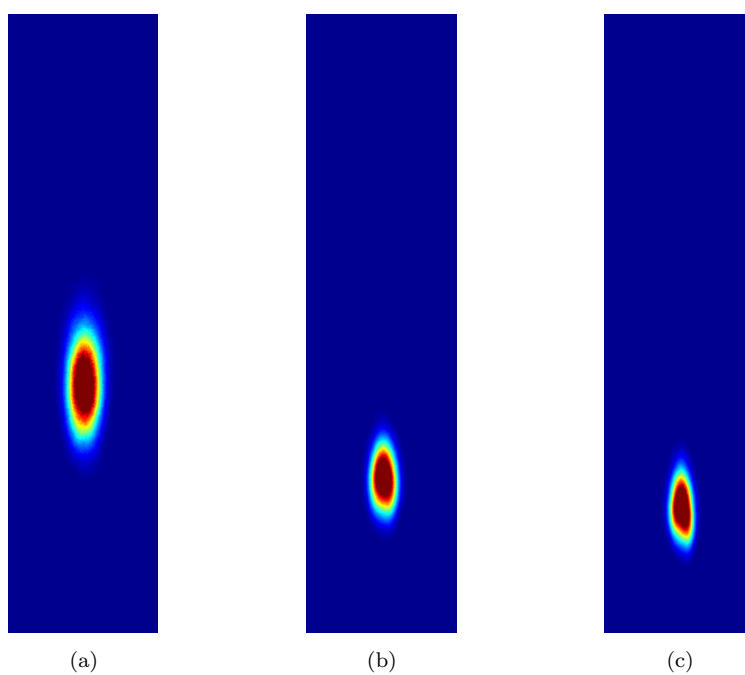
Fig. 28: OH^* Chemiluminescence for H_2 $80\% - CH_4$ 20%: (a) at $T_p \approx 1040\ K$; (b) at $T_p \approx 1100\ K$; (c) at $T_p \approx 1160\ K$;

(a)   (b)   (c)
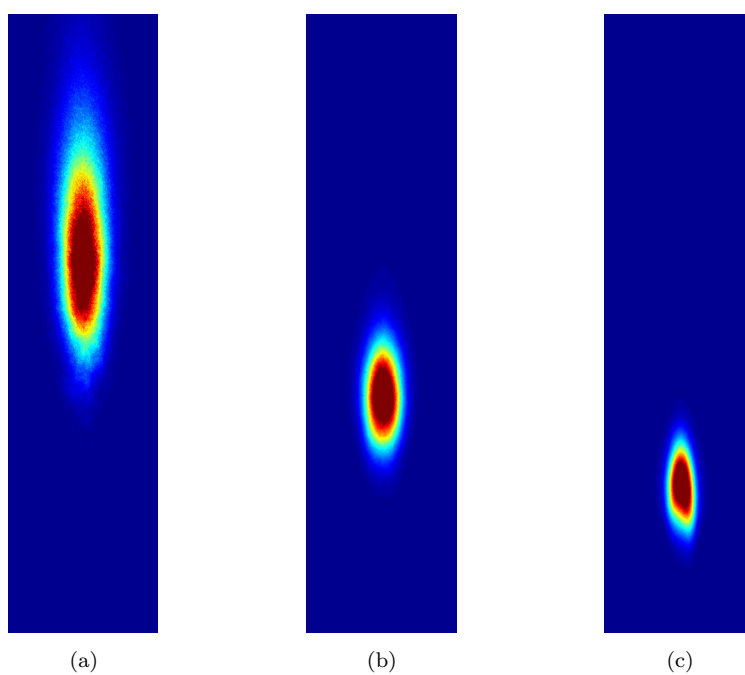
Fig. 29: OH^* Chemiluminescence for $H_2\ 70\% - CH_4\ 30\%$: (a) at $T_p \approx 1070\ K$;
(b) at $T_p \approx 1110\ K$; (c) at $T_p \approx 1190\ K$;

(a)   (b)   (c)
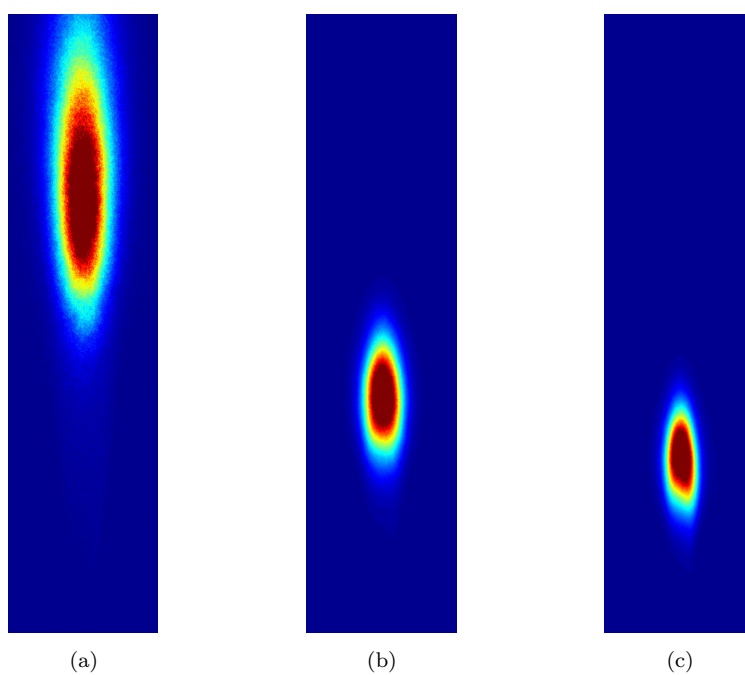
Fig. 30: OH^* Chemiluminescence for $H_2\ 60\% - CH_4\ 40\%$: (a) at $T_p \approx 1140\ K$;
(b) at $T_p \approx 1175\ K$; (c) at $T_p \approx 1230\ K$;

(a)   (b)   (c)
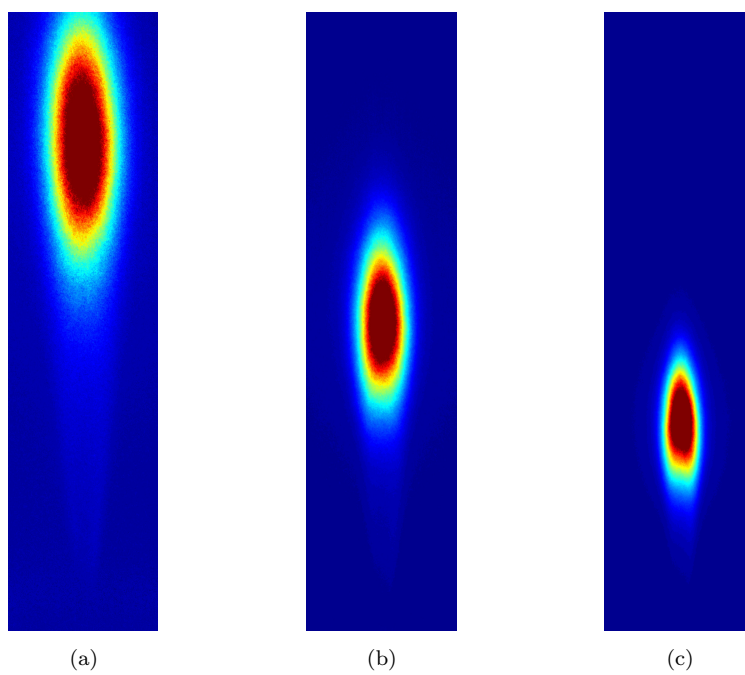
Fig. 31: OH^* Chemiluminescence for H_2 50% $- CH_4$ 50%: (a) at $T_p \approx 1160\ K$;
(b) at $T_p \approx 1200\ K$; (c) at $T_p \approx 1255\ K$;

<div align="center">(a)   (b)   (c)</div>
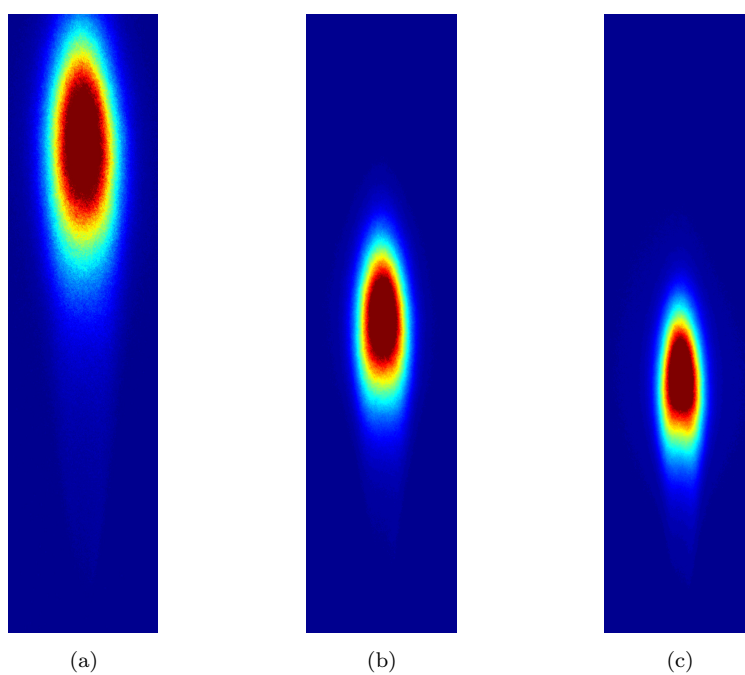
Fig. 32: OH^* Chemiluminescence for H_2 $40\% - CH_4$ 60%: (a) at $T_p \approx 1200\ K$; (b) at $T_p \approx 1240\ K$; (c) at $T_p \approx 1275\ K$;

(a) (b) (c)
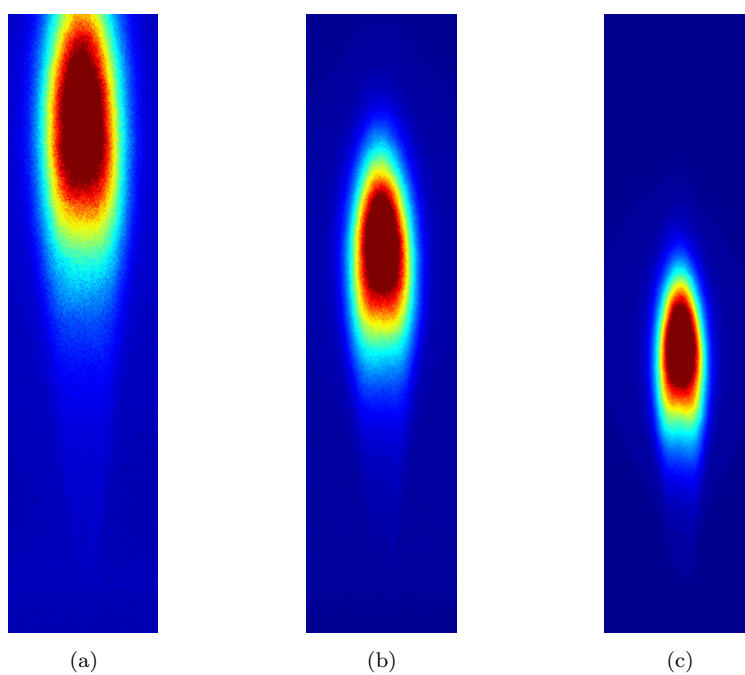
Fig. 33: OH^* Chemiluminescence for H_2 $25\% - CH_4$ 75%: (a) at $T_p \approx 1210\ K$; (b) at $T_p \approx 1275\ K$; (c) at $T_p \approx 1320\ K$;
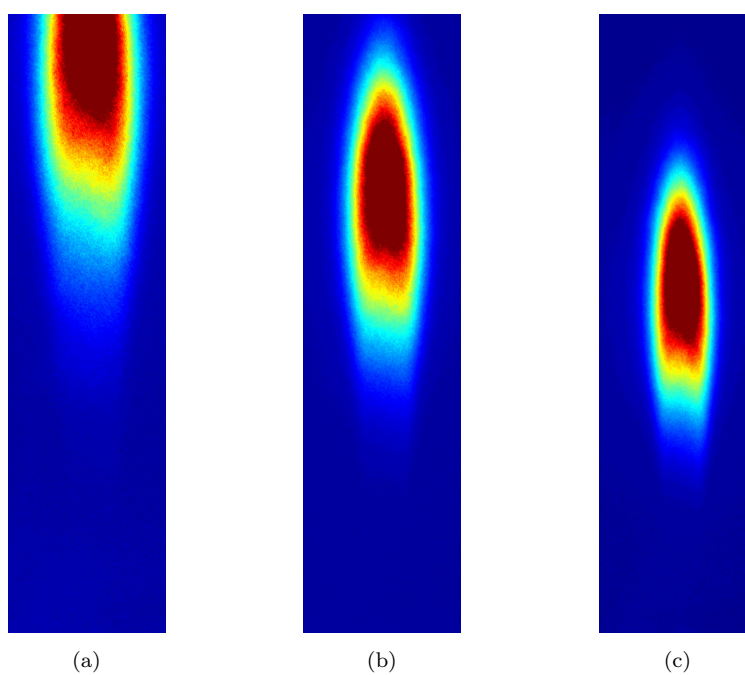
Fig. 34: OH^* Chemiluminescence for H_2 0% $- CH_4$ 100%: (a) at $T_p \approx 1355\ K$; (b) at $T_p \approx 1395\ K$; (c) at $T_p \approx 1425\ K$;

B.2   Hydrogen Blends with Carbon Monoxide

<div align="center">(a)   (b)   (c)</div>
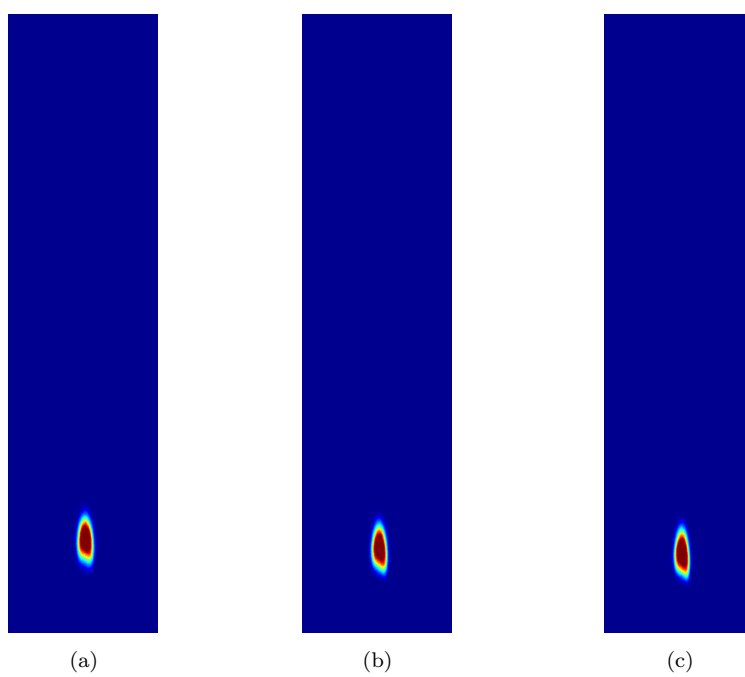
Fig. 35: OH^* Chemiluminescence for H_2 100%: (a) at $T_p \approx 1040\ K$; (b) at $T_p \approx 1070\ K$; (c) at $T_p \approx 1095\ K$;

<center>(a)   (b)   (c)</center>
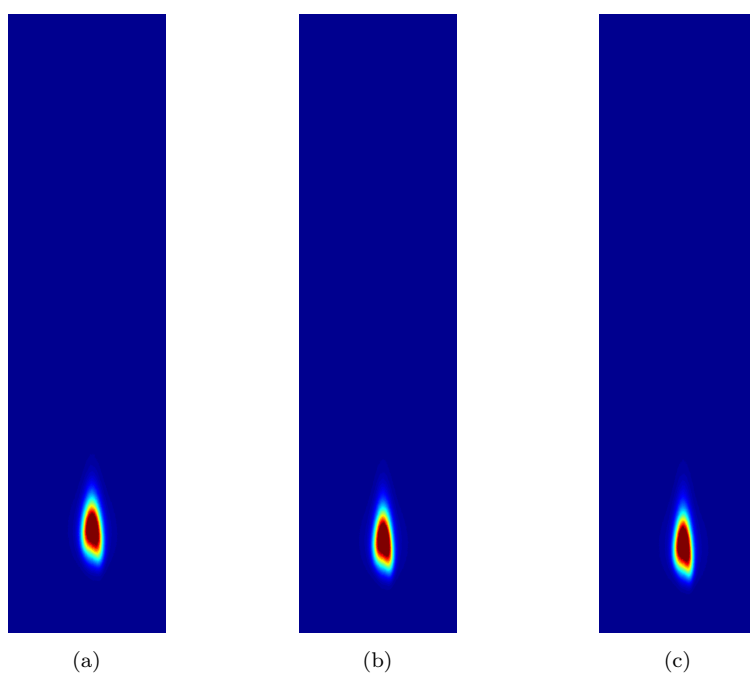
Fig. 36: OH^* Chemiluminescence for H_2 90% $- CO$ 10%: (a) at $T_p \approx 1040$ K; (b) at $T_p \approx 1070$ K; (c) at $T_p \approx 1095$ K;

(a) (b) (c)
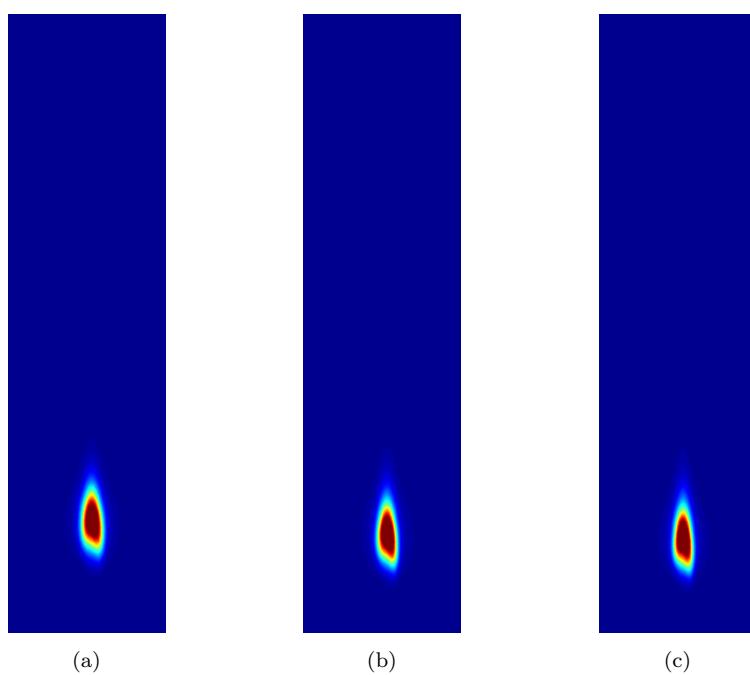
Fig. 37: OH^* Chemiluminescence for H_2 $80\% - CO$ 20%: (a) at $T_p \approx 1040$ K; (b) at $T_p \approx 1075$ K; (c) at $T_p \approx 1095$ K;

(a)   (b)   (c)
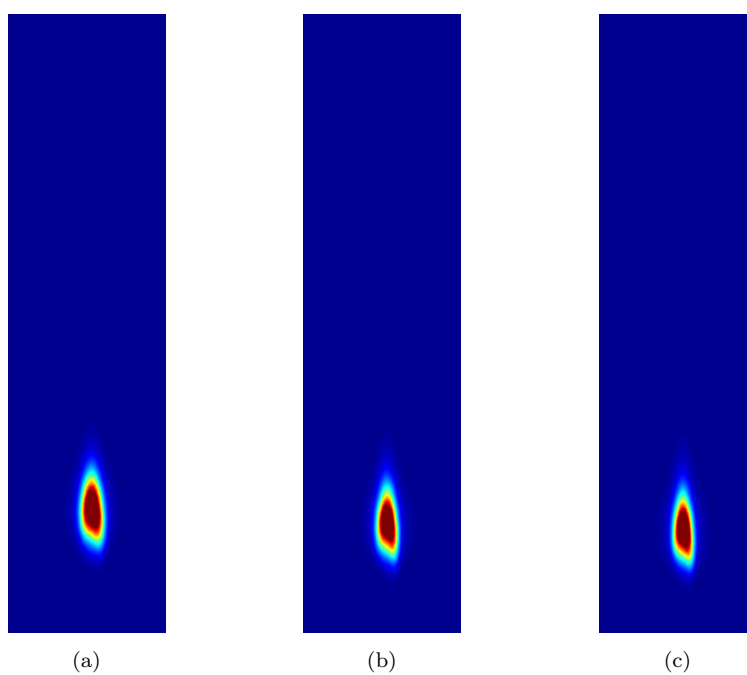
Fig. 38: OH^* Chemiluminescence for H_2 70% $- CO$ 30%: (a) at $T_p \approx 1050\ K$;
(b) at $T_p \approx 1075\ K$; (c) at $T_p \approx 1095\ K$;
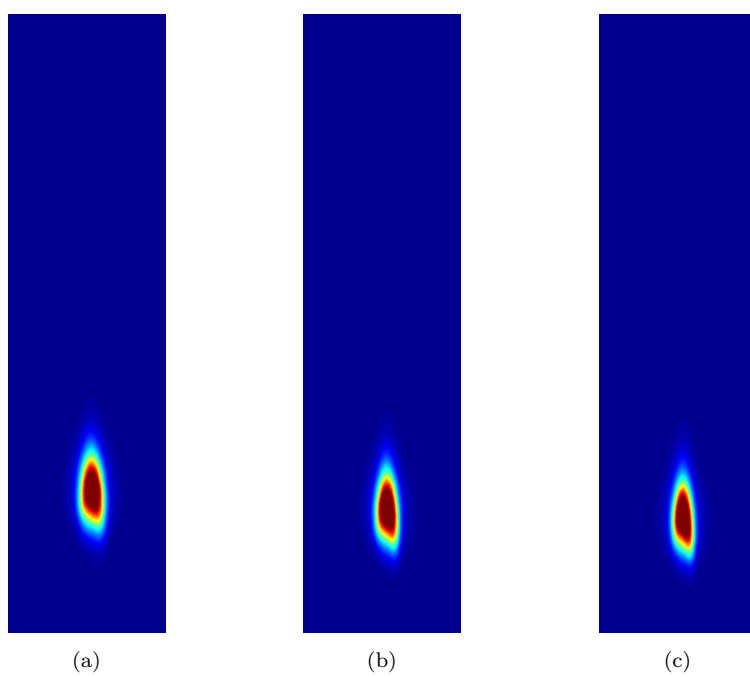
Fig. 39: OH^* Chemiluminescence for H_2 $60\% - CO$ 40%: (a) at $T_p \approx 1050\ K$; (b) at $T_p \approx 1075\ K$; (c) at $T_p \approx 1100\ K$;

(a)   (b)   (c)
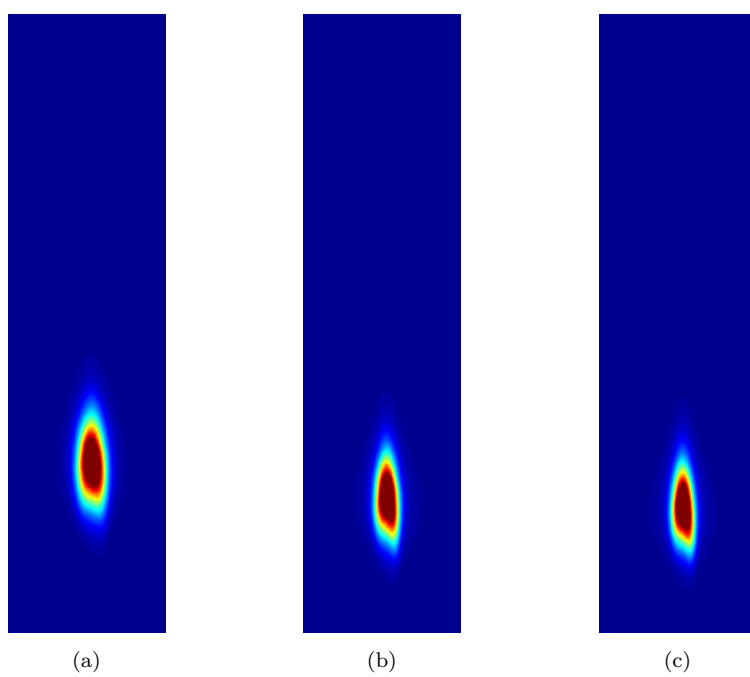
Fig. 40: OH^* Chemiluminescence for H_2 50% $- CO$ 50%: (a) at $T_p \approx 1050\ K$; (b) at $T_p \approx 1095\ K$; (c) at $T_p \approx 1115\ K$;

(a) (b) (c)
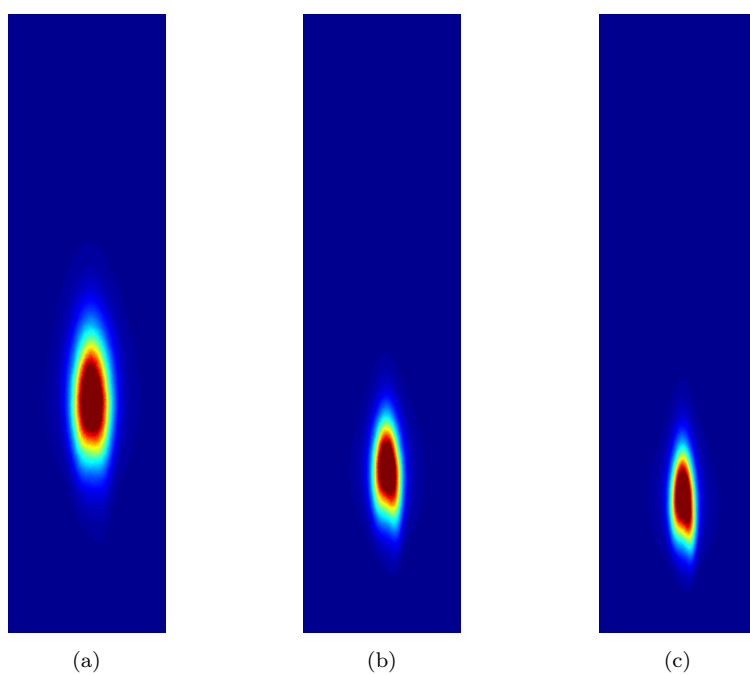
Fig. 41: OH^* Chemiluminescence for H_2 $40\% - CO$ 60%: (a) at $T_p \approx 1045\ K$; (b) at $T_p \approx 1090\ K$; (c) at $T_p \approx 1140\ K$;

(a)   (b)   (c)
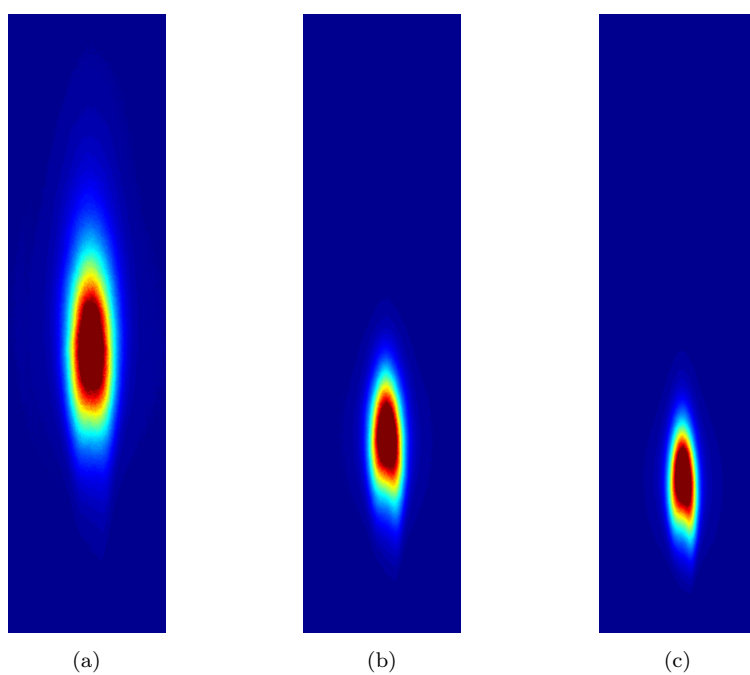
Fig. 42: OH^* Chemiluminescence for H_2 30% $- CO$ 70%: (a) at $T_p \approx 1050\ K$;
(b) at $T_p \approx 1100\ K$; (c) at $T_p \approx 1150\ K$;

B.3   Hydrogen Blends with Methane and Nitrogen Dilution

(a) (b) (c)
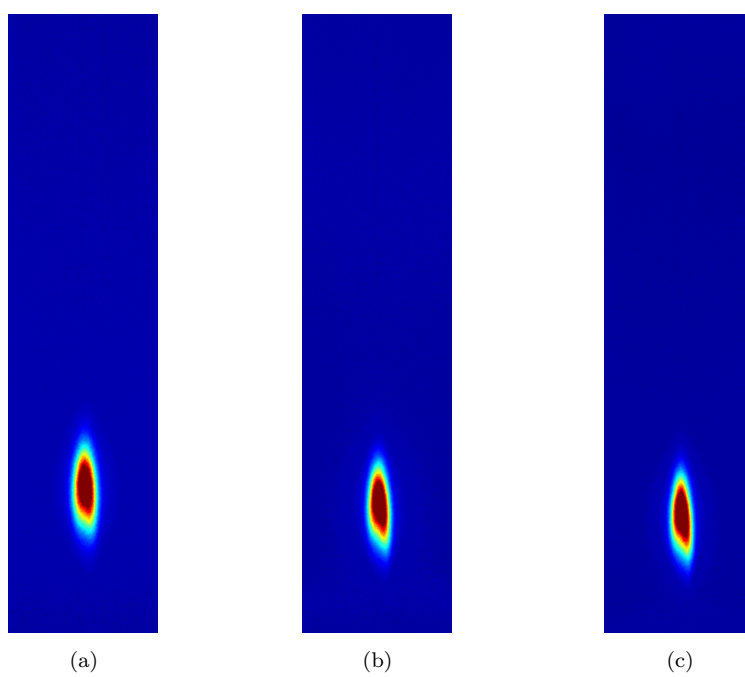
Fig. 43: OH^* Chemiluminescence for H_2 $100\% - N_2$: (a) at $T_p \approx 1040$ K; (b) at $T_p \approx 1070$ K; (c) at $T_p \approx 1090$ K;

(a)   (b)   (c)
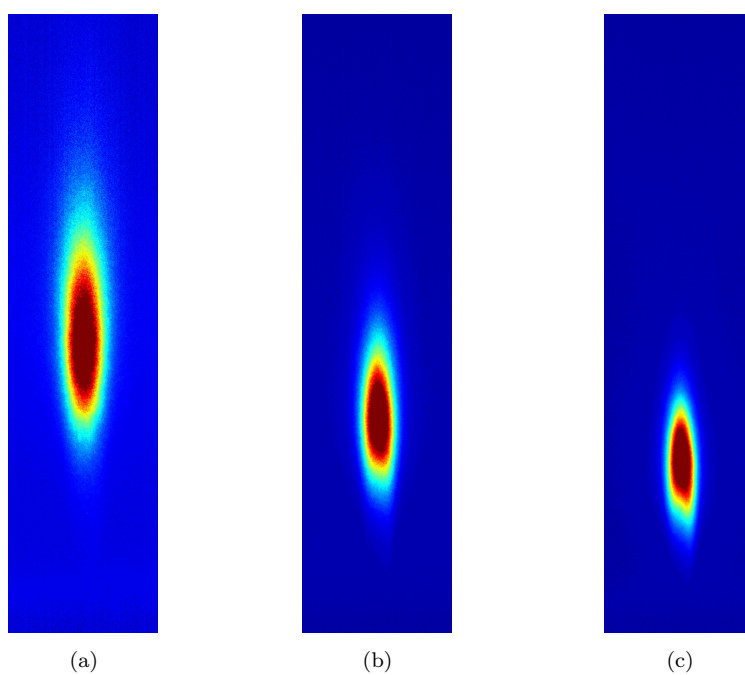
Fig. 44: OH^* Chemiluminescence for H_2 $90\% - CH_4$ $10\% - N_2$: (a) at $T_p \approx$ 1045 K; (b) at $T_p \approx 1075$ K; (c) at $T_p \approx 1125$ K;
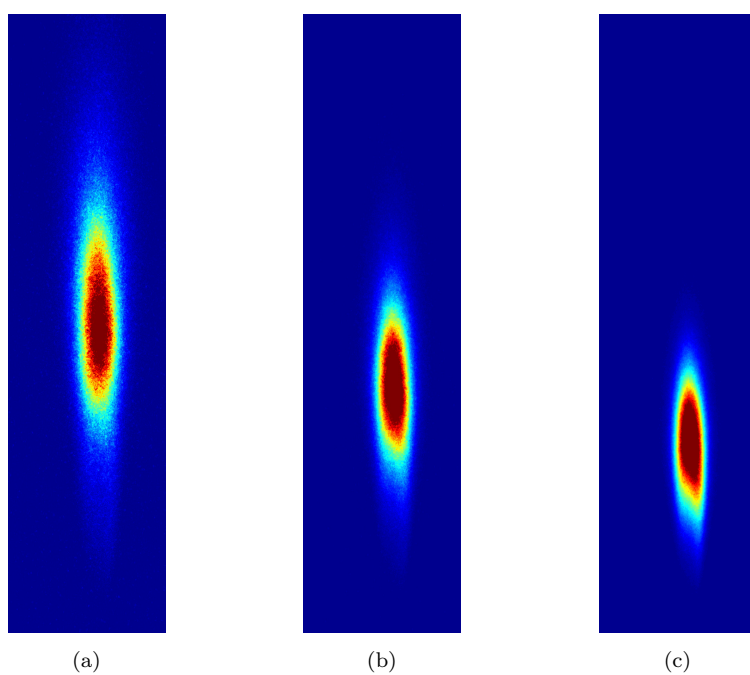
Fig. 45: OH^* Chemiluminescence for H_2 $80\% - CH_4$ $20\% - N_2$: (a) at $T_p \approx$ 1100 K; (b) at $T_p \approx 1140$ K; (c) at $T_p \approx 1185$ K;

(a)   (b)   (c)
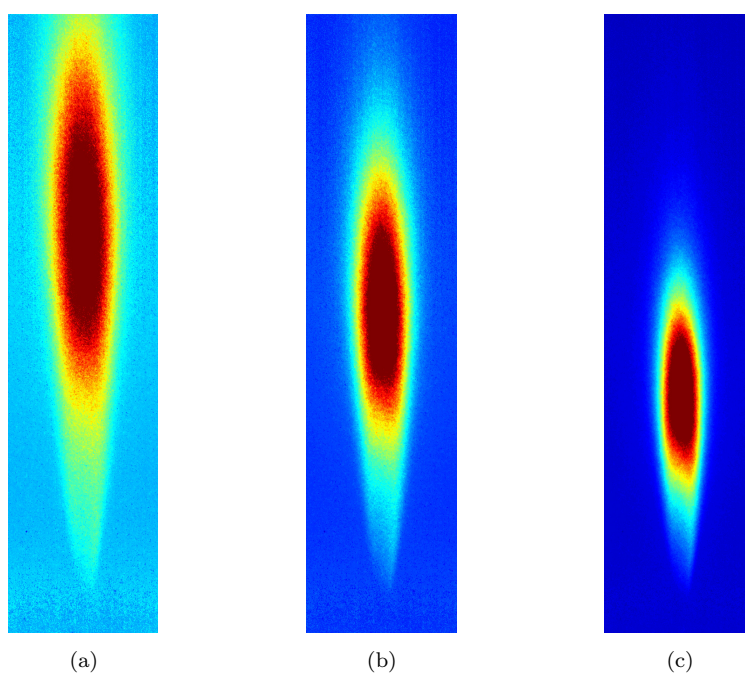
Fig. 46: OH^* Chemiluminescence for H_2 $70\% - CH_4$ $30\% - N_2$: (a) at $T_p \approx$ 1140 K; (b) at $T_p \approx 1160$ K; (c) at $T_p \approx 1210$ K;

(a)   (b)   (c)
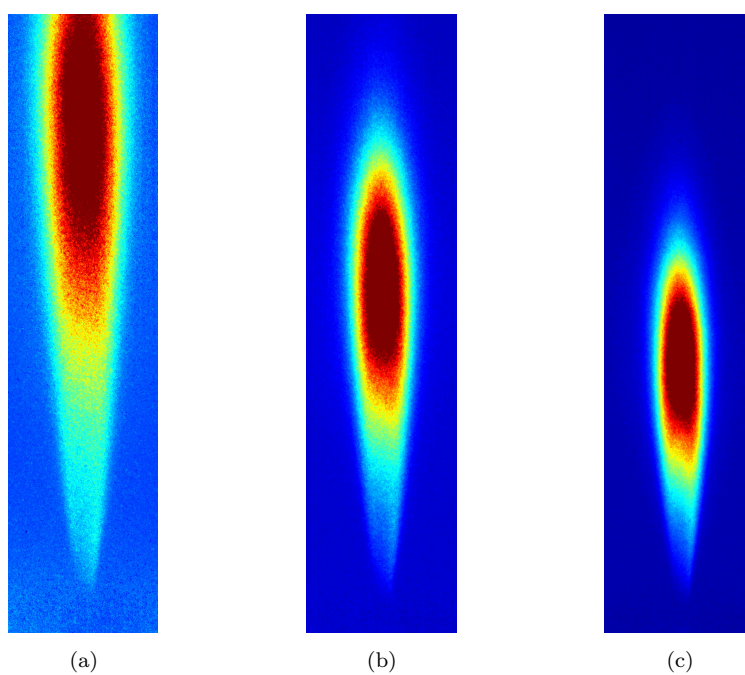
Fig. 47: OH^* Chemiluminescence for H_2 $60\% - CH_4$ $40\% - N_2$: (a) at $T_p \approx$ 1170 K; (b) at $T_p \approx 1210$ K; (c) at $T_p \approx 1250$ K;
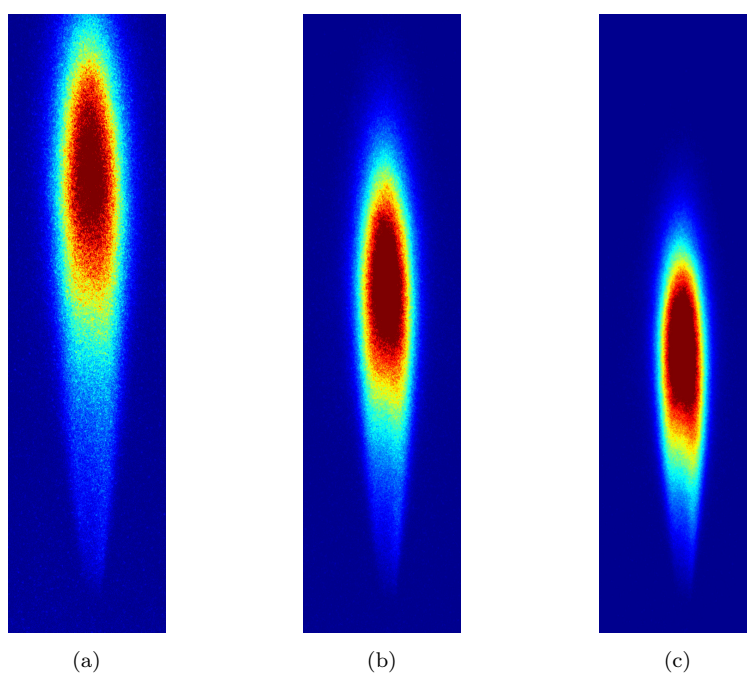
Fig. 48: OH^* Chemiluminescence for H_2 $50\% - CH_4$ $50\% - N_2$: (a) at $T_p \approx$ 1230 K; (b) at $T_p \approx 1270$ K; (c) at $T_p \approx 1310$ K;

<div align="center">(a)   (b)   (c)</div>
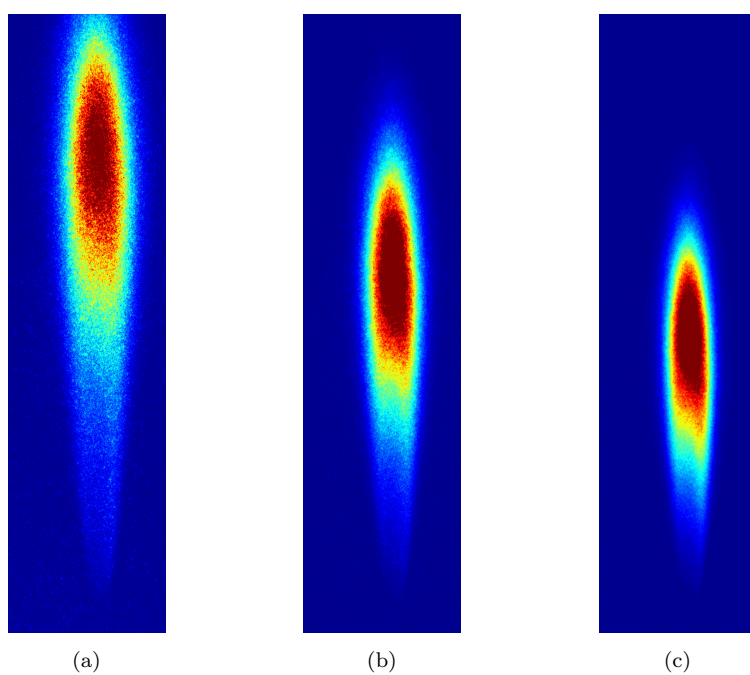
Fig. 49: OH^* Chemiluminescence for H_2 $40\% - CH_4$ $60\% - N_2$: (a) at $T_p \approx$ 1250 K; (b) at $T_p \approx 1290$ K; (c) at $T_p \approx 1330$ K;
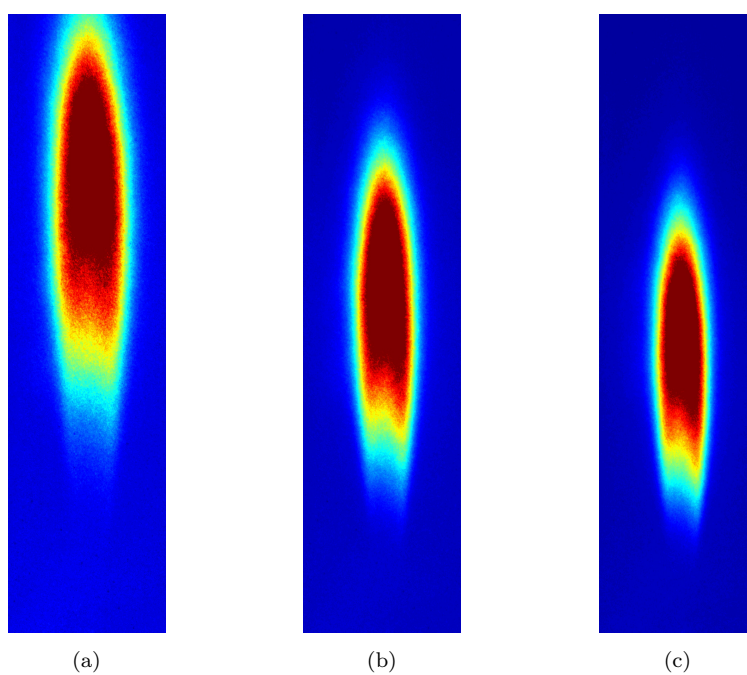
Fig. 50: OH^* Chemiluminescence for H_2 $0\% - CH_4$ $100\% - N_2$: (a) at $T_p \approx$ 1400 K; (b) at $T_p \approx 1450$ K; (c) at $T_p \approx 1485$ K;

B.4 Hydrogen Blends with Carbon Monoxide and Nitrogen Dilution

(a) (b) (c)
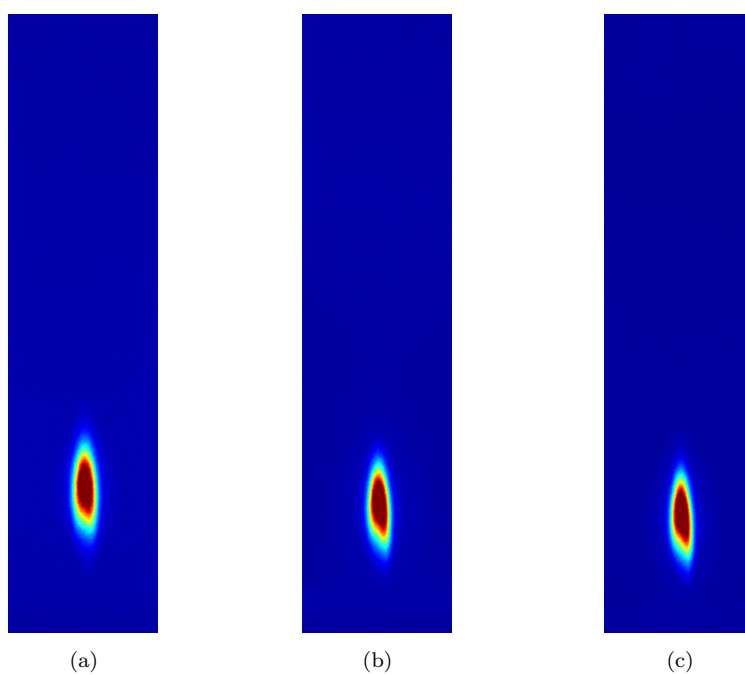
Fig. 51: OH^* Chemiluminescence for H_2 100%: (a) at $T_p \approx 1040\ K$; (b) at $T_p \approx 1070\ K$; (c) at $T_p \approx 1090\ K$;

(a)　　　　　　　　(b)　　　　　　　　(c)
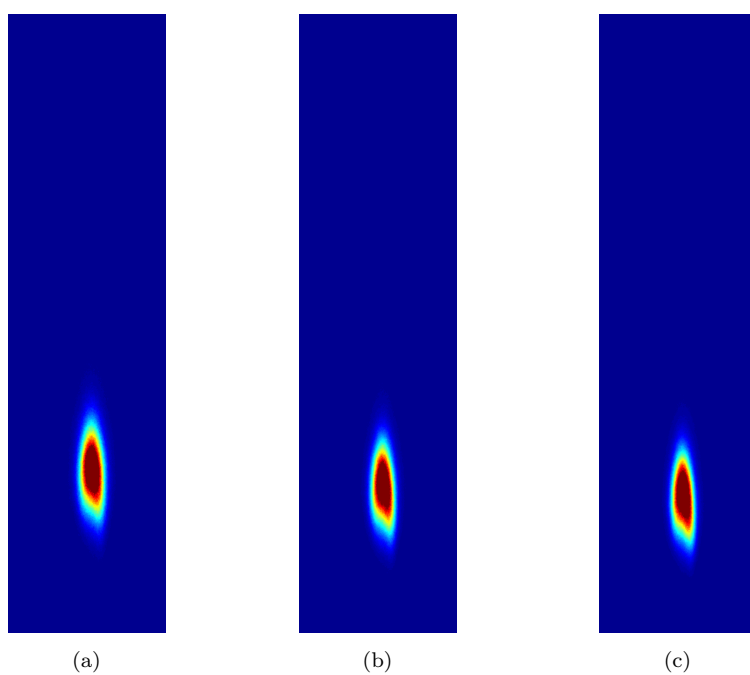
Fig. 52: OH^* Chemiluminescence for H_2 90% $- CO$ 10%: (a) at $T_p \approx 1050\ K$;
(b) at $T_p \approx 1070\ K$; (c) at $T_p \approx 1085\ K$;

(a)   (b)   (c)
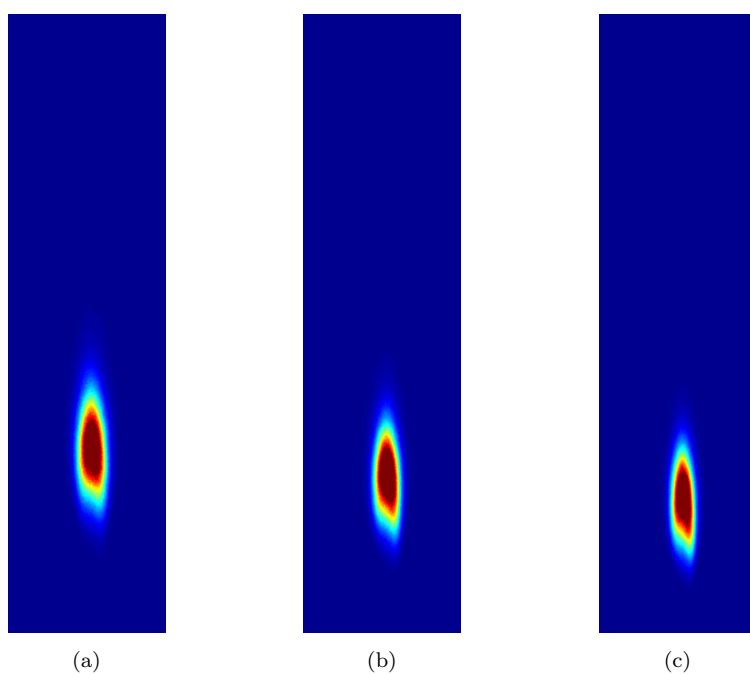
Fig. 53: OH^* Chemiluminescence for H_2 $80\% - CO$ 20%: (a) at $T_p \approx 1050\ K$;
(b) at $T_p \approx 1080\ K$; (c) at $T_p \approx 1125\ K$;
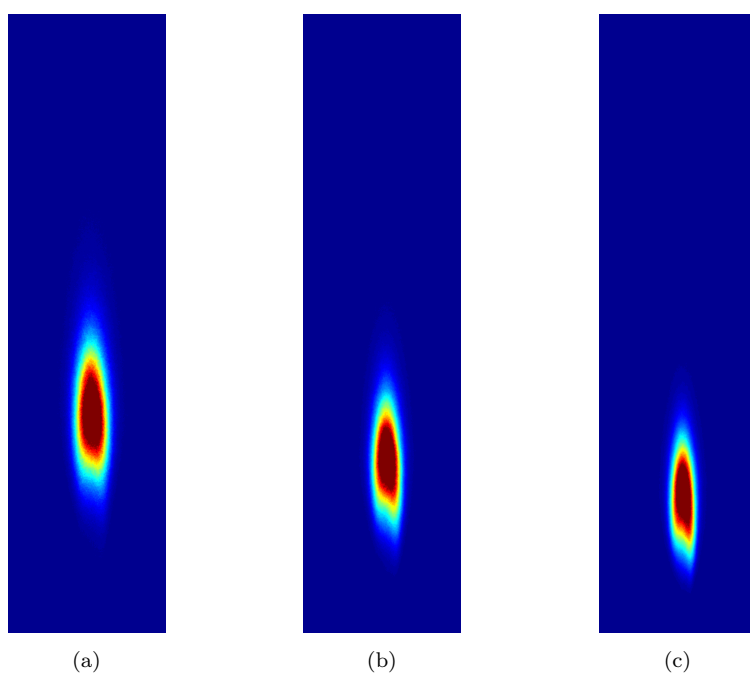
Fig. 54: OH^* Chemiluminescence for H_2 $70\% - CO$ 30%: (a) at $T_p \approx 1050\ K$;
(b) at $T_p \approx 1090\ K$; (c) at $T_p \approx 1150\ K$;

<div align="center">(a)   (b)   (c)</div>
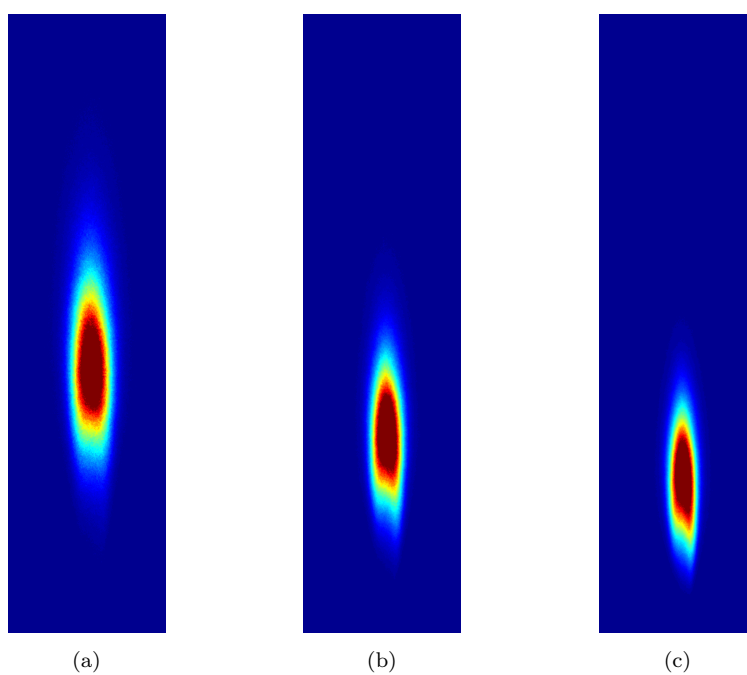
Fig. 55: OH^* Chemiluminescence for H_2 $60\% - CO$ 40%: (a) at $T_p \approx 1050$ K; (b) at $T_p \approx 1090$ K; (c) at $T_p \approx 1150$ K;

(a) (b) (c)
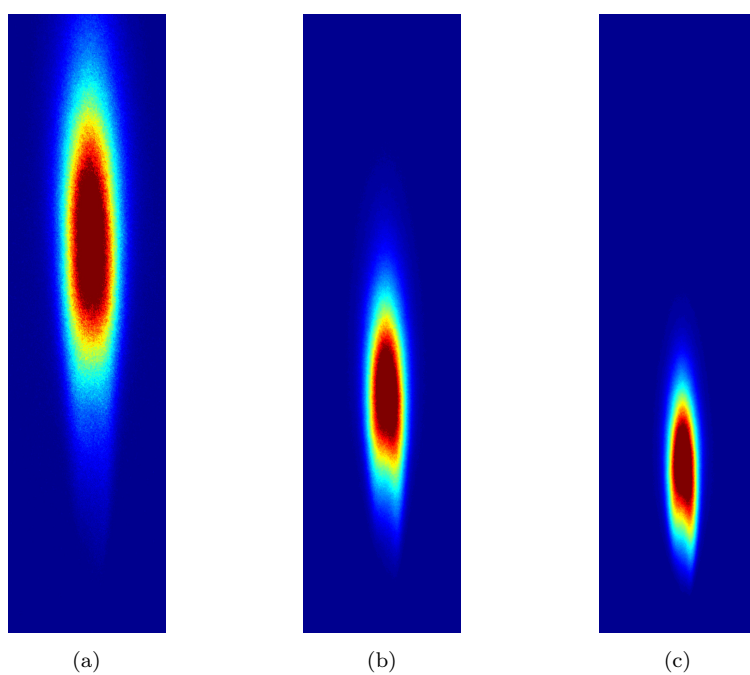
Fig. 56: OH^* Chemiluminescence for H_2 $50\% - CO$ 50%: (a) at $T_p \approx 1045\ K$;
(b) at $T_p \approx 1085\ K$; (c) at $T_p \approx 1160\ K$;

(a)   (b)   (c)
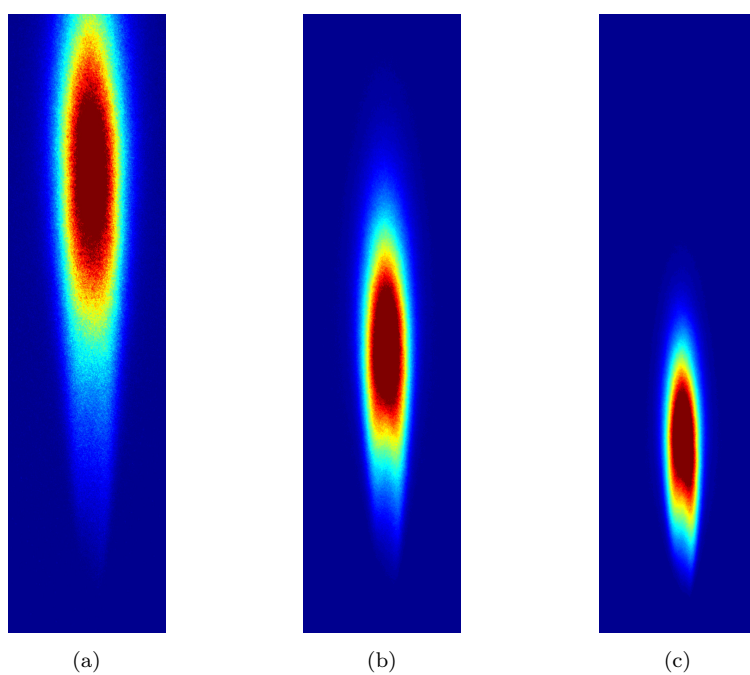
Fig. 57: OH^* Chemiluminescence for H_2 $40\% - CO$ 60%: (a) at $T_p \approx 1050\ K$;
(b) at $T_p \approx 1085\ K$; (c) at $T_p \approx 1155\ K$;
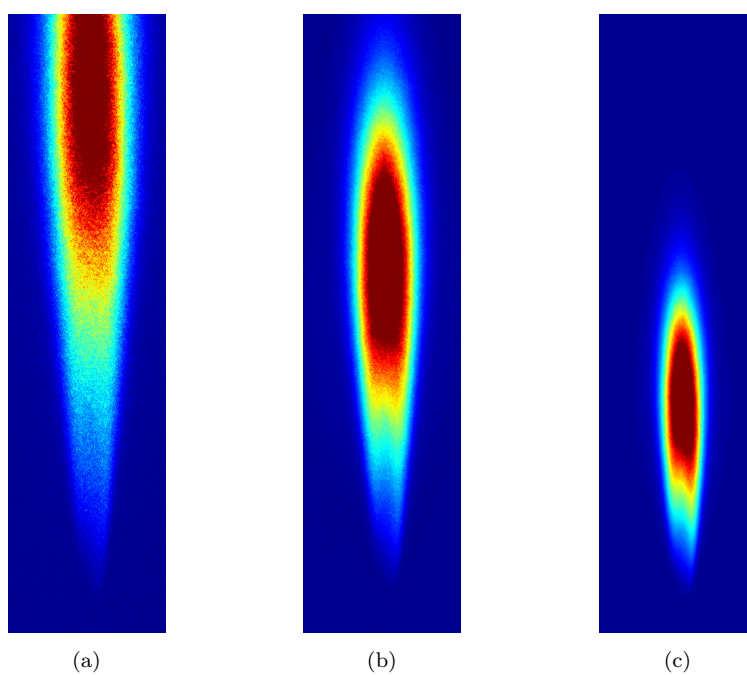
Fig. 58: OH^* Chemiluminescence for H_2 $30\% - CO$ 70%: (a) at $T_p \approx 1050$ K; (b) at $T_p \approx 1085$ K; (c) at $T_p \approx 1150$ K;

References

[1] H. Michels, R.P. Lindstedt, K. Moodie, R. Santon, B.C.R. Ewan, S. Hawksworth and R. Gibson, Literature review of CCGT/CCGE/CHP systems operating on high hydrogen content gases ETI Project no. PE02162, Report 1, February 2012.

[2] R. Cabra, T. Myhrvold, J.Y. Chen, R.W. Dibble, A.N. Karpetis, and R.S. Barlow, Simultaneous laser Raman–Rayleigh–LIF measurements and numerical modeling results of a lifted turbulent H_2/N_2 jet flame in a vitiated coflow, Proc. Combust. Inst. 29 (2002), pp. 1881–1888.

[3] R. Cabra, Turbulent jet flames in a vitiated coflow, Tech. Rep. CR-2004-212887, NASA, 2000.

[4] R. Cabra, J.Y. Chen, R.W. Dibble, A.N. Karpetis, and R.S. Barlow, Lifted methaneair jet flames in a vitiated coflow, Combust. Flame 143 (2005), pp. 491–506.

[5] R. Cabra and R.W. Dibble, 2002; available online at http://www.me.berkeley.edu/cal/VCB.

[6] A.R. Masri and R.W. Bilger, 2003; available online at http://www.aeromech.usyd.edu.au/thermofluids.

[7] K. Gkagkas and R.P. Lindstedt, Transported PDF modelling with detailed chemistry of pre– and auto–ignition in CH_4/air mixtures, Proc. Combust. Inst. 31 (2007), pp. 1559–1566.

[8] K. Gkagkas and R.P. Lindstedt, The impact of reduced chemistry on auto-ignition of H_2 in turbulent flows, Combust. Theory. Model. 13, (2002), pp. 606-643.

[9] A.R. Masri, R.R. Cao, S.B. Pope, and G.M. Goldin, Pdf calculations of turbulent lifted flames of H_2/N_2 fuel issuing into a vitiated co-flow, Combust. Theory Model. 8 (2004), pp. 1–22.

[10] Q. Tang, J. Xu, and S.B. Pope, Probability density function calculations of local extinction and NO production in piloted–jet turbulent methane/air flames, Proc. Combust. Inst. 28 (2000), pp. 133–139.

[11] R.P. Lindstedt, S.A. Louloudi, and E.M. Vaos, Joint scalar probability density function modeling of pollutant formation in piloted turbulent jet diffusion flames with comprehensive chemistry, Proc. Combust. Inst. 28 (2000), pp. 149–156.

[12] R.P. Lindstedt and S.A. Louloudi, Joint scalar transported probability density function modeling of turbulent methanol jet diffusion flames, Proc. Combust. Inst. 29 (2002), pp. 2147–2154.

[13] H. Wang and S.B. Pope, Comparisons of detailed reaction mechanisms in non-premixed combustion, 5th US Combustion Meeting Paper 55 (2007).

[14] TRIDELTA GmbH; available online at http://www.tridelta.de/tridelta-gruppe-unternehmensgruppe-en.html.

[15] Omega Engineering Inc., 2012; available online at http://www.omega.com/.

[16] LaVision GmbH, 2012; available online at http://www.lavision.de/en/.

[17] National Instruments Corporation; available online at http://www.ni.com/3/.

[18] Bronkhorst High-Tech B.V.; available online at http://www.bronkhorst.com/.

[19] R.K. Cheng and A.K. Oppenheim, auto-ignition in methane/hydrogen mixtures, Combustion and Flame, Volume 58, Issue 2, (1984), pp. 125–139, ISSN 0010-2180, 10.1016/0010-2180(84)90088-9.

[20] S. Gersen, N.B. Anikin, A.V. Mokhov, and H.B. Levinsky, auto-ignition of Methane/Hydrogen Mixtures in a Rapid Compression Machine. International Journal of Hydrogen Energy, Vol. 33, (2007), pp. 1957–1964. Mediaterranian Agronomic Institute of Chania.

[21] M. Ilbas, A.P. Crayford, I. Yilmaz, P.J. Bowen, N. Syred, Laminar-burning velocities of hydrogenair and hydrogenmethaneair mixtures: An experimental study, International Journal of Hydrogen Energy, Volume 31, Issue 12, (2006), pp. 1768–1779, ISSN 0360-3199, 10.1016/j.ijhydene.2005.12.007.

[22] T.G. Scholte, P.B. Vaags, Burning velocities of mixtures of hydrogen, carbon monoxide and methane with air, Combustion and Flame, Volume 3, (1959), pp. 511–524.

[23] V.D. Sarli, A.D. Benedetto, Laminar burning velocity of hydrogenmethane/air premixed flames, International Journal of Hydrogen Energy, Volume 32, Issue 5, (2007), pp. 637–646, ISSN 0360-3199, 10.1016/j.ijhydene.2006.05.016.

[24] C.J.Sung and C.K. Law, Fundamental Combustion Properties of H2/CO Mixtures: Ignition and Flame Propagation at Elevated Pressures, Combustion Science and Technology, 180:6, (2008), pp. 1097–1116

[25] T. Lieuwen, V. McDonell, E. Petersen and D. Santavicca, Fuel Flexibility Influences on Premixed Combustor Blowout, Flashback, auto-ignition, and Stability. Journal of Engineering for Gas Turbines and Power, 130, (2008), p. 011506.

[26] C.G. Fotache, Y. Tan, C.J. Sung, and C.K. Law, Ignition of CO=H2=N2 versus heated air in counterflow: Experimental and modeling results., Combust. Flame, 120, (2000), pp. 417-426.

[27] L.J. Spadaccini, M.B. Colket, Ignition delay characteristics of methane fuels, Progress in Energy and Combustion Science, Volume 20, Issue 5, (1994), pp. 431–460, ISSN 0360-1285, 10.1016/0360-1285(94)90011-6.

[28] E. Mastorakos, T.A. Baritaud, and T.J. Poinsot, Numerical simulations of auto-ignition in turbulent mixing flows, Combust. Flame 109 (1997), pp. 198–223.

[29] R.R. Cao and S.B. Pope, The influence of chemical mechanisms on PDF calculations of nonpremixed piloted jet flames, Combust. Flame 143 (2005), pp. 450–470.

[30] R. Hilbert and D. Thevenin, auto-ignition of turbulent non-premixed flames investigated using direct numerical simulations, Combust. Flame 128 (2002), pp. 22–37.

[31] J. Janicka, W. Kolbe, and W.J. Kollmann, Closure of the transport equation for the probability density function of turbulent scalar fields, J. Non-Equil. Thermod. 4 (1979), pp. 47–66.

[32] R.R. Cao, S.B. Pope, and A.R. Masri, Turbulent lifted flames in a vitiated coflow investigated using joint PDF calculations, Combust. Flame 142 (2005), pp. 438–453.

[33] J. Li, Z. Zhao, A. Kazakov, and F.L. Dryer, An updated comprehensive kinetic model of hydrogen combustion, Int. J. Chem. Kinet. 36 (2004), pp. 566–575.

[34] H. Sun, S.I. Yang, G. Jomaas, and C.K. Law, High-pressure laminar flame speeds and kinetic modeling of carbon monoxide/hydrogen combustion, Proc. Combust. Inst. 31 (2007), pp. 439–446.

[35] R.P. Lindstedt and E.M. Vaos, Transported PDF modeling of high-Reynolds-number premixed turbulent flames, Combust. Flame 145 (2006), pp. 495–511.

[36] R.P. Lindstedt, H.-C. Ozarovsky, R.S. Barlow, S.A. Louloudi, and A.N. Karpetis, Progression of localized extinction in high Reynolds number turbulent jet flames, Proc. Combust. Inst. 31 (2007), pp. 1551–1558.

[37] E.R. Hawkes, R. Sankarana, J.C. Sutherland, and J.H. Chen, Scalar mixing in direct numerical simulations of temporally evolving plane jet flames with skeletal CO/H_2 kinetics, Proc. Combust. Inst. 31 (2007), pp. 16331640.

[38] Z. Wu, S.H. Starner, and R.W. Bilger, Lift–off heights of turbulent H_2/N_2 jet flames in a vitiated coflow, In: Honnery, D.R. (Ed.), Proceedings of the 2003 Australian Symposium on Combustion and the Eight Australian Flame Days (2003).

[39] R.L. Gordon, S.H. Starner, A.R. Masri, and R.W. Bilger, Further characterisation of lifted hydrogen and methane flames issuing into a vitiated coflow, Proc. 5th Asia-Pacific Conf. Combust., University of Adelaide (2005), pp. 333–336.

[40] R.P. Lindstedt and S.A. Louloudi, Joint-scalar transported PDF modeling of soot formation and oxidation, Proc. Combust. Inst. 30 (2005), pp. 775–783.

[41] R.P. Lindstedt and H.C. Ozarovsky, Joint scalar transported PDF modeling of non-piloted turbulent diffusion flames, Combust. Flame 143 (2005), pp. 471–490.

[42] C.G. Speziale, S. Sarkar, and T.B. Gatski, Modelling the pressurestrain correlation of turbulence: an invariant dynamical systems approach, J. Fluid Mech. 227 (1991), pp. 245–272.

[43] S.B. Pope, PDF Methods for turbulent reacting flows, Prog. Energy Combust. Sci. 11 (1985), pp. 119–192.

[44] D.L. Baulch et al., Evaluated kinetic data for combustion modeling: Supplement II, J. Phys. Chem. Ref. Data 34 (2005), pp. 757–1555.

[45] N. Peters, Numerical Simulation of Combustion Phenomena, Springer-Verlag, Berlin, 1985.

[46] N.K. Aluri, S.P.R. Muppala, and F. Dinkelacker, A numerical study promoting algebraic models for the Lewis number effect in atmospheric turbulent premixed bunsen flames, Flow Turb. Combust. 75 (2005), pp. 149–172.

[47] N.K. Aluri, P.K.G. Pantangi, S.P.R. Muppala, and F. Dinkelacker, Substantiating a fractal based algebraic reaction rate closure of premixed turbulent combustion for high pressure and Lewis number effects, Combust. Flame 145 (2006), pp. 663–674.

[48] J.W. Sutherland, J.V. Michael, A.N. Pirraglia, F.L. Nesbitt, and R.B. Klemm, Rate constant for the reaction of $O(^3P)$ with H_2 by the flash photolysis-shock tube and flash photolysis-resonance fluorescence techniques; $504K \leq T \leq 2495K$, Proc. Combust. Inst. 21 (1986), pp. 929–941.

[49] D.L. Baulch et al., Evaluated kinetic data for combustion modelling, J. Phys. Chem. Ref. Data 21 (1992), pp. 411–734.

[50] D.L. Baulch et al., Evaluated kinetic data for combustion modeling. Supplement I, J. Phys. Chem. Ref. Data 23 (1994), pp. 847–1033.

[51] M.A. Mueller, T.J. Kim, R.A. Yetter, and F.L. Dryer, Flow reactor studies and kinetic modeling of the H_2/O_2 reaction, Int. J. Chem. Kin. 31 (1999), pp. 113–125.

[52] C.T. Bowman, R.K. Hanson, D.F. Davidson, W.C. Gardiner Jr., V. Lissianski, G.P. Smith, D.M. Golden, M. Frenklach, and M. Goldenberg, available online at http://www.me.berkeley.edu/gri_mech/

[53] F.G. Cerru, A. Kronenburg, and R.P. Lindstedt, Systematically reduced chemical mechanisms for sulphur oxidation and pyrolysis, Combust. Flame 146 (2006), pp. 437–455.

[54] G.P. Smith et al., available online at http://www.me.berkeley.edu/gri_mech/

[55] G.B. Skinner, and G.H. Ringrose, Ignition Delays of a Hydrogen–Oxygen–Argon Mixture at Relatively Low Temperatures, J. Chem. Phys. 42 (1965), pp. 2190–2192.

[56] G.L. Schott, and J.L. Kinsey, Kinetic Studies of Hydroxyl Radicals in Shock Waves. II. Induction Times in the Hydrogen-Oxygen Reaction, J. Chem. Phys. 29 (1958), pp. 1177–1182.

[57] E.L. Petersen, D.F. Davidson, M. Rohrig, and R.K. Hanson, Shock-Induced Ignition of High-Pressure H_2-O_2-Ar and CH_4-O_2-Ar Mixtures, AIAA Paper 95-3113, 31st AIAA/ASME/SAE/ASEE Joint Propulsion Conference and Exhibit, San Diego (1995).

[58] R.K. Cheng, and A.K. Oppenheim, auto-ignition in methane–hydrogen mixtures, Combust. Flame 58 (1984), pp. 125–139.

[59] D.A. Masten, R.K. Hanson, and C.T. Bowman, Shock Tube Study of the Reaction $H + O_2 \rightarrow OH + O$ Using OH Laser Absorption, J. Phys. Chem. 94 (1990), pp. 7119–7128.

[60] J.P. Hessler, Calculation of reactive cross sections and microcanonical rates from kinetic and thermochemical data, J. Phys. Chem. A 102 (1998), pp. 4517–4526.

[61] S.M. Hwang, S.-O. Ryu, K.J.D. Witt, and M.J. Rabinowitz, High temperature rate coefficient measurements of $H + O_2$ chain-branching and chain-terminating reaction, Chem. Phys. Let. 408 (2005), pp. 107–111.

[62] J.V. Michael and J.W. Sutherland, Rate constant for the reaction of H with H_2O and OH with H, by the flash photolysis–shock tube technique over the temperature range 1246–2297 K, J. Phys. Chem. 92 (1988), pp. 3853–3857.

[63] J.W. Sutherland, P.M. Patterson, and R.B. Klemm, Rate constants for the reaction, $O(^3P)+H_2O \rightleftharpoons OH+OH$, over the temperature range 1053 K to 2033 K using two direct techniques, Proc. Combust. Inst. 23 (1990), pp. 51–57.

[64] W. Tsang and R.F. Hampson, Chemical kinetic data base for combustion chemistry. Part I. Methane and related compounds, J. Phys. Chem. Ref. Data 15 (1986), pp. 1087–1279.

[65] S. J. Lim, Two-Dimensional Signal and Image Processing, J Englewood Cliffs, NJ, Prentice Hall (1990), eq. 9.44 − 9.46

[66] J. Cohen and K.R. Westberg, Chemical kinetic data sheets for high-temperature chemical reactions, J. Phys. Chem. Ref. Data 12 (1983), pp. 531–590.

[67] J.V. Michael, M.C. Su, J.W. Sutherland, J.J. Carroll, and A.F. Wagner, Rate constants for $H+O_2+M \rightarrow HO_2+M$ in seven bath gases, J. Phys. Chem. A 106 (2002), pp. 5297–5313.

[68] J. Troe, Modeling the temperature and pressure dependence of the reaction $HO+CO \rightleftharpoons HOCO \rightleftharpoons H+CO_2$, Proc. Combust. Inst. 27 (1998), pp. 167–175.

[69] C.J. Cobos, H. Hippler, and J. Troe, High-pressure falloff curves and specific rate constants for the reactions $H+O_2 \leftrightarrow HO_2 \leftrightarrow HO+O$, J. Phys. Chem. 89 (1985), pp. 342–349.

[70] J.V. Michael, J.W. Sutherland, L.B. Harding, and A.F. Wagner, Initiation in H_2/O_2: Rate constants for $H_2+O_2 \rightarrow H+HO_2$ at high temperature, Proc. Combust. Inst. 28 (2000), pp. 1471–1478.

[71] Ch. Kappel, K. Luther, and J. Troe, Shock wave study of the unimolecular dissociation of H_2O_2 in its falloff range and of its secondary reactions, Phys. Chem. Chem. Phys. 4 (2002), pp. 4392–4398.

[72] H. Hippler, J. Troe, and J. Willner, Shock wave study of the reaction $HO_2+HO_2 \rightarrow H_2O_2+O_2$: Confirmation of a rate constant minimum near 700 K, J. Chem. Phys. 93 (1990), pp. 1755–1760.

[73] J. Warnatz, in Combustion Chemistry, W.C. Gardiner, Jr., ed., Springer–Verlag, New York, 1984, pp. 197.

[74] L. Brouwer, C.J. Cobos, J. Troe, H.R. Dubal, and F.F. Crim, Specific rate constants k(E,J) and product state distributions in simple bond fission reactions. II. Application to $HOOH \rightarrow OH+OH$, J. Chem. Phys. 86 (1987), pp. 6171–6182.

[75] H. Hippler and J. Troe, Rate constants of the reaction $HO+H_2O_2 \rightarrow HO_2+H_2O$ at $T \geq 1000$ K, Chem. Phys. Let. 192, (1992), pp. 333–337.

[76] H. Hippler, H. Neunaber, and J. Troe, Shock wave studies of the reactions HO+H_2O_2→H_2O+HO_2 and HO+HO_2→H_2O+O_2 between 930 and 1680 K, J. Chem. Phys. 103 (1995), pp. 3510–3516.

[77] J.Y.D. Trujillo, T.G. Kreutz, and C.K. Law, Ignition in a counterflowing nonpremixed CO=H2-Air system. Combust. Sci. Technol., 127, (1997), pp. 1-27.

[78] S.B. Pope, Turbulent Flows, Cambridge University Press, (2000), ISBN 0521598869.